Università degli Studi di Palermo
Dipartimento di Ingegneria Civile, Ambientale e Aerospaziale
Area Ingegneria Idraulica e Ambientale

XXIII Ciclo del Dottorato di Ricerca in Ingegneria Idraulica e Ambientale
Tesi per il conseguimento del titolo

Using Satellite precipitation data to support local climatology and weather monitoring. Application to Sicilia.

Francesco Lo Conti

Tutor:
Dr. Leonardo V. Noto

Coordinatore del Dottorato:
Prof. Enrico Napoli

Sede Amministrativa: Università degli Studi di Palermo
Settore Scientifico Disciplinare: Costruzioni idrauliche e marittime e idrologia (ICAR/02)

Palermo, Febbraio 2012

Ringraziamenti

Desidero ringraziare tutte le persone che in maniera consepevole o inconsapevole mi hanno permesso di giungere a questo momento.

In particolare ringrazio il mio tutor e mentore di questa ennesima esperienza universitaria, il Dr. Valerio Noto, per avermi guidato e supportato con fiducia e pazienza.

Ringrazio tutte le persone e i colleghi dell'Università che in diversi momenti mi sono stati di aiuto e di supporto.

Il Prof. Sorooshian e tutte le persone del CHRS della University of California, Irvine, per avermi calorosamente ospitato e dato la possibilità di fare un'esperienza "dell'altro mondo".

La mia famiglia per non aver mai distolto il suo amorevole sguardo su di me.

Gli amici, le persone amiche e le persone buone con cui ho incrociato la via e che in qualche modo mi hanno aiutato e hanno contribuito a riempire di contenuti questo tempo.

Lettera di fine apprendistato

L'arte è lunga, la vita breve, il giudizio arduo, l'occasione fuggevole.
Facile è agire, difficile pensare; gravoso agire secondo il pensiero. Ogni inizio è lieto, la soglia è il luogo dell'attesa. Il fanciullo si meraviglia, l'impressione lo determina, egli impara giocando, la serietà lo sorprende. L'imitazione ci è innata, ciò che è da imitare non è riconoscibile facilmente. È raro incontrare l'eccellenza, più raro apprezzarla.
L'altezza ci attira, non i gradini; con l'occhio fisso alla vetta noi amiamo comminare in piano. L'arte può essere appresa solo in parte, l'artista ne abbisogna per intero. Quelli che la conoscono a metà sbagliano sempre e parlano molto; chi la possiede tutta desidera soltanto fare e parla di rado oppure tardi. I primi non hanno segreti nè forza, il loro insegnamento è come pane cotto in forno che piace e sazia per una sola giornata; ma non si può seminare la farina, non si devono macinare i semi.
Le parole sono buone, ma non sono il meglio. Il meglio non si manifesta con le parole. Lo spirito che ci fa agire è supremo. Soltanto lo spirito può capire e riprodurre l'azione. Nessuno sa ciò che fa quando opera rettamente; ma del mal fatto siamo sempre coscienti. Chi agisce solo per segni è un pedante, un ipocrita o un imbroglione. Di costoro ce n'è parecchi e si trovano bene insieme. Le loro chiacchiere tengono indietro il discepolo, e la loro ostinata mediocrità angustia i migliori.
L'insegnamento del vero artista dischiude l'animo; perché là dove mancano le parole parla l'azione. Il vero discepolo impara a ricavare l'ignoto dal noto e s'avvicina al maestro.

Wolfang Goethe - *Wilhelm Meister, gli anni dell'apprendistato*

Contents

List of Figures

List of Tables

Abstract

Precipitation is one major variable for many applications and disciplines related to water resources and the earth system. Satellite retrieval systems, rain-gauge network and radar systems are complement to each other in terms of their coverage and capability of monitoring precipitation. Satellite rainfall estimates systems produce data with global coverage that can provide information in areas for which data from other sources are unavailable. Without referring to ground measurement, satellite-based estimates can be biased. Although some gauged adjusted satellite precipitation products are developed, an effective way of integrating multi-sources of precipitation information is still a challenge.

In this study we selected the area of Sicilia island (Italy) having high density rain gauges to evaluate of satellite precipitation products. Sicilia has an area of 26,000 Km^2 and the gauge density of the network considered in this study is about 250 Km^2/gauge. It is an island in the Mediterranean sea with a particular climatology and morphology, which is considered as an interesting test site for satellite precipitation products on the European mid-latitude area. Four only satellite products (CMORPH, PERSIANN, PERSIANN-CCS and TMPA-RT) and two adjusted products (TMPA and PERSIANN Adjusted) have been selected for the study. Evaluation and comparison between selected products is performed with reference to the data provided by the gauge network of Sicilia and using statistical and graphical tools.

Results show that bias is considerable for all satellite products and some considerations about larger area climatology and passive microwave retrieval algorithms are reported to address this issue.

A post-retrieval tool is developed for the local study area that is able to improve features of an input satellite product, such as unbiasness and spatial resolution. Such a tool is useful to enlarge the suitability of satellite products even for other applications in addition to climatology.

Sommario

Le precipitazioni costituiscono una delle grandezze più importanti per diverse applicazioni e discipline legate al ciclo delle acque e alle scienze della terra. I sistemi di stima da satellite, le reti di pluviografi e i radar meteorologici, risultano complementari per quanto riguarda la copertura da essi fornita e le caratteristiche di stima delle precipitazioni. Le stime da satellite producono informazione con copertura globale che risulta essenziale in aree dove non è possibile disporre di altre stime. Senza il riferimento a misure a terra, le stime da satellite possono risultare distorte. Nonostante siano state sviluppate procedure di utilizzo complementare con dati da reti pluviografiche, tale integrazione di diverse fonti di dati di precipitazione necessita ulteriori approfondimenti e miglioramenti.

In questo studio è stata selezionata la Sicilia come area di studio per un'analisi di valutazione dei prodotti di stima di precipitazione da satellite. La sicilia ha un'area di 26,000 Km^2 e la densità degli strumenti della rete pluviografica utilizzata è di circa 250 Km^2/strumento. La Sicilia è un'isola nel Mar Mediterraneo con una particolare climatologia e morfologia, e quindi risulta un interessante sito di studio dei prodotti di stima delle precipitazioni da satellite nell'area europea. Vengono scelti quattro prodotti che utilizzano soltanto informazione satellitare (CMORPH, PERSIANN, PERSIANN-CCS e TMPA-RT) e due prodotti corretti con dati di precipitazione da reti pluviografiche (TMPA e PERSIANN Adjusted). L'analisi e il confronto tra i prodotti selezionati è stata effettuata con riferimento ai dati forniti dalla rete pluviografica disponibile e utilizzando strumenti statistici e di visualizzazione.

I risultati mostrano un considerevole livello di distorsione per tutti i prodotti e alcune considerazioni sulla climatologia a larga scala e sugli algoritmi di derivazione della pioggia vengono riportate per l'analisi di questi risultati.

Viene sviluppato uno strumento di elaborazione post-acquisizione dei dati per il miglioramento di alcune caratteristiche dei dati in input nell'area in esame, ovvero la correttezza della stima e la risoluzine spaziale. Questo strumento risulta utile al miglioramento dell'adeguatezza delle stime fornite dai prodotti satellitari anche per applicazioni diverse dalla climatologia.

Introduction

Precipitation is related to several main geophysical and atmospheric processes and its knowledge is usually a key factor for understanding and modeling related processes and their interaction. For several meteorological and climatological purposes, ranging from weather-forecasting to descriptive climatology, precipitation data is directly required as main variable of interest. Other applications use precipitation as primary input data into models, e.g. hydrologic models usually require precipitation data as input forcing variable. On the other hand achieving precipitation knowledge, as needed for most application, is not a trivial issue and it constitutes a field of interest for the scientific research itself. Complex physic conceptualization and representation, high uncertainties in weather and atmospheric modeling, high spatio-temporal variability and related degree of uncertainties in the estimation, are just a few features that determine the difficulties on retrieving and treating precipitation data.

Given both the strong interest for precipitation knowledge and such difficulties, precipitation information retrieving systems have received a great effort on developing tools and procedures to obtain data as reliable and suitable as possible. Some recent review papers provided an overall analysis of precipitation measurement state of the art and related fields of interest helping on focus some major feature.

Gruber and Levizzani (2008) presented an assessment of global precipitation products aiming on identifying the most likely areas where one can expect significant improvement to the understanding of the distribution and variability of global precipitation, with a particular emphasis on future monitoring. Michaelides *et al.* (2009) addressed a general review of precipitation aspects related to measurements and applications, describing retrieval procedures and devices, with their related features and capabilities, distinguishing between measurements (namely describing devices: impact disdrometers, image scan disdrometers, accumulation gauge, tipping bucket, weighing rain gauge, optical

rain gauge) and remote sensing (ground radar and satellite estimates). Moreover they illustrated precipitation aspects related to climatology and implication on numerical models and data assimilation procedures. Authors highlighted that combination of precipitation data from various sources presents the problem of data representativeness since ground-based measurements represent points sparsely distributed over an area while remote sensing data represents volumes related to a continuous surface. Data representativeness issues affect the error and uncertainty estimation on retrievals that however constitutes another important aspect to be investigated deeper by the scientific community. Finally the study pointed out how remote sensing techniques is susceptible to large biases and errors because of too many degrees of freedom in the physical satellite retrieval algorithms resulting in an underconstrained retrieval problem.

Kidd and Huffman (2011) described the previous stages of satellite precipitation estimates up to the present and depicted the expected developments based on new missions availability, algorithms improvements and applications requirements. In particular authors state that precipitation products derived from satellite ovservations have now reached a good level of maturity with ongoing research and development to improve the accuracy and the resolution, temporal and spatial, of these products. Authors identified the future developments of quantitative precipitation estimates on the continuation of operational missions for hydrometeorological applications and utilization/exploitation of long term data sets critical for climate monitoring. Finally they highlighted the necessity for further work needed to continue to develop error estimates that are vital to hydrological modeling and water resource assessment.

All these studies contribute to understand the innovative and leading role of satellite estimates given its unrivalled strength on observing precipitation with global coverage and spatio-temporal continuity. The necessity to fully understand satellite estimates capabilities, limits and uncertainties, is exploited by a number of evaluation studies that cover a wide area of objectives and geographic location. Still this activity is nowdays ongoing, and while several issues and observations have been introduced that help on correcting and improving satellite retrieval systems, a lot of efforts have to be faced to better characterize estimates features.

Motivation on developing satellite systems to measure precipitation on global scale, arose mainly from climatological studies. Indeed, given the low requirements of such applications in terms of temporal and spatial resolutions, they offered the possibility to explore potentialities offered by available sensors and technologies. As interest for getting improved estimates was augmented by potentialities shown by first applications and their scientific utility, a growing

amount of resources was made available for realizing satellite systems devoted to the observation of weather and atmospheric variables. The launch of the *Tropical Rainfall Measurement Mission* (TRMM) satellite system, with a specific precipitation oriented design and the first radar sensor pointing hydrometeors from the space, constituted a corner stone for the exploitation of remote sensing potentialities on measuring precipitation from space. Such developments permitted to obtain estimates with improved resolutions features respect to those needed for climatological purposes, thus allowing for introducing satellite precipitation estimates on other fields where typically ground-based data were considered as precipitation source. The framework of satellite resources that has been consolidated up to now, is constituted by two main data sources: infrared data, provided by sensors aboard of geostationary satellites, and passive microwave data from sensors aboard of low orbiting systems. Coupling these information, resulted being a key strategy, since the first kind of data are characterized by high temporal and spatial coverages but limited physical relationship with hydrometeors structure, while the second able to obtain estimates based on a physical base, but are sampled with low resolutions by low orbiting satellites.

Most used passive microwave retrieval algorithms are based on a Bayesian approach to extract precipitation information from a database of CRM (*cloud resolving model*) simulations outputs coupled with a radiative transfer model. Several issues concerning passive microwave retrieval algorithms have been pointed out. Michaelides *et al.* (2009) highlighted that the use of CRM databases in the satellite retrieval algorithms may introduce large biases because CRM simulations are highly individual and do not satisfy the requirement for general algorithm applicability. Further issues related to satellite precipitation estimates arise as remote sensing of mid and high latitude precipitation is especially challenging because of some factors that affect the retrieval, i.e. light intensity occurrences often close to the range of detection by sensors, snow precipitation occurrences that require particular treatments in the retrieval and related change of surface emissivity (Bennartz, 2007). Issues about mid-latitude retrieval are confirmed by Sohn *et al.* (2010) that reported how some of the main satellite precipitation products show considerable underestimation over the Korea Peninsula. Finally Kidd *et al.* (2012) reported an overall underestimation by satellite products on Europe area and addressed some difficulties arising on mid and high latitude such as those related to low intensities, frozen precipitation occurrences and issues with the surface backgrounds.

However different approaches have been developed to achieve such blended estimates that are available to scientific community users. In order to achieve more robust estimates, other approaches introduced a further merging step with

ground-based measurements from collections of rain-gauge networks data. Such methods provide less biased estimates, respect to only-satellite usually precipitation estimates that often present a relevant bias level. In order to use rain-gauge data to correct satellite estimates, latency time on availability of data increases because adjustment procedures are based on ground data at large time scale (usually monthly data are adopted).

Since satellite precipitation products represent a relative new tool, and given the reported criticism that affects estimates, performing evaluation studies is a worth activity, useful to understand real capabilities and potentialities referred either to general purposes or particular applications.

The IPWG (*International Precipitation Working Group*) is committed in conducting several studies in order to carry out a systematic evaluation activity for operational satellite algorithms referred to continental scale. Among IPWG activities, PEHRPP (*Pilot Evaluation of High Resolution Precipitation Products*), was established to evaluating, inter-comparing and validating many operational high resolution precipitation algorithms. In particular PEHRPP aims to characterize errors on many spatial and temporal scales and geographic regions. Beyond IPWG and PEHRPP activities, others studies have been carried out with similar targets comprising different datasets to retrieve information about products and algorithms features.

Kidd *et al.* (2012) carried out an evaluation study for main satellite precipitation products, referred to Europe area. Results of their analyses are effective on pointing out a series of weaknesses on retrieval algorithms that result particularly relevant on the considered European and Mediterranean area. Moreover other studies take into account a singular satellite product among the most used. Some of the more analyzed evaluation activities concern the capability to reproduce climatology information, the representation of particular events, hydrological performances within models, uncertainty and error characterization related to possible explaining factors as elevation and land/sea origin, retrieving algorithms and comparisons between different products. Moreover the evaluation activity has to be considered geographically referred since performances can be related to spatial and geographic features.

The effective usage of satellite precipitation estimates, depends on the suitability of these data against the requirements of the applications. A compared analysis of satellite estimates potentialities and suitability with respect to other precipitation sources for typical application involving precipitation, highlights how they result being particularly promising not only for climatological purposes, but even for weather and meteorological applications, given the time readiness on which data are available, and for hydrological applications because

of their spatial coverage. But even some weaknesses result affecting and compromising the effective suitability for each application. These aspects lead to the opportunity of further elaboration of satellite products, in order to get a higher level of usability. While some of these weaknesses require substantial review of retrieval algorithms and will benefit of future missions, sensors and technologies, others can be faced directly improving satellite products estimates. Among most important tasks potentially applicable, further bias adjustment based on more detailed ground precipitation knowledge, and spatial downscaling, are expected to significantly increase suitability of satellite estimates in particular for local hydrological applications. Whenever there is not the necessity of having data in real time, bias adjustment is faced by applying a correction procedure based on global rain-gauge network data collections. Such an estimate is suitable for most hydrological applications, off-line meteorological and weather studies, and particularly for climatological studies and investigations. Just for climatological purposes, some robust blended satellite-ground data estimates have been developed by the scientific community. The most important are the *Global Precipitation Climatology Project* (GPCP) discussed on section 1.5, and the *CPC Merged Analysis of Precipitation* (CMAP). Furthermore some satellite precipitation algorithms have been designed to provide even a bias-corrected version of the same product, as those describe on sections 1.4.1 and 1.4.5.

Another approach on adjusting satellite estimates can arise from the opportunity to reach the desired bias correction in real-time respect the retrieving time. Such an operation is justified by the increasing effectiveness on retrieving and delivering data from remote sensing data management systems, and successive precipitation elaboration, that often presents a higher readiness level than corresponding ground-based data. A Bayesian approach has been recently proposed and used to represent the relationship between historical satellite and rain-gauge precipitation retrievals, that is used to correct real-time satellite estimates. Another aspect to be considered on making satellite estimates available for many applications, can arise from resolutions requirements. For example hydrological applications usually require spatial resolution lower than that of common satellite precipitation products. In this case downscaling procedures offer a valid tool to produce derived estimates at lower resolution.

Given this depiction of satellite precipitation estimates, a study of exploration of their features, potentialities and weaknesses, referred to Sicilia island has been carried as main goal of this thesis. Such study is constituted of an evaluation analysis of most important satellite precipitation products developed so far, including both only-satellite and bias-adjusted products. Moreover the development of a post-retrieval supporting tool to improve features of retrieved

data has been performed in order to increase their suitability. Such a tool considers an "on-line" bias-adjustment procedure and the producing of statistical spatial downscaled maps.

In particular, in the evaluation analysis, some of the most consolidated satellite precipitation products are evaluated and compared against data from a rain-gauge network for the area of Sicilia for the period 2007-2008. This case study is particular interesting because it can be useful to understand some satellite products features related to particular spatial and geographic characteristics as Sicilia is placed in the Mediterranean Sea which well represents the transition area between North-Africa climatic regime and the European climatic regime. Since adjusted products are considered in the analysis, considerations about global ground-based datasets with reference to the Mediterranean area, can be obtained from the elaborations.

A coupled bias adjustment-spatial downscaling procedure is proposed in this thesis with reference to the Sicilia area and based on local rain-gauge network data. Criteria for developing such a tool, have been derived from a study of satellite estimates features that need further improvements and possible suited tasks to apply on these data.

Finally the overall contribution of this thesis is to provide an overall analysis of satellite precipitation estimates, with emphasis on their performances and features on the Mediterranean area, and considering further elaboration of such estimate in order to improve their usability.

Chapter 1

Satellite precipitation retrieval systems

Beginning of meteorological and atmospheric remote sensing is usually identified with the launch of the first *Television InfraRed Observing Satellite* (TIROS-1) on April 1960. In order to coordinate activities and efforts on developing observation systems of weather, the *World Meteorological Organization* (WMO) established the *World Weather Watch* program in 1963. The *Global Observing System* (GOS; WMO, 2005) was charged with providing long-term stable datasets required by international organizations and the user community. In the last years many efforts have been done on developing satellite systems, precipitation and other variables retrieval algorithms and procedures as well as on delivering data, information and related scientific knowledge. *Tropical Rainfall Measuring Mission* (TRMM) launch has determined and influenced the most important developments on retrieving precipitation from space so far, and the future *Global Precipitation Mission* (GPM) is expected to stimulate further advancements and improvements.

Precipitation retrievals are more complex than other typical atmospheric variables such as the *total precipitable water* (TPW) and *column liquid water* (CLW) because they involves satellite measurements of cloud containing both water droplets and ice particles.

The main sources of information from satellite systems on measuring meteorological and atmospheric variables, are the *infrared* (hereafter IR) data and the *passive microwave* (PMW) data. IR sensors are familiar to most forecaster with

excellent coverage from *geostationary earth orbiting* (GEO) satellites and fine spatial resolution. However, when clouds are present, IR sensors observe only the temperature of the cloud tops. In contrast PMW sensors on polar satellites, comprised on the *low earth orbiting* (LEO) satellite systems, observe emissions from water and ice within clouds to produce more reliable quantitative precipitation estimates. Another important satellite source of information is given by the active space based microwave or radar sensors. Satellite radar have a role in the overall precipitation monitoring missions, producing the highest accuracy in both the vertical and horizontal dimensions.

While retrieval algorithms that use only of GEO-IR or LEO-PMW data have been developed, the most effective results emerged from the algorithm developments activity, consider the blended usage of both these sources in such a way that main strengths from each source are kept.

Given high uncertainties and numerous issues that characterized satellite precipitation estimates during their development years, the main field on which they resulted being suitable was climatology as it requires low space and time resolutions, then allowing for using satellite precipitation in an aggregated form. Suitability of satellite precipitation for climatological applications, results from the unprecedented possibility offered by satellites to estimate precipitation over sea where usually a very scarce information was provided by traditional measures. Moreover, since climatological applications usually do not require particular data readiness, the possibility to perform a further merging with ground-based information has been explored by specific climatological techniques. The most used of such datasets are the *Global Precipitation Climatology Project* (GPCP Huffman *et al.*, 1997; Adler *et al.*, 2003) and the *CPC Merged Analysis of Precipitation* (CMAP Xie and Arkin, 1996b). GPCP data has been adopted as reference data for the developing of adjusting procedures for operational satellite precipitation products.

Information about sensors and tecniques are described on the next subsections, while algorithms descriptions follow in the sections 1.2 and 1.3. Then blended retrieval techniques are described on section 1.4 followed by description of GPCP procedure on section 1.5. Finally main expected future developments on satellite systems and retrieval products is reported on section 1.6.

1.1 Sensors and techniques

As already described, the satellite framework related to precipitation information and retrievals, is usually divided in to two broad categories: *geosta-*

tionary earth orbiting (GEO) satellites and *low earth orbiting* (LEO) satellites, which include polar-orbiting satellites. Figure 1.1 provides a schematic, not in scale, representation of both systems. Descriptions of GEO and LEO systems are reported on next paragraphs.

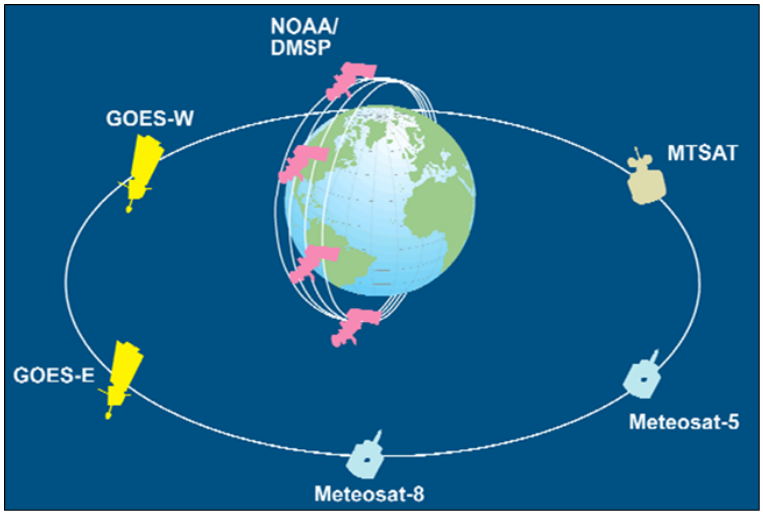

Figure 1.1: GEO-LEO schematic representation.

1.1.1 GEO satellites

GEO satellite systems are able to provide continuous observation related to the area of interest since they orbit at the same rate as the Earth turns such that they appear stationary to a location on the Earth's surface. Although these systems have different characteristics, still they share main features. In particular their orbiting height above the equator is about 35,800 km and visible (VIS) and IR data resolutions is 1 km and 4 km respectively. GEO systems considered in precipitation retrieval are described in the following sections.

- **Meteosat Second Generation**
  It is operated by the *European Organization for the Exploitation of Meteorological Satellites* (EUMETSAT). Meteosat satellites provide coverage related to Europe area. Its primary instrument is the *Spinning Enhanced Visible and InfraRed Imager* (SEVIRI) that provide data from 12 spectral

channels from visible to thermal infrared. In particular 8 thermal infrared channels are useful on estimating temperatures of clouds, oceans and land. SEVIRI provide a permanent imaging of the observed are with a time resolution of 15 minutes. Spatial coverage and more detail about Meteosat program, are reported on figure 1.2 and table 1.1.

Table 1.1: Meteosat satellite characteristics

Satellite	**Meteosat-7**	**Meteosat-8**	**Meteosat-9**
Programme	Meteosat First Generation	Meteosat Second Generation	Meteosat Second Generation
Longitude	57.5^oE	9.5^oE	0^oE
Lifetime	1997-2013	2002-2018	2005-2022

- **Geostationary Operational Environmental Satellites**
  Geostationary Operational Environmental Satellites (GOES) system provide data coverage about USA and South America. It is operated by NOAA-NESDIS (*National Environmental Satellite, Data, and Information Service*) for supporting weather forecasting, severe storm tracking, and meteorology research. Two GOES satellites, called GOES-East (longitude 75^oW) and GOES-West (longitude 135^oW), work simultaneously to fully cover Alaska, Hawaii, the entire continental United States, South America and the Pacific and Atlantic Ocean (see figure 1.3). The main mission is carried out by the primary payload instruments, the *Imager* and the *Sounder*. The *Imager* is a multichannel instrument that senses infrared radiant energy and visible reflected solar energy from the Earth's surface and atmosphere. The *Sounder* provides data for vertical atmospheric temperature and moisture profiles, surface and cloud top temperature, and ozone distribution.

- **Feng-Yun-2**
  Feng-Yun-2 (FY-2) satellites system (Feng-Yun means "winds and clouds" in Chinese) is operated by the *National Satellite Meteorological Center* (NSMC) of CMA (*China Meteorological Administration*). FY-2 observe the Asia-Pacific region from a longitude position of 105^oE. The main sensor onboard FY-2 is the VISSR (*Visible and Infrared Spin-Scan Radiometer*). VISSR is a 3 channels device: visible channel is 0.55-1.05 μm, infrared channel is 10.5-12.5 μm and water vapour channel is 6.2-7.6 μm. In the visible channel, the resolution is equal to 1.25 km. In the infrared and

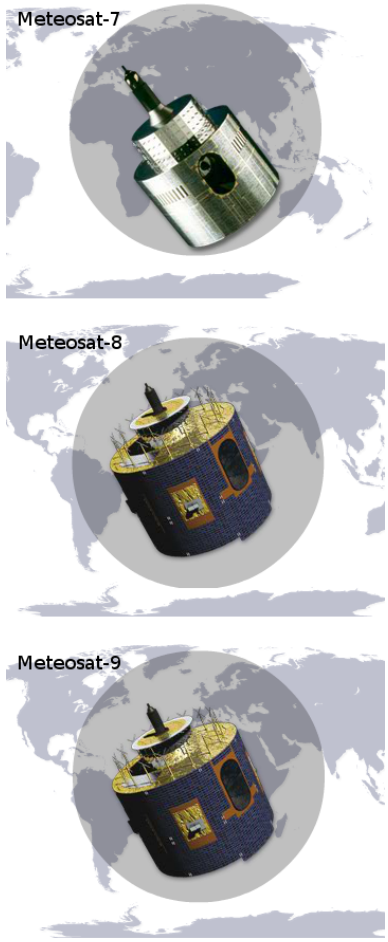

Figure 1.2: Coverage of Meteosat satellites.

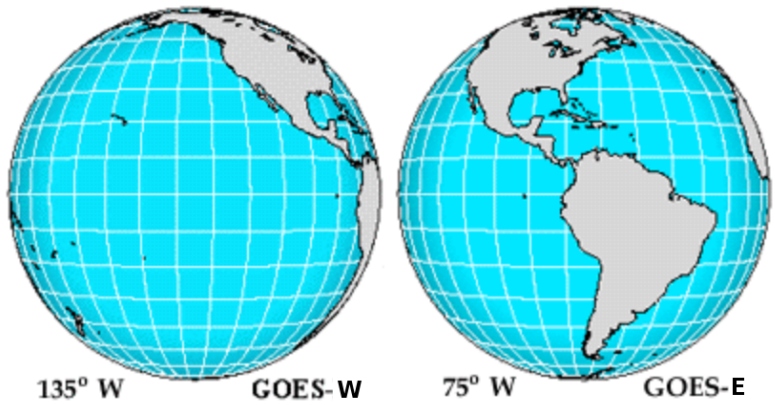

Figure 1.3: GOES-East and GOES-West coverage.

water vapour channels, the resolution is equal to 5 km.

- **Japanese Multifunctional Transport Satellite series**
  Multifunctional Transport Satellites (MTSAT) are geostationary satellites owned and operated by the Japanese Ministry of Land, Infrastructure and Transport and the *Japan Meteorological Agency* (JMA), and provide coverage for the hemisphere centred on 145^{o}E (MTSAT-2). The visible light camera has a resolution of 1 km; the infrared cameras have 4 km (referred to the equator latitude).

A depiction of GEO satellites position and coverage is shown on figure 1.4.

1.1.2 LEO satellites

Since IR bands can be used only to infer top cloud characteristics, other spectral bands are needed in order to infer physics of precipitation and cloud properties. Given the spectral feature of atmosphere constituents, PMW data results being a very important information source. PMW sensors have been designed in particular for polar orbiting satellite missions. Descriptions of most important satellite missions follows along with their related PMW sensor.

- **Defense Meteorological Satellite Program (DMSP)**
  The DMSP is run by *National Oceanic and Atmospheric Administra-*

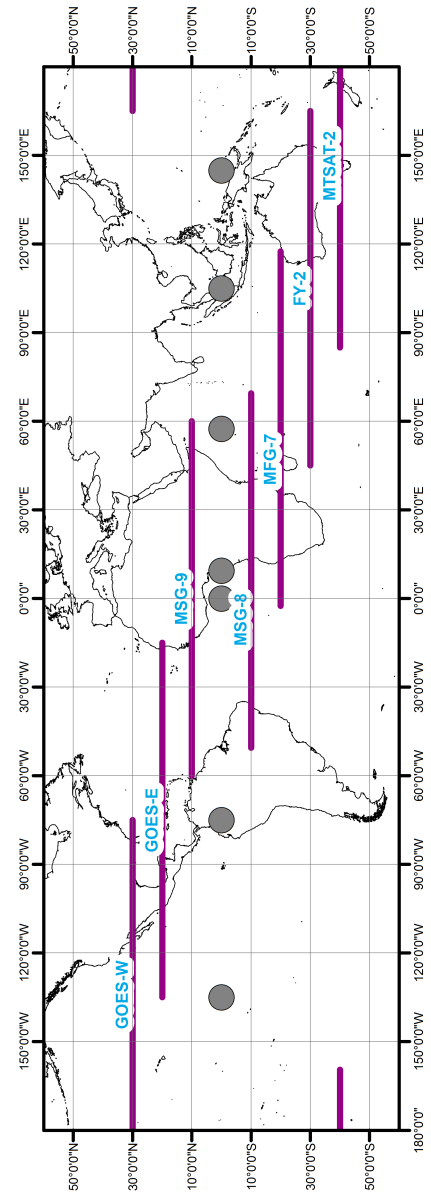

Figure 1.4: GEO satellites longitude indication and observation range approximatively considered equal to 60 degrees.

tion (NOAA) for monitoring meteorological, oceanographic and solar-terrestrial physics. Each DMSP satellite has a 101 minute, sun-synchronous near-polar orbit at an altitude of 830 km above the surface of the earth.

The PMW instruments on board DMSP satellites is the *Special Sensor Microwave/Imager* (SSM/I) flown on board the DMSP Block 5D-2 satellites. It measures brightness temperature at 19.35, 22.235, 37 and 85.5 GHz. With the exception of 22.235 GHz band, both horizontal and vertical polarization are sampled by SSM/I.

- **NOAA satellites**
  NOAA-15/16/17 satellites are weather forecasting satellites operated by NOAA and working on a sun-synchronous orbit on an altitude between 800 and 850 km above the earth orbiting every around 101 minutes. Main instruments hosted by NOAA satellites are the *Advanced Microwave Sounding Unit* (AMSU), the *Advanced Very High Resolution Radiometer* (AVHRR) and the *High Resolution Infrared Radiation Sounder* (HRIS).

  The *Advanced Microwave Sounding Unit - B* (AMSU-B) is a multichannel cross-track microwave radiometer with five bands: 89.9±0.9, 150±0.9, 183.31±1.00, 183.31±3.00, 183.31±7.00 GHz.

- **Tropical Rainfall Measuring Mission (TRMM)**
  TRMM is a joint mission between NASA and JAXA, the Japanese space agency mission. It has been specifically designed to measure rainfall on the tropical area and to study weather and atmosphere on the earth. TRMM make use of both active and passive microwave instruments for the first-time. Such a combination of instruments make possible observing weather phenomenon deriving different features. Orbit altitude is 402.5 km.

  Main instruments on board TRMM are the *Visible and Infrared Scanner* (VIRS), the *TRMM Microwave Imager* (TMI) and the *Precipitation Radar* (PR). TMI designing was based on SSM/I sensor. Indeed they are similar on many feature and even the bands frequencies are the same except that TMI has the additional 10.7 GHz channel useful for an improved response for high rainfall rates common in tropical rainfall. TRMM data is the reference information for several retrieving precipitation systems. This information is often used, within precipitation retrieval algorithms, by means of a series of products derived directly from TRMM sensors (see figure 1.6). These are organized in a four level scheme. Level 1 corresponds to raw data measured by sensors and directly derived radiances,

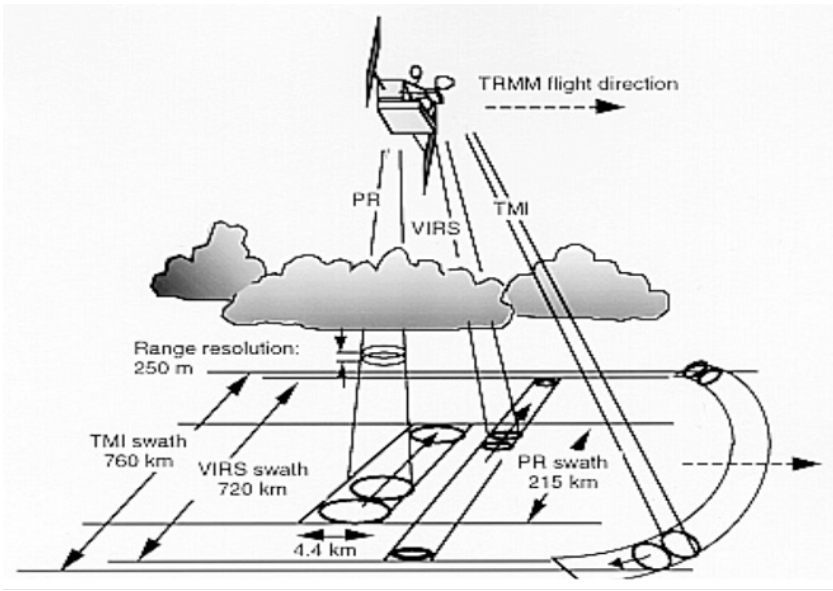

Figure 1.5: TRMM instruments representation.

reflectivities and temperatures. On level 2 physical variables are derived from level 1 data (mainly precipitation and precipitation related fields). These data are further elaborated on level 3 that provides aggregated values and statistic fields. Finally level 4 is given by coupling previous levels data with those from other sensors and sources.

- **EOS Aqua**
  Aqua is a NASA Earth Science satellite mission named for the large amount of information that the mission is collecting about the Earth's water cycle, including evaporation from the oceans, water vapor in the atmosphere, clouds, precipitation, soil moisture, sea ice, land ice, and snow cover on the land and ice. Additional variables also being measured by Aqua include radiative energy fluxes, aerosols, vegetation cover on the land, phytoplankton and dissolved organic matter in the oceans, and air, land, and water temperatures. Aqua flies on a near-polar low-Earth orbit 705 km above the earth. The *Earth Observing System* (EOS) Aqua platform records PMW data by means of the *Advanced Microwave Scanning*

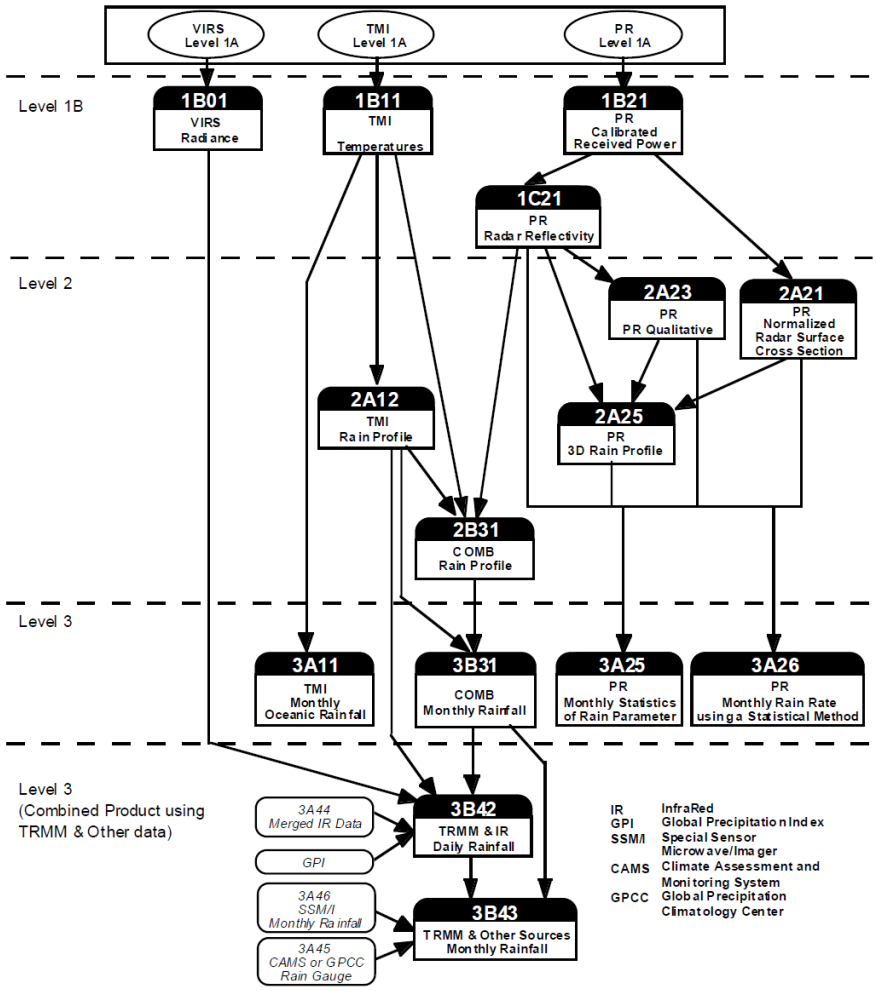

Figure 1.6: TRMM sensors derived products scheme.

Radiometer (AMSR-E). Its band frequencies are 6.925, 10.65, 18.7, 23.8, 36.5, 89 GHz.

A summary of PMW sensors features is given on table 1.2.

Table 1.2: PMW sensors and related satellite characteristics.

Sensor	Spatial resolution [km] (footprint at $\sim$ 85 GHz)	Frequencies (GHz)	Satellite altitude (km)
TMI (TRMM)	4.6x6.9	10.7, 19, 22, 37, 85	402
SSM/I (F-13/14/15)	13x15	19, 22, 37, 85	800-850
AMSU-B (NOAA-15/16/17)	15x15	89, 150 and three at $\sim$ 183 GHz	830
AMSR-E (Aqua)	6x4	6.9, 10.7, 18.7, 23.8, 36.5, 89	705

1.1.3 Remote sensing of atmosphere and precipitation

Estimating atmospheric, water content and precipitation features using electromagnetic radiation measured by satellite sensors, requires to identify which bands can be useful for these purposes. Figure 1.7 illustrates the atmospheric transmission along the electromagnetic spectrum along with approximate indications of the bands of radiation that are absorbed and transmitted by the earth's atmosphere. While atmospheric window (transmitted bands) are important since remote sensing of the surface is only possible in these bands, absorption bands are also important, because related radiation and absorption can be used to obtain profiles of temperature, water vapour and precipitation down through the depth of the atmosphere from sounders or profilers.

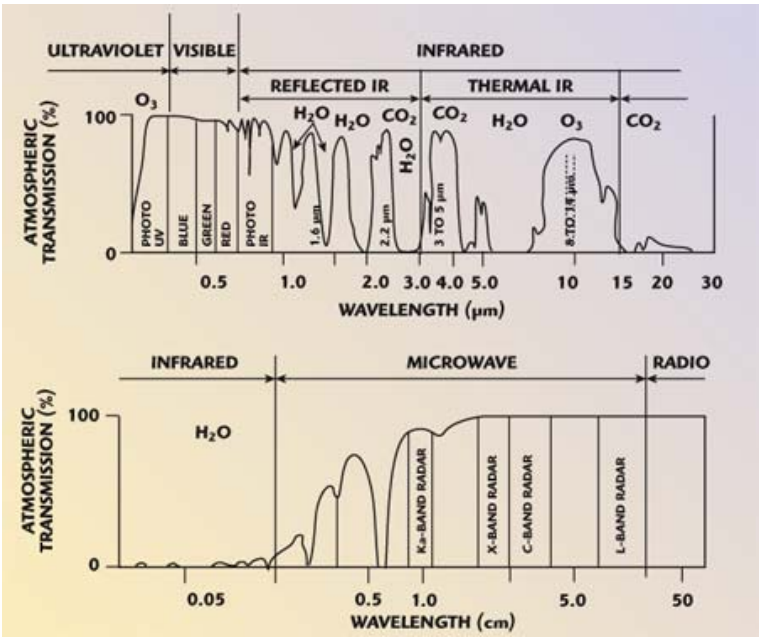

Figure 1.7: Atmospheric transmission along the electromagnetic spectrum.

Two main strategies can be identified among precipitation information retrieval methods: the first approach consists on using bands that interacts with atmosphere components, allowing for inferring precipitation information based on a physical approach. Microwave bands constitutes the main source for such methods. The second makes use of absorbtion bands to infer information related to top-cloud features obtained from emitted radiation; in particular, thermal infrared bands are mainly used to derive top-cloud temperature.

In the following paragraphs, passive microwave precipitation retrieval algorithms (that constitutes the main satellite precipitation estimation source) and usage of IR bands and other sources are described.

1.2 PMW algorithms

Looking more closely at a hypothetic convective rain cloud (figure 1.8) it is possible to see how the various satellite observations can be used to quantify pre-

cipitation. Above the freezing level the cloud is dominated by a mixture of small, medium and large ice particles or solid hydrometeors. This is the regime where the higher-frequency microwave channels would be most effective on observing precipitation. As the larger ice hydrometeors falls through the freezing level, the resulting melting produces falling raindrops or liquid hydrometeors and the lower-frequency microwave channel become the preferred observing tool. Below cloud base, the raindrops form a rain shaft.

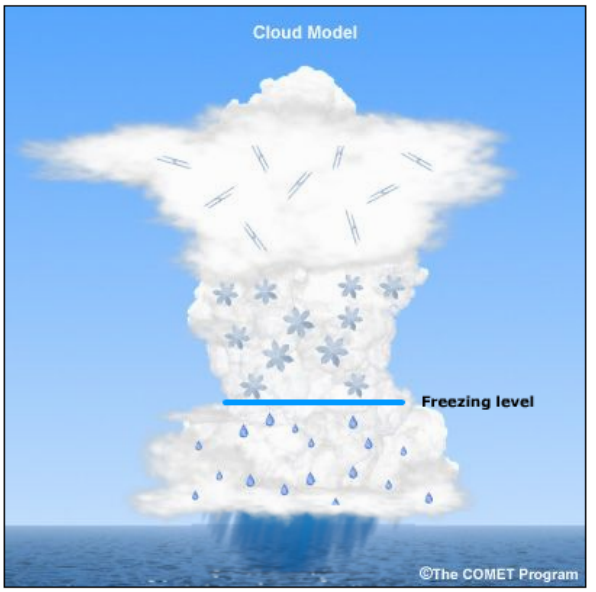

Figure 1.8: Convective rain cloud representation.

A passive IR remote sensing observing strategy for inferring precipitation, relies on the observation of the energy emitted from cloud tops. Therefore no information about either the frozen or liquid hydrometeors is contained in this upwelling energy. The only information is the top cloud temperature providing only a rough idea of the precipitation rate. The lower PMW frequencies, often referred as "emissions" channels, measure precipitation mainly from the energy emitted by medium-to-large-sized raindrops while the higher frequencies, or "scattering" channels, retrieve the energy scatter by ice particles above the freezing level and are sensitive to emission from small raindrops and scattering

and attenuation of energy by precipitation-sized ice particles (see the electromagnetic spectrum on figure 1.9).

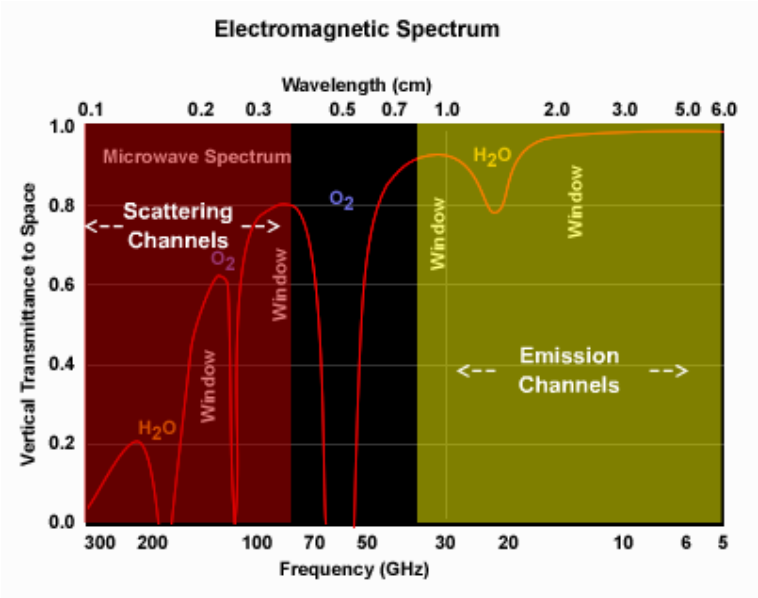

Figure 1.9: Microwave vertical transmittance spectrum.

Therefore the lower-frequency energy (typical 37 GHz channel) coming from the surface is augmented by emission from liquid hydrometeors and cloud water. Above the ocean, energy leaving the cloud is greater than the surface-based energy entering the base of the cloud from below. The fundamental limitation of microwave precipitation retrieval over land using emission channels is that the magnitude of microwave energy from precipitation and surrounding land are similar.

High-frequency microwave scattering channels, such as 85 GHz, provide different information than lower frequency microwave or IR channels. Upwelling energy come from the surface, cloud water and raindrops below the freezing level. However, above the freezing level, the energy is attenuated due to scattering by precipitation-sized ice particles. The energy leaving the cloud is less than what came originally from the surface. Thus the effect of this large ice-particles is to depress brightness temperature seen by the satellite.

Unique characteristics of microwave identification of clouds and precipitation, referring to SSM/I and TMI channels, include the following:

At 85-91 GHz:

- Deep convection appear relatively cold;
- Water clouds and moist air masses have warm brightness temperatures over water surfaces;
- Imagery can penetrate thin cirrus canopies and reveal internal storm structure;
- Imagery is able to distinguish deep convection, but can not always see low-level circulations when associated primarily with low-level water clouds;
- Spatial resolution is higher than for imagery at lower microwave frequencies.

At 37 GHz:

- Water clouds and precipitating clouds appear warm against a relatively cold ocean;
- Upwelling radiation is largely unaffected by ice particles, which allows imagery to highlight low-level cloud features;
- Imagery resolves details missed by 85-91 GHz;
- Imagery shows regions of low-level clouds and rain.

Examples of precipitation algorithms based on the "emission" principle were presented by Wilheit *et al.* (1991) and Chang *et al.* (1999). In order to reduce uncertainties of emission algorithms at the pixel level, algorithms such as those developed by Petty (1994) and Aonashi and Liu (2000) rely on an approach similar to that above mentioned, but with additional frequencies used to constrain the problem. The additional channels, unfortunately, do not provide any additional direct information about the surface rainfall. Instead, the additional channels are used to help describe some property of the underlying cloud, such as its convective or stratiform nature or whether the scene corresponds to deep or shallow convection. This information is then used, in conjunction with appropriate parameterizations, to better constrain what the vertical rain profile or its horizontal inhomogeneity might be. As such, these methods can reduce the uncertainty at the pixel level, but only at the expense of additional assumptions

and parameterizations that must themselves be validated if a complete error model is to be generated.

As microwave frequencies increase, the amount of scattering due to ice particles commonly found in raining clouds increases too. This scattering acts to reflect upwelling radiation back to the surface, lowering the observed brightness temperatures. While all frequencies display some amount of scattering, the behavior is most evident in the 85-GHz channel of the SSM/I where brightness temperature depressions of as much as 150 K can be observed over convective updrafts. Algorithms which make use of this relationship are generally referred to as "scattering" algorithms. Examples of this type of algorithm can be found in Kidd and Barrett (1990), Grody (1991) and Adler *et al.* (1994).

In addition to emission and scattering algorithms, there are also a number of multichannel regression algorithms. Examples of these may be found in Bauer and Schlnessel (1993), or the SSM/I calibration/validation algorithm described by Olson *et al.* (1991). The algorithms are based upon theoretical radiative transfer computations to derive regression statistics. In so doing, however, these algorithms become sensitive to the assumed vertical structure of rain systems. Unless the ratios of cloud water, rain water, and ice in the cloud systems are assumed correctly, these schemes are susceptible to the same uncertainties found in pure scattering algorithms. To avoid some of these problems, Liu and Curry (1992) have developed alternative approaches in which emission signatures are used to determine rainfall while scattering signatures are used to help define the nature of the precipitation. To overcome the inhomogeneous rainfall problem, Petty (1994) has developed a technique that employs normalized polarization and scattering indices.

An even more complex family of algorithms is the Bayesian approaches that employ *cloud resolving models* (CRMs). These algorithms are described by a number of authors (e.g. Mugnai *et al.*, 1993; Kummerow and Giglio, 1994; Smith *et al.*, 1994; Marzano *et al.*, 1999; Bauer, 2001; Kummerow *et al.*, 2001). In these methods, the CRM outputs are coupled with radiative transfer calculations to construct *a priori* databases of satellite observables along with the cloud model hydrometeor fields. A Bayesian or probabilistic approach is then used to compute the most likely *a posteriori* distribution when constrained by the actual measurements. Unlike the previous multifrequency approaches, these schemes can make direct use of explicit physical mechanisms contained in the CRMs to link satellite observables to the rain structure. The disadvantage of these approaches is their susceptibility to errors in the *a priori* database in terms of the accuracy of the microphysical details provided by the CRM (Panegrossi *et al.*, 1998), the completeness of the CRM databases, and the fidelity of model

outputs on capturing differences in climate regimes. These climate regime biases can be difficult to observe at individual validation sites because of the large random noise associated with individual clouds. They are, however, critical to understanding climate signals and trends.

1.3 IR data and others supporting precipitation sources

Even though PMW data represents the most important data source in retrieving precipitation on global scale using satellite information, most relevant precipitation estimation products, usually make use of other data sources. Coupling several data sources allows for improving PMW estimates features keeping the strengths from each source. The fundamental data sources taken into consideration are the IR data from GEO satellite systems, the active microwave information, essentially from the TRMM's PR, and the ground based data with the related collecting systems.

1.3.1 IR data

Among other satellite resources, IR information is essential for improving spatial and temporal resolutions. Nevertheless it can be used even to directly produce precipitation data, considering the relationship with the top cloud temperature. The primary advantage of IR-based techniques is the high temporal frequency of images, for example, up to 15 minutes for GOES and *Meteosat Second Generation* (MSG) geostationary satellites. The most important example of using IR data to retrieve precipitation is the *GOES Precipitation Index* (GPI) (Arkin and Meisner, 1987). The GPI precipitation estimate is computed using this expression:

$$Precipitation\,(mm) = FRAC \times RATE \times TIME$$

where FRAC is the fractional coverage of IR pixels < 235K over a reasonably large domain (50 km $\times$ 50 km and larger), RATE is fixed equal to 3 mm/hour and TIME is the number of hours over which FRAC was compiled. The GPI shows large bias over equatorial Africa and Indonesia, where virga[1] clouds may

[1](Also called Fallstreifen, fallstreaks, precipitation trails.) Wisps or streaks of water or ice particles falling out of a cloud but evaporating before reaching the earth's surface as precipitation (from AMS Glossary of meteorology: *http://amsglossary.allenpress.com/glossary*).

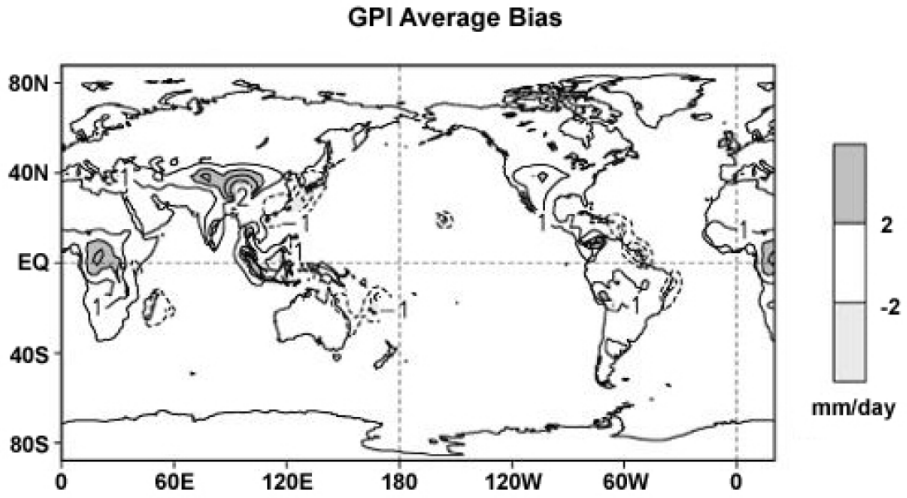

Figure 1.10: Time-average precipitation bias (1996-2003) for the GPI satellite estimates in mm day^{-1} (Smith *et al.*, 2006).

be interpreted as surface rainfall, and over high mountains, where snow may be interpreted as precipitation (figure 1.10, Smith *et al.*, 2006).

IR-only techniques suffer from some weaknesses compared with radar because the lower-resolution satellite IR can not detect convective-scale structure and rain from warm clouds. In addition, thick cirrus and convective precipitation appear similar. This means that satellite IR-only techniques tend to underestimate precipitation early in the lifecycle of convective systems, when warm rain processes dominate, and overestimate precipitation in the decaying stages when cold cirrus is common. As will be exposed in the next section, IR data are more often coupled with PMW data to improve the spatial and temporal resolutions. Many approaches have been proposed to obtain this data-merging. One of this consists on using IR data to infer the movement of hydrometeors allowing for the translation of the PMW estimates available on a raw temporal scale. Another is given by the infilling of PMW precipitation estimates using those obtained from IR (e.g. GPI) previously calibrated. Finally it is possible using the IR-rain rate relationship as main retrieving tool, using PMW data to improve it and characterizing this relationship for several cloud-hydrometeor classes. Other merging procedures have been proposed in literature and will be

exposed in the satellite blended techniques section.

1.3.2 Active microwave data

The development of specific satellite missions dedicated to the investigation of the atmosphere and clouds, like TRMM and CloudSat, has led to the opportunity to carry radar instruments to infer hydrometeor properties from the space rather than from the ground. The radar instrument onboard of TRMM and that onboard of CloudSat are respectively the *Precipitation Radar* (PR) and the *Cloud Profiling Radar* (CPR). The TRMM PR is operationally used for calibration operations of precipitation measurements and for blended products with PMW data. Main features of TRMM PR are reported on table 1.3.

Table 1.3: Characteristics of TRMM Precipitation Radar

Radar type	Pulse radar
Frequency	13.796, 13.802 GHz
Polarization	Horizontal
Sensitivity	$<$0.5 mm h^{-1}
Range resolution	250 m
Horizontal resolution	5 km
Swath width	250 km
Observational range	Surface to 15 km (minimum)

Here a general description of TRMM PR is provided as it is the most exploited satellite radar by operational precipitation products.

As illustrated on figure 1.6, the operational PR precipitation product is the TRMM 2A25. The algorithm used since version 5 is described by Iguchi *et al.* (2000). The 2A25 algorithm retrieves the precipitation profiles in two steps. It estimates the true effective reflectivity factor (Z_e) from the measured vertical profile of reflectivity factor (Z_m) first. It then converts the estimated effective reflectivity factor (Z_e) into the rainfall rate (R). The step to estimate Z_e from Z_m correspond to the estimation of attenuation correction. Since almost all attenuation at the Ku-band originates in rain itself, the profile of Z_m contains some information about the attenuation. However, the relationship between Z_e and the specific attenuation due to precipitation, depends on the type of precipitation particles (e.g. snow or rain), their drop size distribution (DSD) and their temperature. This dependence is crucial in attenuation correction when the attenuation becomes large. The step to convert Z_e to R also depends on

the same factors related to electromagnetic properties of precipitation particles as well as their DSD. The algorithm uses the surface echo to extract the DSD information that gives an important constraint in both attenuation correction and Z_e-R conversion. In this step, the type of precipitation particles at each range and their initial distribution is assumed to be known. If the phase of precipitation particles is incorrectly assumed, the estimated DSD parameters may be biased.

The dual-frequency precipitation radar that will be carried by the future *Global Precipitation Mission* (GPM) will be useful on extracting further information about the attenuation by precipitation that can be used to identify the phase state of particles.

PR data is used even in the TRMM 2B31 algorithm that merge this information with the TRMM TMI data. This product is characterized by a good quality precipitation estimate as it comes from two physically related data sources, but its spatial and temporal resolution is rather low. It is used as calibration data in the TMPA algorithm described on section 1.4.

1.3.3 Ground-based data

Traditional measurements of precipitation using rain-gauge networks, have an important role even in the satellite measurement era. Since the new estimate tools derived from satellite data still are characterized by high uncertainties and the uncertainty estimate itself is an open issue, coupling these estimates with ground based data is important to reduce errors and in particular the bias error. As will be illustrated in the next sections and chapters, precipitation estimates based on satellite data only, result being affected by systematic bias error. The usage of ground based data and in particular of rain-gauge network data, has been widely adopted on developing climatological precipitation datasets, where timing requirements are not so strictly then allowing for the latency time needed to retrieve global scale ground data.

The *Global Precipitation Climatology Centre* (GPCC) has been established in year 1989 on request of the *World Meteorological Organization* (WMO). It is operated by the *Deutscher Wetterdienst* (DWD, National Meteorological Service of Germany) as a German contribution to the *World Climate Research Programme* (WCRP). Mandate of GPCC is the global analysis of monthly precipitation on earth's landsurface based on *in situ* rain-gauge data. Since its start, the centre is the *in situ* component of the WCRP *Global Precipitation Climatology Project* (GPCP).

The GPCC is based on the estimate of a precipitation mean climatology

and of the anomalies from it, then assumed as climatological "normals". The *Precipitation Climatology* dataset focus on the period 1951-2000 and consists of data from around 50,650 stations (see figure 1.11). This climatology comprises normals collected by WMO, delivered by the countries to GPCC or calculated from time-series of monthly data (with at least 10 complete years of data). In case that time series of sufficient length (more than 40 years) for the period 1951-2000 were not available from a specific station, then climatological normals have also been calculated for 30-year reference periods 1961-1990, 1951-1980 or 1971-2000 with at least 20 years of data. If even this was not possible for a station, then normals have been calculated for the period 1931-1960, or for any other period with at least 10 complete years of data. Given the *Precipitation Climatology* background, a *First Guess* product and a *Monitoring* product are produced. Moreover a *Full Data Reanalysis* dataset and the *Variability Analysis of Surface Climate Observations* (VASClimO) dataset are produced using particular data treatment and quality procedures. These monthly precipitation analysis prod-

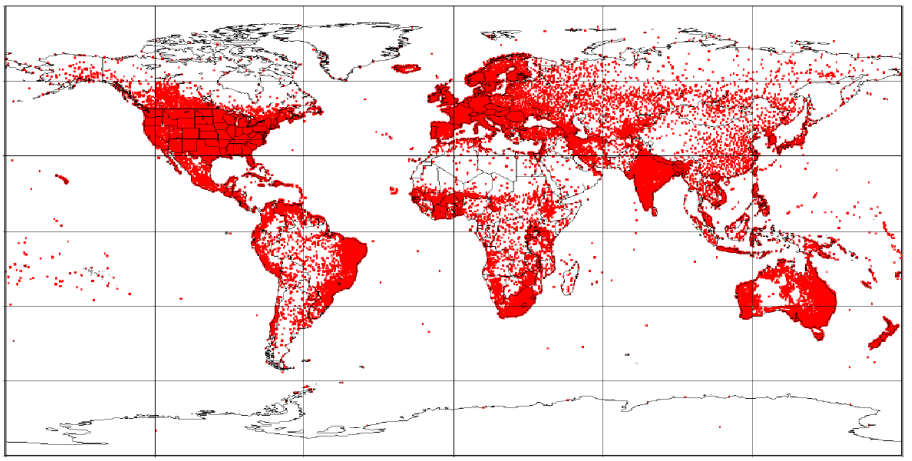

Figure 1.11: Location of the globally distributed stations featuring measurement periods longer than 10 years within the GPCC database.

ucts (except *VASClimO* dataset) are based on anomalies from climatological normals at the stations, or where no station normal is available, from GPCC's high resolution gridded climatology. The anomalies are spatially interpolated by the analysis method SPHEREMAP that is a variant of the spherical-coordinate adaptation of Shepard's method, (Wilmott *et al.*, 1985) and, for the *Monitor-*

ing and *Full Data Reanalysis* products, the gridded anomaly analyses are then superimposed on GPCC's background climatology.

In particular, the *First Guess* product of the monthly precipitation anomaly is based on interpolated precipitation anomalies from more than 6,000 stations worldwide. Data sources are synoptic weather observation data (SYNOP) received at DWD via the WMO *Global Telecommunication System* (GTS) and climatic mean (mainly 1951-2000, or other reference periods as described before) monthly precipitation totals at the same stations extracted from GPCC's global normals collection. An automatic-only quality-control (QC) is applied to these data. Since September 2003, GPCC *First Guess* monthly precipitation analyses are available within 5 days after end of an observation month. Main application purpose is to serve as input for near-realtime drought monitoring applications.

The *Monitoring* product of monthly precipitation for global climate monitoring is based on synoptic weather observation data and monthly climatological reports received near-realtime via GTS from ca. 7,000 8,000 stations (after a high level quality control procedure) and is available within about 2 months after observation month. This is the GPCC product with the longest history: Operational monthly analysis started with year 1986 and has continuously been done every month since then. The analyses are based on automatic and intensive manual quality control of the input data. The GPCC Monitoring Product is the *in situ* component of the satellite-gauge combined precipitation analyses of GPCP (Huffman *et al.*, 1997; Adler *et al.*, 2003) and CMAP (Xie and Arkin, 1996b, 1997). It also supports regional climate monitoring.

The *Full Data Reanalysis* product is much higher accurate than compared with the GPCC near real-time products mentioned above. Therefore, its application is recommended for hydrometeorological model verification and water cycle studies. This analysis product is based on all stations, near real-time and non real-time, in the GPCC data base supplying data for the individual month. The data coverage per month varies from less than 10,000 to more than 45,000.

The *VASClimO 50-Year* dataset supplies gridded time-series of monthly precipitation for climate variability and trend studies. It is based on data being selected with respect to a complete temporal data coverage and homogeneity of the time-series. A general description of the GPCC data processing and analysis system is given by Rudolf (1993).

Beyond GPCC, other rain gauge datasets considered for climatological purposes and used within the GPCP (see section 1.5) are the *Global Historical Climate Network* (GHCN), operated by NOAA/NCDC (*National Climate Data Center*) and the *Climate Assessment and Monitoring System* (CAMS) operated

by the CPC/NCEP (*Climate Prediction Center, National Centers for Environmental Prediction*) and NOAA.

1.4 Satellite blended techniques

1.4.1 TMPA/TMPA-RT

In TMPA-RT/TMPA systems (Huffman *et al.*, 2007), precipitation related passive microwave data are collected by a variety of LEO satellites, including the TMI on TRMM, SSM/I on DMSP, AMSR-E on Aqua and AMSU-B on NOAA satellite series. Passive microwave fields of view (FOVs) from TMI, AMSR-E, and SSM/I are converted to precipitation estimates at the *TRMM Science Data and Information System* (TSDIS) with sensor-specific versions of the *Goddard Profiling Algorithm* (GPROF; Kummerow *et al.*, 1996); Olson *et al.* (1999) provide information about subsequent use of GPROF in the TMPA.

Passive microwave FOVs from AMSU-B are converted to precipitation estimates at the *National Environmental Satellite, Data, and Information Service* (NESDIS) with operational versions of the Zhao and Weng (2002) and Weng *et al.* (2003) algorithm. Ice water path (IWP) is computed from the 89- and 150-GHz channels, with a surface screening that employs ancillary data. Precipitation rate is then computed based on the IWP and precipitation rate relationships derived from cloud-model data computed with the fifth generation *Pennsylvania State University-National Center for Atmospheric Research* (Penn State-NCAR) *Mesoscale Model* (MM5). The AMSU-B algorithm can discriminate between precipitating and non-precipitating ice-bearing clouds but cannot provide information on precipitation systems that lack the ice phase. The multichannel conically scanning passive microwave sensors (TMI, AMSR-E, SSM/I) have a similar limitation over land, so the AMSU-B estimates are roughly comparable. However, over ocean the conical scanners also sense liquid hydrometeors, providing additional sensitivity, including the precipitation from clouds that lack the ice phase. As a result, the AMSU-B estimates are relatively less capable in detecting precipitation over ocean. The lack of the lightest rain occurs in all ocean areas, but it is most important in the subtropical area, where all of the rain events are light. A second issue in the current AMSU-B algorithm is that it neglects calibration differences across the swath due to variations in the size of individual FOVs. This variation introduces unphysical variability into the resulting AMSU-B estimates that must be corrected in a future release (Joyce and Ferraro, 2006).

The second major data source for the TMPA is the window-channel (10.7 μ) IR data that are being collected by the international constellation of GEO satellites. In contrast to the sparse temporal sampling of the passive microwave data, the GEO-IR data provide excellent time-space coverage. The CPC office at the *NOAA/National Weather Service* (NWS) merges the international complement of GEO-IR data into half-hourly 4x4 km equivalent latitude-longitude grids (hereafter the "CPC merged IR") (Janowiak *et al.*, 2001). The IR brightness temperatures, T_b, are corrected for zenith angle viewing effects and intersatellite calibration differences. For TMPA research estimates generated prior to the start of the CPC merged IR dataset in early 2000 (see figure 1.12), a GPCP dataset (also produced at CPC) that contains 24-class histograms of GEO-IR T_b data on a 3-hourly, 1^o x 1^o latitude-longitude grid covering the latitude band 401^oN-S (hereafter the "GPCP IR histograms") (Huffman *et al.*, 2001) is used. This dataset also includes grid-box-average *GOES Precipitation Index* (GPI) (Arkin and Meisner, 1987) estimates computed from LEO-IR data recorded by the NOAA satellite series. These LEO-GPI data are used in the TMPA to fill gaps in the GEO-IR coverage, most notably in the Indian Ocean sector, where there was no GEO-IR coverage before Meteorological Satellite 5 (Meteosat-5) began providing observations there in June 1998. All IR-based precipitation estimates share the limitation that the T_b's primarily correspond to cloud-top temperature, and implicitly cloud height. Arkin and Meisner (1987) showed that such information is poorly correlated to precipitation at fine time/space scales but is relatively well correlated at scales larger than about 1 day and 2.5^o x 2.5^o of latitude-longitude. Finally, the research TMPA also makes use of three additional data sources: the *TRMM Combined Instrument* (TCI) estimate, which employs data from both TMI and PR as a source of calibration (TRMM product 2B31; Haddad *et al.*, 1997a,b); the GPCP monthly rain gauge analysis developed by the *Global Precipitation Climatological Center* (GPCC, see section 1.5); and the *Climate Assessment and Monitoring System* (CAMS) monthly rain gauge analysis developed by NOAA/CPC (Xie and Arkin, 1996a). During the early TMPA design work, the authors realized that they could obtain (restricted) access to the requisite microwave and IR data within a few hours of observation time. "Real time" (or more strictly, near-real time) production makes the estimates useful to several new classes of users. At the same time, experience indicated that bias adjustments based on monthly gauge data materially improve the accuracy of the estimates (Huffman *et al.*, 1995). These considerations led to the two-track approach of computing both real-time (RT) and research products. In the following paragraphs the research product approach is described, then the necessary changes that distinguish the RT algorithm are

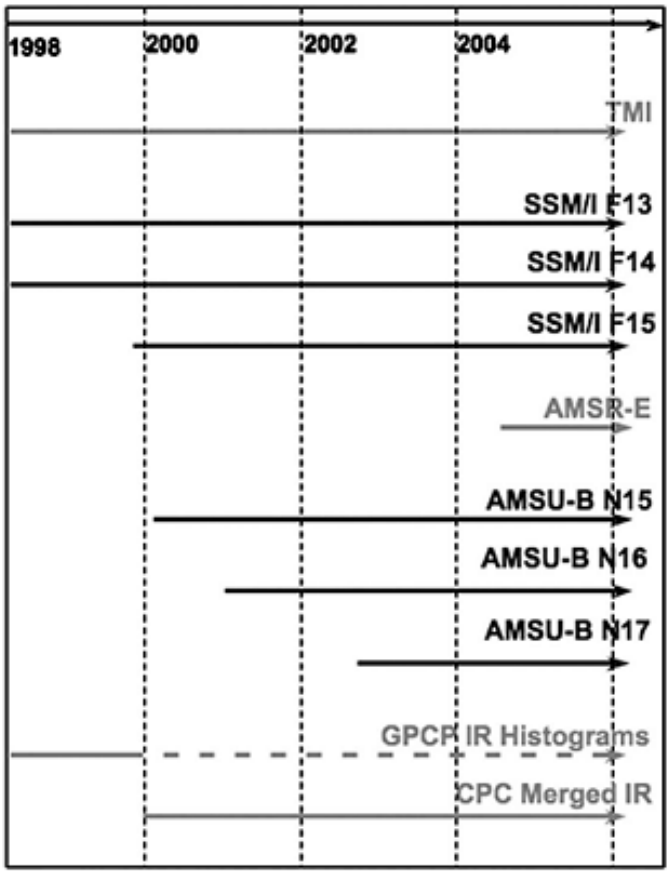

Figure 1.12: Data availability during the TRMM era for satellite sensors used in the TMPA. Solid lines denote periods where the data are used in the research product, and dashing indicates they are available but not used (Huffman *et al.*, 2007)

.

introduced.

The TMPA estimates are produced in four stages: 1) the microwave precipitation estimates are calibrated and combined, 2) infrared precipitation estimates are created using the calibrated microwave precipitation, 3) the microwave and IR estimates are combined, and 4) rain gauge data are incorporated. Figure 1.13 presents a block diagram of the TMPA estimation procedure. Each TMPA precipitation field is best interpreted as the precipitation rate effective at the nominal observation time.

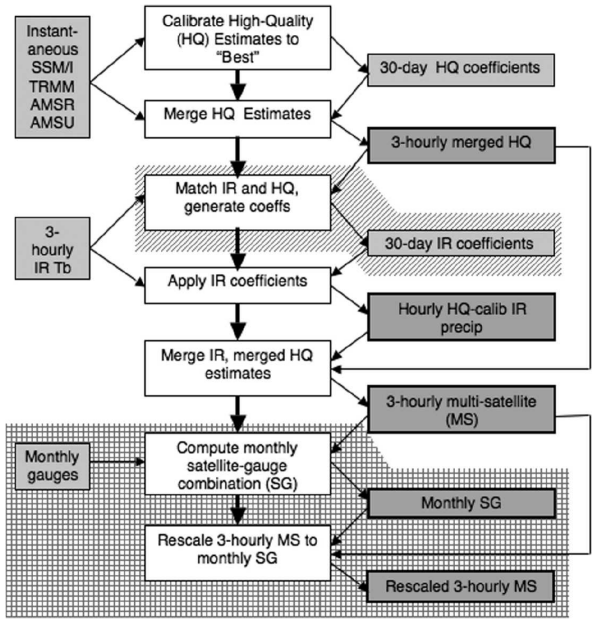

Figure 1.13: Block diagram for both the RT and research product algorithms, showing input data (left side), processing (center), output data (right side), data flow (thin arrows), and processing control (thick arrows). The items on the slanted shading run asynchronously for the RT algorithm, and the items on the grid shading are only performed for the research product. Best in the top center shaded box is the TMI—GPROF precipitation estimate for the RT algorithm and the TMI–PR combined algorithm precipitation estimate for the research product (Huffman *et al.*, 2007).

1. **High Quality (HQ) microwave estimates**
   All of the passive microwave data are converted to precipitation estimates and averaged to the 0.25^o spatial grid over the time range ± 90 minutes from the nominal 3-hourly observation time. The gridded estimates are adjusted to a "best" estimate using probability matching (Miller, 1972). The calibrating data source for the post-real-time TMPA is the TCI. Since the TCI only occasionally intersects any of the sensors other than TMI, a TCI-TMI is computed and then applied to TMI-calibrated values of the other sensors to estimate the TCI-calibrated values. Preliminary work showed that the TMI calibrations of the other sensors' estimates are adequately represented by climatologically based coefficients representing large zonal bands for ocean and single calibrations for land (for each sensor). The calibrations are computed for a month of match-ups to ensure stability and representativeness, except the TMI-AMSR-E calibration requires 2 months of data to meet these goals. The calibration month in the post-real-time system is a calendar month. In the event of multiple overpasses covering a HQ (high quality) grid box in a 3-h interval, data from TCI and TCI-adjusted TMI, AMSR-E, and SSM/I are averaged together, while TCI-adjusted AMSU-B estimates are used if no other microwave estimate is available.

2. **Variable Rain Rate (VAR) IR estimates**
   As shown in Table 1.4, the post-real-time TMPA uses two different IR datasets. Before 7 February 2000, each grid box's histogram in the 1^o x 1^o 3-hourly GPCP IR histogram dataset is averaged to a single value for the grid box, and plane-fit interpolated to the 0.25^o grid. Thereafter, the CPC Merged IR is averaged from its native 4 x 4 km^2-equivalent to 0.25^o resolution and combined into hourly files as $\pm$ 30 min. from the nominal time. Histograms of time-space matched HQ precipitation rates and IR T_b's are accumulated for a calendar month, and then probability matched to create spatially varying T_b rain-rate look-up tables that are applied to that month of IR data. There is no precipitation when the 0.25^o x 0.25^o-average T_b is greater than the local rain-no rain threshold value, while colder T_b's are assigned larger precipitation rates. The highest rain/lowest T_b calibration tends to fluctuate unphysically, so a climatological fitted curve is substituted for the coldest 0.17% of the T_b-precipitation rate curve. Once computed, the HQ-IR calibration coefficients are applied to each 3-h interval IR dataset during the calendar month.

3. **Combined HQ and VAR estimates**

Table 1.4: Summary of input datasets used in the TMPA. The shaded entries are only used in the post-real-time product. All others appear in both the real-time (perhaps for only part of the record) and the post-real-time. A space scale of pixel indicates that the data are accessed at the native resolution of the original pixels, while a time scale of swath indicates that the values are instantaneous and observed at times that depend on location and orbit geometry.

Algorithm	*Input data*	*Space scale*	*Time scale*	*Areal coverage*	*Time coverage*
GPCC gauge analysis	$\sim$ 6500 surface stations	1^o	Monthly	Global land	1998-present
CAMS gauge analysis	$\sim$ 6500 surface stations	0.5^o	Monthly	Global land	1998-present
TRMM Combined Instruments	TRMM PR and TMI	Pixel	Swath	Global land	1998-present
GPROF	TMI	Pixel	Swath	40^oN-40^oS	1998-present
	SSM/I	Pixel	Swath	70^oN-70^oS	1998-present
	AMSR-E	Pixel	Swath	70^oN-70^oS	June 2003-present
NESDIS High Frequency	AMSU-B	Pixel	Swath	Global	January 2007-present
VAR	all GEO and LEO IR T_b's	1^o	3 hour	40^oN-40^oS	1998-6 Feb. 2000
	all GEO IR T_b's	4 km	30 min	60^oN-60^oS	7 Feb. 2000-present

This product is intended to provide the "best" estimate of precipitation in each grid box at each observation time. Combining data is relatively easy for passive microwave estimates because the sensors are quite similar and GPROF is used for most retrievals, but it is much harder for the HQ and VAR fields. Currently the HQ estimates are used wherever they exist, and then the remaining grid boxes are populated with VAR estimates. The resulting data fields have a mix of statistical properties, so users for whom homogeneous statistics are important may choose to work with the HQ or VAR estimates alone.

4. **Rescaling to monthly data**
The last stage in the post-real-time TMPA is to compute the satellite-gauge adjustment and then rescale the individual 3-hourly grids to sum to the monthly value. Experience shows that sub-monthly accumulations

of gauge data are not reported with sufficient density to warrant direct inclusion in a global algorithm that provides sub-monthly resolution. This issue was solved in the sub-monthly GPCP datasets by scaling the short-period estimates to sum to a monthly estimate that includes monthly gauge data. All of the individual HQ+VAR fields are summed over a calendar month to create a monthly multi-satellite (MS) field. The MS and gauge fields are combined as in Huffman *et al.* (1997) to create a post-real-time monthly satellite-gauge combination, which is a TRMM product in its own right (3B43 in Version 6). Then the field of satellite-gauge/MS ratios is computed and used to scale each 3-hourly HQ+VAR field in the month.

5. **RT algorithm adjustments**
   The real-time and post-real-time systems are designed to be as similar as possible; however, a real-time system cannot reach into the future, so the calibration month is taken as a trailing accumulation of approximately 6 pentads. Through 2004, new coefficients were computed at the end of each pentad, but thereafter the coefficients were recomputed every three hours to better represent heavy-rain outbreaks. A second important difference is the choice of calibrator for the HQ field; the TMI precipitation is used in the real-time because the TCI is only computed after real-time. Finally, there is not sufficient gauge data to drive a MS-gauge combination in the RT system.

1.4.2 CMORPH

The *Climate Prediction Center* CPC *Morphing*, (Joyce *et al.*, 2004) method makes use of the availability of global half-hourly IR data as a means to propagate PMW derived precipitation, producing spatially and temporally complete global precipitation analyses. Since the IR data provide good measurements of cloud top properties, IR data can be used to detect cloud system movements. A system known as WINDCO was developed to detect and estimate cloud motions from geostationary satellites (Smith and Philips, 1972). The first phase of the WINDCO program used an automated process that selects cloud targets that are either the coldest clouds or near regions where the IR gradient is strong (Herman, 1992). Dills and Smith (1992) devised a specialized cloud relative motion tracking technique using geostationary IR and visible data. The purpose for computing cloud system advection vectors (CSAVs) for this project is to propagate PMW derived global rainfall each half hour. This requires total

automation, and precludes the use of visible imagery.

Information about collection and organization of IR data, PMW data and related rainfall estimation algorithms, are not reported here and in the following blended techniques paragraphs, since they do not differ from those reported on the TMPA/TMPA-RT paragraph.

The direction and speed of cloud tops as detected by satellite IR may not always correlate well with the propagation of the lower precipitating layer of the system. An optimal spatial lag correlation scale would be large enough to include the sharp contrast of the cloud shield edges with the earth's surface thus helping to focus on the motion of the entire cloud system. However, if the spatial resolution is too large, the resulting CSAV information may miss the variability of the steering currents that provide propagation of cloud system complexes. After various tests it was concluded that spatially lagging overlapping 5^o latitude/longitude IR regions centered at 2.5^o latitude/longitude intervals provide a good measure of the movement of entire cloud systems while capturing the bulk of variations in the steering currents. More details on deriving CSAVs for use in CMORPH can be found in Joyce *et al.* (2004).

Early versions of CMORPH used CSAVs directly to propagate PMW derived precipitation. However, it was soon determined that the west to east and south to north advection rates were too fast in the North Hemisphere mid-latitudes. To correct this, a speed adjustment procedure was developed by first computing rainfall advection vectors by spatially lagging hourly U.S. NEXRAD Stage II (Klazura and Imy, 1993) radar rainfall (mapped to the same 8-km grid) in the exact same dimensions and manner CSAVs are computed from IR. The frequency distribution of hourly CSAV and radar rainfall advection rates indicated that north to south rates are quite similar but that west to east CSAV speeds were about twice as fast compared to the radar-derived vectors, and south to north rates were 3-4 times faster. These systematic differences are consistent with several case studies that show the tendency of IR features to quickly stream to the north-east on the east side of long wave troughs with the actual rainfall also moving in this direction but at a slower rate. The incorporation of this adjustment procedure into the CMORPH processing has resulted in improved propagation of precipitation features. For consistency with the North Hemisphere, the meridional adjustment is applied to vectors of the opposite sign in the South Hemisphere in order to reduce the same long wave trough effect. Further tests have shown that there is scant seasonal dependence in the relationship between the IR-derived and radar derived advection vectors.

The PMW rainfall propagation process begins by spatially propagating initial fields of 8-km half-hourly instantaneous PMW analysis estimates (t + 0

h) forward in time, by the discrete distance of the corresponding zonal and meridional vectors. Two auxiliary fields that are maintained along with each precipitation estimate are: (1) time stamp (t = 0 for instantaneous) in which the units represent the time, in half-hourly increments, since the scan of the PMW satellite overpass used to define that pixel and (2) satellite identification. All PMW satellite pixels (including those with zero precipitation) within each 2.5^o latitude/longitude region are propagated in the same direction and distance to produce the analysis for the next half hour (t + 0.5 h). Finally, if a PMW-derived precipitation estimate from a new scan at "t + 0.5 h" is available at a particular pixel location, then that estimate overwrites the propagated estimate and the associated time stamp for that pixel is set to a value of zero. Otherwise, the time stamp is incremented by a value of "1". This entire process is repeated each half hour. The propagation process is graphically illustrated in figure 1.14. An initial 0330 GMT time analysis of instantaneous ("t = 0 h") PMW rainfall (figure 1.14a, leftmost plot) is propagated forward to produce analyses at "t = 0.5 h" and "t + 1 h" (figure 1.14a) using the IR-derived propagation vectors. This analysis is actually propagated one more time step to "t + 1.5 h" (not shown), but in this case all values are overwritten by precipitation estimates from an updated PMW scan (figure 1.14a, rightmost plot) that became available at the "t + 1.5 h" time step (0500 GMT). The continuity of the propagated rainfall clusters in the "t + 0.5 h" and "t + 1.0 h" fields can be appreciated by comparing them with the updated PMW analysis (figure 1.14a, rightmost plot).

In addition to propagating rainfall estimates forward in time, a completely separate process is invoked in which instantaneous rainfall analyses are spatially propagated backward in time using the same propagation vectors used in the forward propagation, except for reversing the sign of those vectors. The results are stored separately from those computed in the forward propagation process. Thus for the above example, the "t = 1.5 h" updated observed PMW precipitation (figure 1.14b, rightmost plot) is propagated backwards to the "t = 0 h" time frame (Figure 2b, leftmost plot). When all propagated fields have been computed, the "t = 0 h" analysis that contains observed data overwrites the propagated estimates for that time stamp. By propagating the rainfall analyses temporally in both directions, the propagation speed and direction is improved over doing this in a single direction (in time) only. To this point only forward/backward propagation of initial/updated PMW derived rainfall patterns, when and where PMW data are not available, has been shown. Changes in the intensity and shape of the rainfall features are accomplished by inversely weighting both forward and backward propagated rainfall by the respective temporal distance from the initial and updated observed analyses. This process is re-

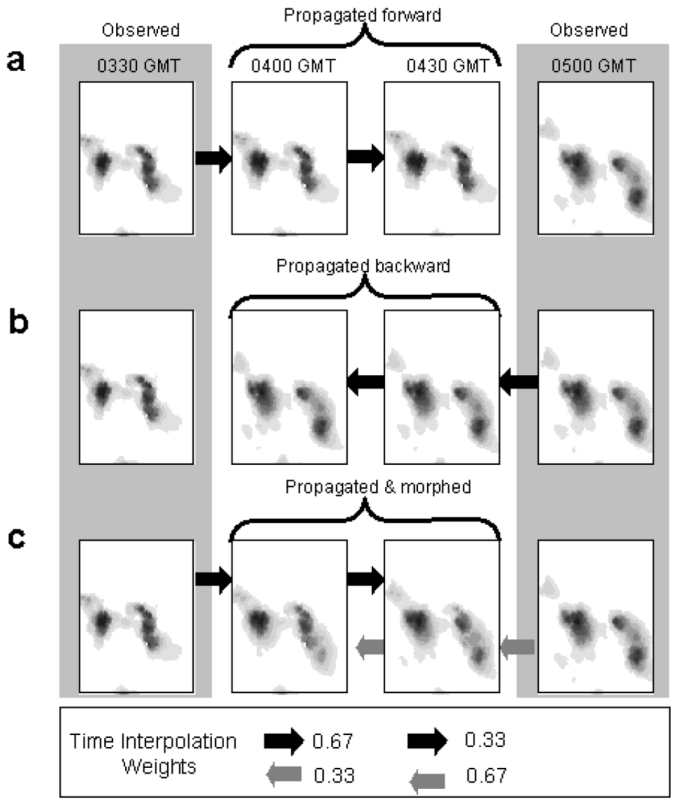

Figure 1.14: Depiction of the propagation and morphing process for a region in the South Pacific. The analyses at 0330 UTC and 0500 UTC are actual passive microwave estimates, i.e., no propagation or morphing has been applied to these data. The 0400 UTC and 0430 UTC are: (a) propagated forward in time, (b) propagated backward in time, and (c) propagated and morphed.

ferred here as "morphing", and it is representted graphically in figure 1.14c. At each pixel location, the process by which the 0400 UTC (t + 1/2 h) estimate is produced (figure 1.14c, second plot from the left) involves creating a weighted mean as follows:

$$P_{morph(t+1/2hr)} = 0.67 \cdot P_{forward(t+1/2hr)} + 0.33 \cdot P_{backward(t+1/2hr)}$$

where $P_{forward}$ is the PMW rainfall estimate forward propagated from initial scan (0330 UTC) and $P_{backward}$ is the PMW rainfall estimate backward propagated from updated scan (0500 UTC). Similarly, the CMORPH value for the 0430 GMT analysis is computed as:

$$P_{morph(t+1hr)} = 0.33 \cdot P_{forward(t+1hr)} + 0.67 \cdot P_{backward(t+1hr)}$$

Each CMORPH estimate's associated time stamp and satellite identification are extracted from the propagated estimate (forward or backward) with the smallest time stamp. For CMORPH derived from instantaneous PMW information, time stamp = 0.

1.4.3 PERSIANN

The development of the *Precipitation Estimation from Remotely Sensed Information using Artificial Neural Networks*, (PERSIANN Hsu *et al.*, 1997; Sorooshian *et al.*, 2000) is based on the more reliable but less frequently sampled instantaneous precipitation rate from microwave sensors to adjust the mapping function of the infrared image of GEO satellites and rainfall rate. The input features of PERSIANN are extracted from the local image texture of the longwave IR imagery (10.2-11.2 μ) of GEO satellites. The mapping function of ANN using IR image to the rainfall map is implemented through these steps:

1. extracting the local image texture, in terms of calculating the mean and variance of IR brightness temperature (T_b) near the calculation pixel;

2. classifying the extracted feature;

3. multivariate mapping of classified texture to the surface rainfall rate.

An adaptive training feature facilitates updating of the network parameters whenever independent estimates of rainfall are available (Hsu *et al.*, 1997; Sorooshian *et al.*, 2000). The parameters of PERSIANN are constantly updated when PMW-based rainfalls are available. The system first used GEO-IR

imagery. It was later extended to use both GEO-IR and VIS imagery and found that the rainfall estimates were improved (Hsu *et al.*, 1999).

The PERSIANN algorithm estimates rainfall rate at each $0.25^o \times 0.25^o$ pixel of every 30 minutes. The estimated rainfall is then integrated to various spatial and temporal scales, such as six-hour, daily, monthly, etc. In the operation of PERSIANN, two PERSIANN algorithms are running in parallel: one is run in the simulation mode and the other in the update mode. The simulation mode generates the surface rain rate at the $0.25^o \times 0.25^o$ resolution at every 30 minutes from the GEO satellites infrared images, while the update mode continuously adjusts the mapping function parameters of PERSIANN based on the fitting error of any pixel for which a PMW instantaneous rainfall estimate is available. The simulation mode generates the regular rainfall rate output, and the update mode improves the quality of the product. The accuracy of the final product, however, depends on many factors, such as the effectiveness of the input feature detection and classification scheme, the accuracy of the individual input-output mapping functions, and the accuracy and frequency of the PMW rainfall estimates used for updating (Sorooshian *et al.*, 2000). Description of the current operation of PERSIANN is listed in figure 1.15. IR imagery is provided by GEO satellites, such as GOES-8, GOES-10, GMS-5, and MeteoSat-6&7 (Janowiak *et al.*, 2001), while PMW rainfall is calculated from the information provided by TRMM, NOAA- 15, -16, -17, DMSP F-13, F-14, and F-15 satellites (Ferraro and Marks, 1995; Kummerow *et al.*, 1998) is used to train the mapping parameters of PERSIANN.

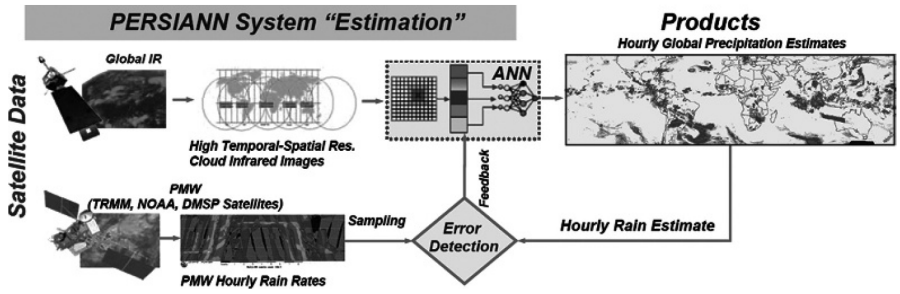

Figure 1.15: PERSIANN scheme (Hsu and Sorooshian, 2008).

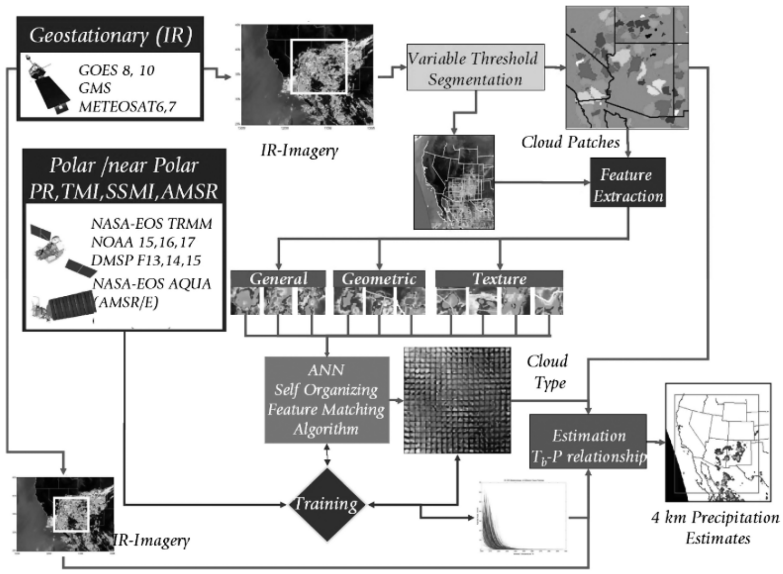

Figure 1.16: PERSIANN-CCS scheme (Hsu and Sorooshian, 2008).

1.4.4 PERSIANN-CCS

A development of the PERSIANN system is to extend the classification features of the GEO-IR image from local texture-based to the cloud patch-based features and to improve the resolution of the retrieved product from lower-resolution of $0.25^o \times 0.25^o$ lat-lon scale to finer resolution of $0.04^o \times 0.04^o$. The designed patch-based algorithm is named as *PERSIANN Cloud-patch Classification* (PERSIANN-CCS, figure 1.16) system (Hong *et al.*, 2004). The PERSIANN-CCS consists of four major steps:

1. IR cloud image segmentation;
2. feature extraction from IR cloud patches;
3. patch feature classification;
4. rainfall estimation.

These image processing and computation steps, briefly discussed below, can be found in Hong *et al.* (2004) and Hsu *et al.* (1997). Those four steps are brief

listed below:

1. *Cloud image segmentation*: cloud segmentation is operated through a process that may eventually divide the image into separable patches. This is operated through a watershed-based segmentation approach (Vincent and Soille, 1991). The algorithm starts with finding the local minima temperature of the IR cloud map, followed by raising the IR temperature gradually and connecting the neighborhood pixels attracted to a same local minimum pixel until all the local minimum basins are separated into distinct patches.

2. *Feature extraction*: the selected patch features are separated into three categories-coldness, geometry, and texture. From these categories we extract representative features such as the cloud height (coldest temperature), cloud size and shape, surface textures, and surface gradients in our study. In addition, all the relevant features are extracted from three temperature threshold levels (220K, 235K, and 253K).

3. *Feature classification*: clustering is proceeded based on the similarities of patches measured in their feature spaces. An unsupervised clustering method, Self-Organizing Feature Map (SOFM), is used to classify patch features into a number of cloud patch categories (Kohonen, 1995; Hsu *et al.*, 1999). After training, cloud patches with similar input features are assigned to a same category. An array of 20x20 (i.e. 400) groups was assigned to the classification category. Cloud patches with similar features are grouped together in the same category or assigned to the neighborhood categories.

4. *Specification of patch rainfall distribution*: the final stage is to specify rainfall distribution to the classified cloud patch categories. At this stage, a large amount of GEO satellite IR image and surface rainfall data is needed. One year of radar (over the continental US) and PMW rainfall estimates of LEO satellites (Ferraro and Marks, 1995; Kummerow *et al.*, 1998) is used to build the rainfall distributions of the classified patch group. The *Probability Matching Method* (PMM) (Atlas *et al.*, 1990; Rosenfeld *et al.*, 1994) was used to match the relationship between the GEO IR temperature and the hourly rainfall rate in each classified IR patch group, with the assumption that the higher rainfall rate is associated with the lower IR temperature. Finally the T_b-R relationship is fitted by an exponential function of five parameters, where parameters were found from the SCEUA optimization algorithm (Duan *et al.*, 1992).

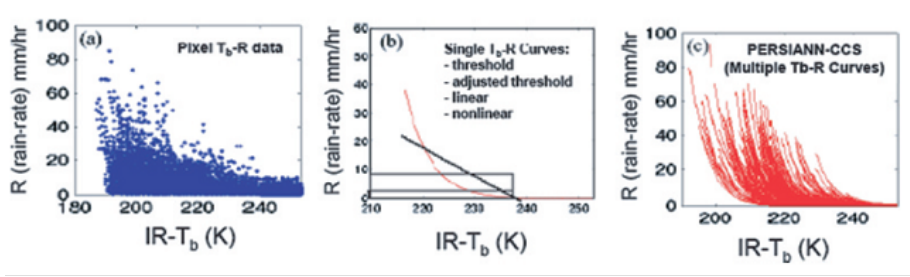

Figure 1.17: (a) scatterplot of Tb-R relationship, (b) fitting Tb-R from one-single function, and (c) fitting Tb-R using multiple fitting functions (PERSIANN-CCS) (Hsu and Sorooshian, 2008).

Figure 1.17 shows the fitting of the IR brightness temperature (T_b) to the rainfall rate from one-single function and multiple function (PERSIANN-CCS) approaches. The scatterplot of the GEO-IR image and radar rainfall (figure 1.17a) shows that the T_b-R relationship is quite wide spread, which cannot be well fitted by a single polynomial curve (figure 1.17b). Instead of fitting through one single fitting function, approaches were developed to use limited PMW rainfall to correct the T_b-R relationship. Although the results show improvement over those unadjusted estimates, the effectiveness of the algorithms, however, largely relied on the blending procedures to modify the mapping function spatially and temporally. PERSIANN-CCS, on the other hand, creates a large amount of fitting curve to generate rainfall rates from IR image (figure 1.17c). With distinguishable features based on IR cloud coldness, size, and textures, each classified cloud patch is assigned a specific T_b-R curve. In the case study, 400 classifications were assigned and therefore multiple T_b-R curves were used to the fitting of the scatter points in figure 1.17a. Compared to other fittings using one-single function, PERSIANN-CCS gives great potential to provide improved estimates.

1.4.5 PERSIANN Adjusted

PERSIANN bias adjusted (PERSIANN-adj) product is obtained by computing a correction factor α as the ratio of GPCP rainfall and PERSIANN rainfall at 2.5^o grids at monthly scale. The monthly bias is then spatially downscaled and removed from PERSIANN 0.25^o resolution estimates using the correction factor α. GPCP monthly rainfall inherently considers gauge measurement and several

satellite-based rainfall and model estimates (Adler *et al.*, 2003). PERSIANN-adj maintains total monthly precipitation estimate of GPCP, while retains the spatial and temporal details made available through PERSIANN estimate (0.25^o lat/long and hourly). The hourly 0.25^o lat/long PERSIANN-adj data together with the listed satellite and multi-sensor precipitation products are integrated from their original resolution onto a common 6-h and monthly 0.25^o x 0.25^o resolution to be used in the study time scales.

1.4.6 Other blended techniques

The possibility to merge LEO-PMW and GEO-IR data has been exploited by a number of algorithms that have not been used in the analyses that are exposed in the next chapters. Brief descriptions of these methods are reported to have a complete reference framework of blended techniques methods.

NRL blended techniques The *Naval Research Laboratory* blended technique(Turk and Miller, 2005) is based upon an adaptive analysis of temporally and spatially matched pixels from all available GEO VIS/IR and PMW observations, and TRMM PR (2A25) data (Turk *et al.*, 2009). The NRL technique has three stages: collocation of GEO VIS/IR and LEO-PMW data to build 2^ox2^o lookup tables of IR-T_b to PMW rain rates; conversion of IR data into instantaneous rain rates via lookup table and finally updating of accumulations for each 3-h period. Additional corrections are applied based upon model-generated wind vectors for upslope and downslope orographic effects and growth/decay of the clouds based upon the changes in the IR-T_b, are used to intensify or lighten the rain rates (Vicente *et al.*, 2002). The baseline product is a global (60^oN to 60^oS latitude) map of 3-h accumulated precipitation, starting in mid-2000 and updated every 3 h.

SCaMPR The *Self-Calibrating Multivariate Precipitation Retrieval* algorithm (Kuligowski, 2002) is self calibrating as it routinely updates the relationship between the predictor (GOES IR brightness temperatures and rain-rate estimates) and target values (SSM/I rain-rate estimates) using recent data and then applies that calibration to subsequent data for a short period of time. The algorithm consists of two parts. First, from a set of 12 available screening parameters, the optimal parameter for separating raining from nonraining pixels (as defined by the SSM/I estimates) is determined, along with the optimal value of the screening parameter. Second, from a set of 16 available amount predictors (one half of which are nonlinear transformations of the first nine), the

best amount predictor for the raining pixels is selected via forward-screening regression.

GSMaP The *Global Satellite Mapping of Precipitation* (Kubota *et al.*, 2007) product combines precipitation estimates from the TMI, AMSR and SSM/I together with those derived from geostationary IR data. The technique provides a number of different combination procedures; the MWR version generates cloud motion vectors from the GEO IR data and morphs the PMW rainfall where PMW overpasses are not present; the MVK version uses a Kalman filter approach to generate precipitation estimates in PMW voids. Comparison of the results against surface radar shows correlations of $\sim$0.8 and low RMSE_s. Product generation is at a nominal 0.1^o resolution every 30 min. The latitude band covered is 60^oN to 60^oS for recent time periods that vary by product. Fully global precipitation products are also available at somewhat coarser time/space resolutions, implicitly aimed at more climate applications.

MICRA The *Microwave Infrared Combined Rainfall Algorithm* (Marzano *et al.*, 2004) is a statistical integration method using the satellite microwave-based rain rate estimates, assumed to be accurate enough, to calibrate spaceborne infrared measurements on sufficiently limited subregions and time windows. The proposed methodology is focused on new statistical technique, namely the *multivariate probability matching* (MPM), aimed at employing both average and texture information as well as multispectral data.

A Neural NetworksBased Fusion Technique to Estimate Half-Hourly Rainfall Estimates from Satellite Passive Microwave and Infrared Data Tapiador *et al.* (2004) developed an algorithm based upon PMW and IR fusion by means of an Artificial Neural Network evaluated among different algorithms and configurations.

PMIR The *Passive Microwave-InfraRed* (Kidd *et al.*, 2003; Kidd and Muller, 2009) technique was devised to combine the information from the PMW and IR datasets through local calibration of the IR Tbs The technique uses data from the SSM/I instrument to derive rain rates from a frequency difference algorithm tuned to surface datasets and the TRMM PR. Co-located and co-temporal IR-T_bs and PMW observations are entered into a data base for each $1^o \times 1^o$ gridbox globally, from which cumulative distribution histograms are generated which map the IR T_b on to the PMW rain rates. The histograms

are updated through a temporal/spatial inverse weighting function in one of two ways: a 'climatological' mode where data up to 5 days either side of the current day are used, and a 'real time' mode where only the previous 5 days data are used. Precipitation products are generated at a nominal 12 km, 30 min resolution.

MIRA In the *Microwave/Infrared Rainfall Algorithm* (Todd *et al.*, 2001), rainfall estimates are produced at the high spatial resolution and temporal frequency of the IR data using rainfall information from the PMW data. An IR T_b-rain rate relationship, variable in space and time, is derived from coincident observations of IR-T_b and PMW rain rate (accumulated over a calibration domain) using the probability matching method. The IR-T_b-rain rate relationship is then applied to IR imagery at full temporal resolution.

LMODEL The model (Bellerby *et al.*, 2009) uses single-band thermal infrared geostationary satellite imagery to characterize cloud motion, growth, and dispersal at high spatial resolution (4 km). These inputs drive a simple, linear, semi-Lagrangian, conceptual cloud mass balance model, incorporating separate representations of convective and stratiform processes. The model is locally updated against microwave satellite data using a two-stage process that scales precipitable water fluxes into the model and then updates model states using Kalman filter. Model calibration and updating employ an empirical rainfall collocation methodology designed to compensate for the effects of measurement time difference, geolocation error, cloud parallax, and rainfall shear.

1.5 The Global Precipitation Climatology Project (GPCP) dataset

When the availability latency time needed to use precipitation data, is not a constrain of the analysis that is being carried out, it can result useful merging satellite data with ground based sources, then producing a more robust precipitation dataset. In particular it can be assumed that such a dataset results having bias error reduced to that of the ground based network used and it is able to reproduce worldwide precipitation patterns at typical climatological spatial and temporal resolutions. Then the most important case of such applications are those inherent the climatology in which precipitation is of fundamental importance given its role in the hydrologic balance on global scale, the

associated latent heating and potentiality on improving climate forecast models. The GPCP represents the effort produced by the *World Climate Research Programme* WCRP *Global Energy and Water Cycle Experiment* GEWEX project to realize a community analyses of global precipitation merging satellite and ground based data. GPCP provides three different products:

- a monthly analysis on a global 2.5^o latitude x 2.5^o longitude grid for the period 1979-present, described by Adler *et al.* (2003);
- a pentad (5 day) global analysis adjusted by the monthly analysis, described by Xie *et al.* (2003);
- a daily, 1^o latitude $\times$ 1^o longitude analysis from January 1997 to the present, as described by Huffman *et al.* (2001), also constrained by the monthly analysis.

The monthly analysis is the main reference for climatic studies and it is even used as reference dataset in the adjustment procedure of some satellite precipitation products. The input datasets used to build this product are reported on table 1.5. The GPCC gauge analysis, described on section 1.3 provides ground reference dataset from about 6500 stations from all around the globe. The CAMS and GHCN gauge analyses are used within the GPCC to provide ground reference data for the pre-GPCC period, that is from 1979 to 1985. The PMW data retrieved from the DMSP SSM/I are used directly as precipitation estimate from the application of an emission-based algorithm on the ocean and a scattering-based algorithm based on the technique developed by Grody (1991) that contains separate components for land and ocean, as well as screening tests for the removal of artifacts caused by various surface types and a particular treatment for coastal areas. The *Adjusted GPI* (AGPI) comes from the elaboration of the GPI using GEO-IR data and IR sensors onboard of LEO satellites, and successive adjustment calibrating with PMW precipitation estimates. Data from the *Television and Infrared Observation Satellite* (TIROS) *Operational Vertical Sounder* (TOVS) aboard the NOAA series of polar-orbiting platforms is used to retrieve a number of meteorological variables, including precipitation using a regression relationship between collocated rain-gauge measurements and several TOVS-based parameters that relate to cloud volume. Within the GPCP elaborations, TOVS estimates are used for filling in data voids on the polar and cold-land regions from which SSM/I estimates are unavailable due to shortcomings in retrieving precipitation information over frozen surfaces. Outside of the zone 40^0N-40^0S, the SSM/I and TOVS data are averaged using equal weighting.

Finally GPCP makes use of the OLR (*Outgoing Longwave Radiation*) *Precipitation Index* (OPI) technique (Xie and Arkin, 1998) based on the use of LEO satellite OLR observations. Lower OLR radiances are directly related to higher cloud tops, which in turn are related to increased precipitation rates. For use as part of the GPCP the OPI estimates are calibrated against the globally complete GPCP estimates from 1988-98 period. During the pre-SSM/I period, the OPI data, calibrated by the GPCP satellite-gauge estimates for the SSM/I period, are used as a replacement for the multisatellite estimates. The OPI estimates calibrated by the GPCP analyses are produced routinely by NOAA/CPC.

Processing of GPCP is described on figure 1.18. The analysis from 1979 to 1985 is given by the OPI estimates calibrated by the GPCP on the successive SSM/I period. Only for the period 1986-1987 OPI estimates replace microwave and TOVS estimates on providing reference data for calibrating IR-GPI estimates(from GEO and LEO). Calibration is performed matching microwave and TOVS or OPI estimates with time corresponding GEO-IR estimates to derive additive and multiplicative microwave/IR calibration factors. The AGPI computed from the merged IR-GPI calibrated datasets represents the multi-satellite estimation reached by GPCP. Eventually the final satellite/gauge product is achieved by averaging the large scale ($5^o \times 5^o$ grid box) of the multisatellite analysis to agree with the large-scale average of the gauges by means of GPCC data (over land and where available). This keeps the bias of the satellite and gauge combination close the presumably small bias of the gauge analysis on a regional scale.

The GPCP dataset is considered as the reference precipitation source for climatological studies. The robustness of its deriving procedure, ensure reliable estimate in particular at large spatial and temporal scales. On figure 1.19 the mean precipitation map for all the globe is reported based on a long period (1979-2001) of observation (Adler *et al.*, 2003). This representation is useful to depict major climatic feature of the globe.

1.6 Future satellite missions and precipitation products

Satellite precipitation estimates is a dynamic field of activity as it is related to the availability of new satellite missions, the development of new algorithms and the exploitation of other sensors and ground sources. Improvements that are expected in the next years regard a wide range of features such as the

Table 1.5: Input dataset used by GPCP.

Algorithm	*Input data*	*Space scale*	*Time scale*	*Areal coverage*	*Time coverage*	*Data provider*
GPCC gauge analysis	~6500 surface stations	2.5°	Monthly	Global land	1986-present	DWD/GPCC
CAMS+GHCN gauge analysis	~6500 surface stations	2.5°	Monthly	Global land	1979-1985	NOAA/CPC
Emission-based PMW estimates	SSM/I on DMSP	2.5°	Monthly	60°N-60°S ocean	July 1987-present	NASA/GSFC Lab. for Atmos.
Scattering-based PMW estimates	SSM/I on DMSP	2.5°	Monthly	Global land	July 1987-present	NESDIS/ORA
AGPI	GEO satellites	2.5^0	Pentad	40°N-40°S	1986-1996	NOAA/CPC
	GEO satellites	2.5^0	Pentad	40°N-40°S	1986-1996	NOAA/CPC
TOVS-based estimates	TOVS sounding data	1°	Monthly	Global	July 1987-present	NASA/GSFC Lab. for Atmos.
OPI	LEO-IR	2.5°	Monthly	Global	1979-June 1987	NOAA/CPC

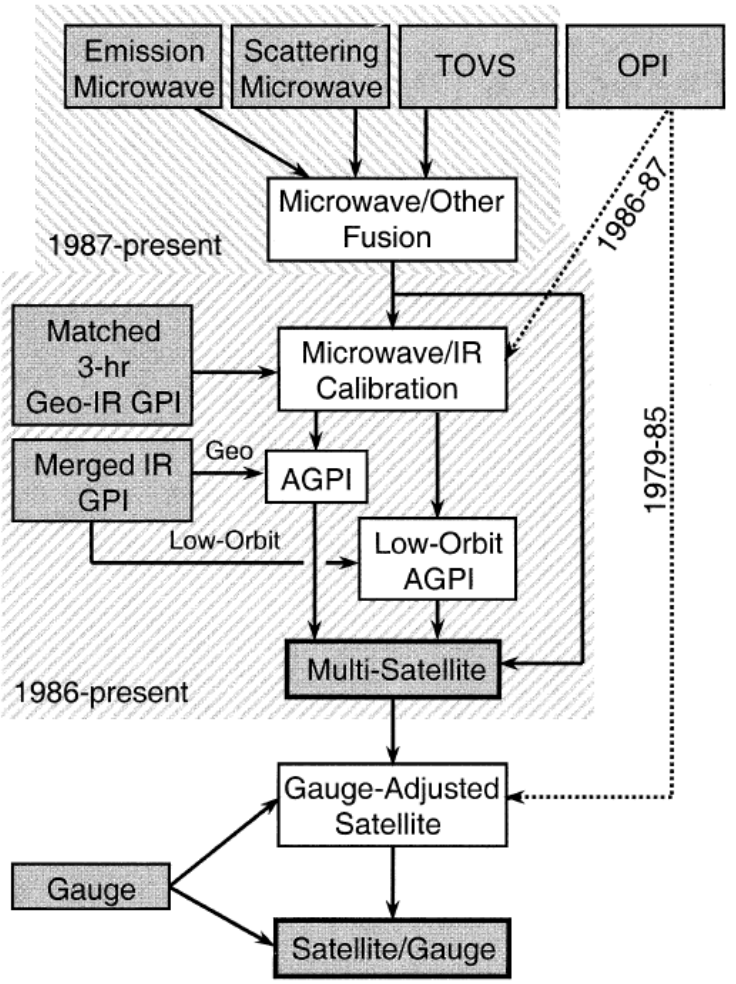

Figure 1.18: Block diagram of GPCP elaboration system (Adler *et al.*, 2003).

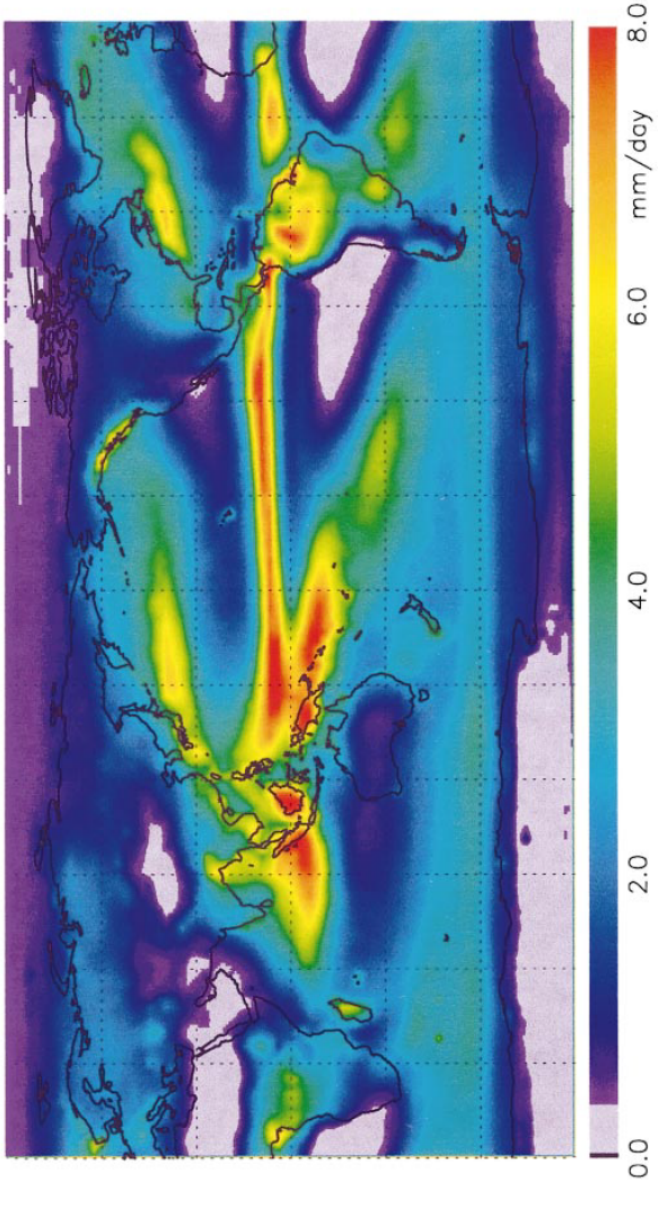

Figure 1.19: Global annual mean precipitation [mm day^{-1}] based on 23 years (1979-2001) observation period from GPCP (Adler *et al.*, 2003).

reinforcement of the physical relationship between radiation measured by sensors and precipitation within the algorithms and particularly from microwave data, the increasing of the revisit time from LEO satellites, the improvements of spatial and temporal resolutions and finally the general improvement of quality of precipitation estimates and estimates performances.

The interest for improving satellite precipitation estimates arise from the possibility to retrieve data well suitable for hydrological applications, capable to give new insights on the knowledge of earth systems and useful for meteorological and weather applications.

Here we want to address main planned satellite missions and precipitation products that are expected to emerge in the next years. The *Global Precipitation Mission* (GPM) is the most important new satellite mission of interest for precipitation estimates since it constitutes an important specific effort for studying precipitation distribution, designed on the basis of the precious TRMM experience. On the algorithm development front, other methods are expected to emerge from scientific activities. Moreover we want to furnish some information about EUMETSAT H-SAF precipitation products that will effectively provide operationally and well supported estimates for the European area, based on solid algorithms and a supporting validation activity.

1.6.1 The Global Precipitation Mission

The purpose of the International *Global Precipitation Measurement* (GPM) Program is to develop a next-generation space-based measuring system which can fulfill the requirements for frequent, global, and accurate precipitation measurements, continuously acquired along with well-defined and quantitative metrics of the measurements' systematic and random errors. For a full description of GPM see Smith *et al.* (2007).

The ultimate goal of the associated GPM mission, which is being developed as an international collaboration of space agencies, weather and hydrometeorological forecast services, research institutions, and individual scientists, is to serve as the flagship satellite mission for a variety of water-related research and applications programs. These include international research programs involved with the *Global Water and Energy Cycle* (GWEC) such as the *World Climate Research Program* (WCRP), *Global Energy and Water Cycle Experiment* (GEWEX), and to support basic research, applications oriented research, and operational environmental forecasting throughout individual nations and consortiums of nations. Because water cycling and the availability of fresh water resources, including their predicted states, are of such immense concern to

most nations, and because precipitation is the fundamental driver of virtually all environmental water issues, developing a space-based, globally inclusive precipitation measuring system has become a pressing issue for a large body of nations.

The design and development of the GPM mission is an outgrowth of valuable knowledge and published findings enabled by the *Tropical Rainfall Measurement Mission* (TRMM) and produced by various US, Japanese, and European Union (EU) research teams, and dedicated individual scientists. From the TRMM experience, from consideration of basic physical principles associated with direct sensing of precipitation from space, and from a realistic view of contemporary economic constraints, it is now recognized that the GPM mission must consist of a constellation of satellites, some dedicated, and some conveniently available through other experimental and operational missions supported by various of the world's space agencies, i.e., in the vernacular of GPM, "satellites of opportunity". The heart of the GPM constellation is the Core satellite, under joint development by NASA and the *Japan Aerospace Exploration Agency* (JAXA). As with TRMM, the basic workshare arrangement between NASA and JAXA is that JAXA will provide the radar and the launch, while NASA will provide the radiometer, the satellite bus, and the ground segment. The Core satellite is the central rain-measuring observatory which will fly both a dual frequency (Ku/Ka-band) precipitation radar called DPR, and a high-resolution, multichannel PMW rain radiometer called *GPM Microwave Imager* (GMI). Launching of GPM Core Observatory into orbit is planned in 2014, that can be considered as the starting of GPM operative phase. The core is required to serve as the calibration reference system and the fundamental microphysics probe to enable an integrated measuring system made up of, typically, eight additional constellation-support satellites. Each support satellite is required to carry one or more precipitation-sensing instruments, but at a minimum, some type of PMW radiometer measuring at several rain frequencies. Fortunately, the GPM constellation has had the welcome attention of the *European Space Agency* (ESA) and a consortium of European and Canadian scientists, who are planning for the contribution of a *European GPM* (EGPM) satellite whose instrument capabilities would strengthen the core measurement scheme. This observatory will be specially outfitted with an advanced rain radiometer using a mix of window and molecular O^2 sounding frequencies, and a Ka-band, high-sensitivity (5 dBZ) radar - a combination of instruments suitable for measurements of light and warm rainfall, moderate to heavy drizzle, and light to moderate snowfall. All these types of precipitation, which are largely outside the dynamic range of the Core satellite's instruments, are very important contributors to the Earth's

water cycle at mid- to high-latitudes, while warm rain and drizzle are significant contributors in the tropics, particularly in the extended marine stratocumulus regions.

The GPM Mission consists of four main components. The first is the space hardware making up the constellation measuring system as described.

The second is the data information system, referred to as the GPM *Precipitation Processing System* (PPS), a system whose functions will be distributed among NASA, JAXA, and ESA, with the main node at the *NASA/Goddard Space Flight Center* (GSFC). The main responsibilities of the PPS are:

1. to acquire level 0 and 1 sensor data (see figure 1.6 for a reference on products data levels);

2. to produce and maintain consistent level 1 calibrated/earth-located radiometer brightness temperatures (T_b) and radar reflectivities (Z_s);

3. to process level 1 data into consistent level 2 and 3 standard precipitation products;

4. to disseminate precipitation products through both "push" and "pull" data transfer mechanisms;

5. to assure archival of all data products acquired or produced by the PPS, either within the PPS or through suitable arrangements with other data archive services.

The third mission component is the internationally organized GPM *ground validation* (GV) program, which will consist of a worldwide network of GV-measuring sites and their associated scientific and technical support organizations.

On table 1.6 a scheme of GPM satellites and related main features is reported.

The fourth mission component is the most valuable of the entire mission; that being the people involved, i.e., the collection of individual scientists, engineers, and program officials making up the various science teams from participating nations, as well as the oversight committee/working group infrastructure that will manage and coordinate the international aspects of the mission. Because the GPM mission is expected to be flexible and fluid in design, enabling space hardware assets to come and go as the situation evolves (referred to as the "rolling wave" constellation approach), allowing for new and changing PPS and GV site facilities and capabilities, and accepting that the underlying scientific effort is a

Table 1.6: Summary of GPM's constellation members. SS=sun-synchronous orbit, NSS non sun-synchronous orbit, DN=local time descending node, AN=local time ascending node, DFR=dual-frequency radar. (Smith *et al.*, 2007).

Satellite	Sponsoring agency	Relevant instruments	Probable launch window (likely orbit)	Unique measuring capabilities
Dedicated constellation members				
GPM Core	JAXA NASA	GMI DPR	2009-10 (400 km, 65-deg, NSS)	Ku/Ka-band DFR
EGPM	ESA	EMMR NPR	2009-10 (600 km, 1430 DN, 2320 AN, SS)	O_2 dual-band channels, 5-dBZ sensitivity Ka-band radar
Megha Tropiques	CNES ISRO	Madras ScaRab	2009-10 (800-km, 20-deg, NSS)	Radiation budget
NASA–Partner	NASA Partner (TBD)	GMI TBD	2011-12 (TBD)	TBD
Satellites of opportunity				
DMSP (F19,F20)	DOD	SSMIS	2006-09 (833 km, 0530-0930 DN,1820-2220 AN, SS)	Operational satellite asset
NPOESS (C1,C2,C3)	IPO (NASA–NOAA–DOD)	CMIS	2009-32 (833 km, 0530-0930-0040 DN, 1820-2220-1330 AN, SS)	Operational satellite asset with eight complimentary meteorological instruments
FY-3 (V1,V2,V3,V4)	NSMC	PMWR	2007-12 (TB km, TBD DN, TBD AN, SS)	Operational satellite asset
GCOM-B1	JAXA	AMSR	2012-TBD (800 km, 1030 DN, 2320 AN, SS)	Experimental satellite asset with three complimentary hydromet instruments
Potential backup satellites				
TRMM	JAXA NASA	TMI, PR	Orbit since 1997 (400 km, 35-deg, NSS)	First PMW radiom in low inc/alt orbit, first space-borne precip radar
CORIOLIS	IPO (NASA–NOAA–DOD), Navy	WindSat	Orbit since 2003 (830 km, 0510 DN, 1800 AN, SS)	First PMW with full stokes vector
AQUA	NASA	AMSR-E	Orbit since 2002 (705 km, 0040 DN, 1330 AN,SS)	1.8-m aperture radiom at 705 km, both window and sounding freqs
NPP	IPO (NASA–NOAA–DOD)	ATMS	2006-07 (830 km, 1030 DN, 2320 AN, SS)	31 GHz plus sounding freqs
METOP	ESA EUMETSAT	AMSU-A	2005-15 (800–850 km, 0930 DN, 2240 AN, SS)	Operational satellite asset with eight complimentary met instruments

shared responsibility, the people involved will practice international diplomacy as well as adhere to their fundamental responsibilities and commitments within their own organizations and sovereign nations.

With these four components, the GPM mission will have the capability to provide physically based retrievals on a global basis, with ∼3-h sampling assured at any given Earth coordinate ∼90% of the time; such frequent diurnal sampling made possible by a mixed nonsunsynchronous/sunsynchronous satellite orbit architecture. Ultimately, however, it will be the people involved that will demonstrate how an internationally sanctioned collective effort can be used to acquire a long-sought measuring capability of one of the Earth's most fundamental variables and one of life's most precious commodities.

1.6.2 H-SAF precipitation products

A new aggregation point of resources for a lot of applications related to the satellite information is provided by the *European Organisation for the Exploitation of Meteorological Satellites* (EUMETSAT). In particular EUMETSAT has designed a collection of activities grouped on a unique hub named *Satellite Application Facilities* (SAFs). SAFs are dedicated centres of excellence for processing satellite data, achieved by utilising specialist expertise from the European Union Member States. SAFs generate and disseminate operational EUMETSAT products and services based on satellite data collected on EUMETSAT. A scheme of SAFs facilities is reported on figure 1.20.

The *Support to Operational Hydrology and Water Management SAF* facility (H-SAF) is charged of providing support for a wide range of applications related to the water cycle and the estimates of water related variables in a hydrological framework. The H-SAF objectives are to provide new satellite-derived products from existing and future satellites with sufficient time and space resolution to satisfy the needs of operational hydrology, and to perform independent validation of the usefulness of the new products for fighting against floods, landslides, avalanches, and evaluation water resources. Three water related variables focused by H-SAF are precipitation, soil moisture and snow. In this framework several precipitation products have been developed that make use of different satellite sources and techniques. A synthesis of main feature offered by these precipitation products, is reported on table 1.7.

H-SAF precipitation products use satellite data from both microwave and infrared sensors, producing either estimates based only on microwave data and microwave-infrared blended estimates. Algorithm approaches are not described here but they recall similar ideas used on other precipitation products, such as

Table 1.7: H-SAF precipitation products descriptions and characteristics (source: *http://hsaf.meteoam.it/precipitation.php*)

Product	Description	Coverage	Cycle	Resolution	Accuracy	Timeliness
PR-OBS-1	Precipitation rate at ground by MW conical scanners (with indication of phase)	Strips of ∼ 1400 km swath crossing the H-SAF area [25-75^{o}N lat, 25^o W-45^o E long] in direction approx. S-N or N-S	Up to six passes/day at approximately 05:30, 08:00, 09:15, 17:30, 20:00 and 21:15 LST	Average: 30 km (computed at 37 GHz) - Best case: 15 km (computed at 90 GHz)	10-20 % (> 10 mm/h), 20-40 % (1-10 mm/h), 50-100 % (< 1 mm/h) - Depending on liquid or solid and land or sea	within 90 min from the observing time
PR-OBS-2	Precipitation rate at ground by MW cross-track scanners (with indication of phase)	Strips of ∼ 2250 km swath crossing the H-SAF area [25-75^{o}N lat, 25W-45^{o}E long] in direction approx. S-N or N-S	Up to six passes/day at approximately 01:40, 09:30, 10:20, 13:40, 21:30 and 22:20 LST	Average along the swath: 40 km - Best case (close to the s.s.p.): 20 km	20-40 % (> 10 mm/h), 30-60 % (1-10 mm/h), 40-80 % (< 1 mm/h) - Depending on type (convective or stratiform)	30 min
PR-OBS-3	Precipitation rate at ground by GEO/IR supported by LEO/MW	The rectangular area of the Meteosat field of view that includes the H-SAF area limited to 60^o N [i.e. 25-60N lat instead of 25-75^{o}N lat, 25^{o}W-45^{o}E long]	15 min	Average over Europe: 8 km (controlled by the IR pixel size)	40-80 % (> 10 mm/h), 80-160 % (1-10 mm/h), not applicable for low rate (more suitable for convective precipitation)	Within 5 min from the end of (real time) acquisition
PR-OBS-4	Precipitation rate at ground by LEO/MW supported by GEO/IR (with flag for phase)	Strips of ∼ 2250 km swath crossing the H-SAF area [25-75^{o}N lat, 25W-45^{o}E long] in direction approx. S-N or N-S	Up to six passes/day at approximately 01:40, 09:30, 10:20, 13:40, 21:30 and 22:20 LST	Average along the swath: 40 km - Best case (close to the s.s.p.): 20 km	20-40 % (> 10 mm/h), 30-60 % (1-10 mm/h), 40-80 % (< 1 mm/h) - Depending on type (convective or stratiform)	30 min
PR-OBS-5	Accumulated precipitation at ground by blended MW and IR	The rectangular area of the stereographic projection that includes the H-SAF area [25-75^{o}N lat, 25^{o}W-45^{o}E long]	Each 3 hours: MW+IR integrated over the previous 3, 6, 12 and 24	Average over Europe: 8 km as intended sampling, ∼ 30 km effective	From PR-OBS-3 or PR-OBS-4: 40 % (lower bias from PR-OBS-4). More accurate for 24-h than for 3-h integration	At fixed times of the day, within 15 min after synoptic hours (00, 03, 06, 09, 12, 15, 18 and 21 UTC)
PR-ASS-1	Instantaneous and accumulated precipitation at ground computed by a NWP model	Mid of Development Phase: COSMO-ME [approx. 30-55^{o}N lat., 5^{o}W-35^{o}E lon.] Domain; Last part of Development Phase: H-SAF area [25-75^{o}N lat, 25^{o}W-45^{o}E long]	6 hr	7 km	For 3-h forecast: precipitation rate 50 %, accumulated: 100 %	At fixed times of the day, 4 h after nominal time of analysis (00, 12)and, in Version-2, 06, 18 UTC)

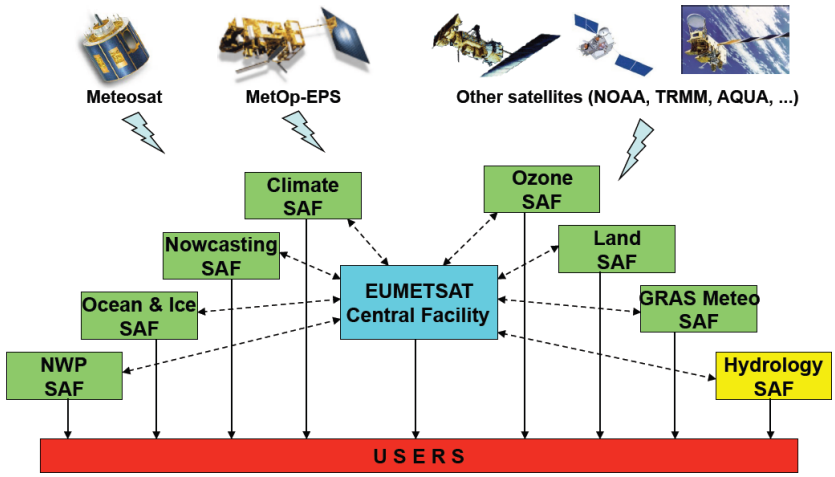

Figure 1.20: EUMETSAT SAFs scheme with some of most important satellite used.

bayesian procedures to produce estimate by coupling a physical representation of hydrometeors and a radiative transfer model, and image morphing approaches to infer cloud movement from infrared image.

H-SAF precipitation products are expected to become reference data for European area since they have adopted robust algorithm principles and finally address more specifically issues related to mid and high latitudes.

A calibration/validation group has been built within H-SAF with the following objectives:

- characterize the product error structure whose knowledge is needed for correct utilisation;
- supporting algorithms and models tuning (i.e., calibration) during their development process;
- collecting routine reporting from end-users and special reporting from experimental activities;
- continuing calibration/validation activities during the pre-operational phase.

This activity is supported by a consistent ground-based network set up by several rain-gauge networks and radars provided by the group members.

Chapter 2

Satellite precipitation evaluation

The progressive exploitation of resources to retrieve measurement and information about precipitation experienced by the scientific community in the last years, has led to a number of precipitation products characterized either by common features and differences. As can be observed from previous chapters, the most important sharing of features is related to the usage of the same sensors data. In particular, satellite data, given the limited number of missions used for these aims, provides an essential information source shared by precipitation information retrieval systems. Differences come from the different usage of satellite data, employment of other data sources, algorithms and procedures, product final features in terms of temporal and spatial resolution, possible geographic preferred focusing. Moreover, different evaluation approaches can result suitable either for *Quantitative Precipitation Estimates* (QPE) and *Quantitative Precipitation Forecast* (QPF) or can fit only one of these categories. Here the emphasis is put on QPE. The complex framework that come out has led to some question about the reliability of each dataset in particular by means of the uncertainty characterization. In the next subsections results from some evaluation studies are reported to illustrate some insights of interests for the analysis reported on this thesis and some major features of satellite precipitation products derived from these evaluation activities.

2.1 General literature review

Evaluating and comparing output from precipitation retrieval systems developed along the satellite era, is of interest for the potential users of these datasets, i.e. institutions and agencies promoting and working on research fields related to precipitation knowledge, and algorithms and products developers. Actually performing a systematic evaluation and comparison activity requires that developers have to play a key role because of their accurate knowledge of the retrieval procedure and the possibility to have full access to the datasets.

First attempts of conducting a systematic validation activity have been registered by the *Precipitation Intercomparison Program* (PIP) and the *Algorithms Intercomparison Program* (AIP) (Arkin and Xie, 1994; Ebert *et al.*, 1996; Barrett *et al.*, 1994; Smith *et al.*, 1998; Adler *et al.*, 2001). These programs were designed to validate especially PMW retrievals. A key role on the precipitation evaluation activity, is nowdays played by the *International Precipitation Working Group* (IPWG), that was established in 2001 as a permanent working group of the *Coordination Group for Meteorological Satellites* (CGMS) and co-sponsored by the WMO. Given the importance of the accuracy analysis related to precipitation estimates, here identified as *High Resolution Precipitation Products* (HRPP), a specific program, the PEHRPP (*Pilot Evaluation of High Resolution Precipitation Products*, Turk *et al.* (2008)), was established. Results so far obtained from this program, have been presented on the first workshop of this program that took place on Germany in 2008. In particular PEHRPP aims to characterize errors on many spatial and temporal scales and geographic regions.

Within and beyond the IPWG, PEHRPP and other evaluation programs, a lot of efforts have been done to achieve the knowledge related to the potentiality of satellite precipitation products. Some of the more analyzed evaluation activities concern the capability to reproduce climatology information, the representation of particular events (e.g. extremes events), hydrological performances within models, uncertainty and error characterization related to possible explaining factors as elevation and land/sea origin, retrieving algorithm analysis and comparisons between different products. Moreover the evaluation activity has to be considered geographically referred since performances can be related to spatial and geographic features.

Several studies perform the analysis considering the entire coverage provided by the dataset, that is at global scale. Gottschalck *et al.* (2005) considered different precipitation datasets as potential input for the *Global Land Assimilation System* (GLAS). Ebert *et al.* (2007) compard some satellite products and NWP

(*numerical weather prediction*) model output data, finding that they complement each other as the first are more accurate during summer and at lower latitudes while NWP models show better performance during winter and at higher latitudes. Sapiano (2010) evaluated and compared some satellite blended products on global scale against GPCP data, highlighting that satellite products tend to be lower than GPCP over mid-latitude oceans and higher over land and some parts of the tropical ocean. Tian and Peters-Lidard (2010) built an uncertainties global map indirectly considering the spread given by six different satellite precipitation products reaching a raw global characterization of error associated with precipitation estimates at global scale.

Moreover particular studies take into account singular satellite product among the most used and/or particular reference area for the evaluation considerations. Hong *et al.* (2007) examined PERSIANN-CCS performances on Northwestern Mexico using the *North American Monsoon Experiment* (NAME) *Event Rain Gauge Network* (NERN) and showing that the dataset is able to reproduce the precipitation field and that an elevation-dependent bias is observed. Habib *et al.* (2009) took into consideration TMPA dataset and evaluated its estimate against radar and raingauge measurements for particular heavy events localized in Lousiana, USA. It turned out that TMPA estimates reported reasonable levels of rainfall detection especially when light rainfall rates are excluded and that they tend to overestimate small rain rates and underestimate large rain rates. Zeweldi and Gebremichael (2009) evaluated CMORPH dataset against radar data on Oklahoma reporting positive bias in summer and negative bias in winter. Sohn *et al.* (2010) reported an evaluation study of some major satellite products over the Korea peninsula. The study reports that all the datasets underestimate precipitation and points out some PMW algorithms known issues as possible reasons. Kidd *et al.* (2012) recently addressed the performances of satellite precipitation products on Europe area, comparing some of the more important operational blended algorithms (TMPA, CMORPH, NRL blended technique, PERSIANN) along with the GPI-IR precipitation estimates and the *European Centre for Medium-Range Weather Forecasting* ECMWF operational forecast model. Precipitation data from the European radar network, supported by the GPCC precipitation gauge analysis, has been used as reference data for this validation. Results highlight the necessity of addressing deficiencies in retrieval algorithms for mid and high latitude, and in particular during cold season since lower performances than those on warm season are observed, and overall underestimation is reported by satellite products.

Even though this is not an exhaustive list of evaluation, comparison and validation studies, it is effective on illustrating how results are highly variable

depending on the purpose of the analysis, the spatial and temporal scale considered and the geographic location just to name the most important features. Moreover it is notable as a wide range of tools can be used as benchmark on performing evaluation studies.

2.2 Evaluation indexes and tools for satellite precipitation products

The development of precipitation products has been accompanied by a corresponding effort on validating results. The evaluation activity has been carried out in particular using available ground data, therefore for precipitation over land. The emphasis on conducting these verification analyses is related on the objective of the application for which the dataset is considered. The nature of these application can greatly vary as well as the requirements for precipitation data considered.

For climatological studies, data is evaluated considering large spatial and temporal resolutions (tipically 2.5^o, monthly rainfall). Therefore errors on shorter time and space scale are unimportant. But users interested for applying data on other application, may not accept these errors. Hydrologists need accurate estimates of rain volume at the catchment scale. In NWP data assimilation of satellite rainfall, experience suggests that detecting the correct rain location and type may be more important than getting the correct amount. For flash flood warning and tropical rainfall potential, it is not only important to correctly detect the occurrence of rainfall, but to be able to estimate the maximum rain rates.

Given the wide range of applications that can make use of satellite precipitation products, several analyses and tools can be considered in order to carry out such evaluations. Moreover same indexes and elaboration can provide different information e.g. considering spatial and temporal resolutions or considering aggregation, temporal trend or mapping evaluation indexes.

This variegation on evaluation tools has been highlighted by PEHRPP activity since in the first meeting group a dedicated session on *error metrics* has been organized. An exhaustive discussion about evaluation tools is provided by Rossa *et al.* (2008). A fundamental classification among tools, that is widely recognized, considers two main indexes classes:

- *Continuous verification statistics* to measure the accuracy of predicted or estimated rain amount;

- *Categorical verification statistics* to measure the accuracy of predicted or estimated rain occurrences.

Moreover other tools have been designed, to investigate particular features. Below description of main indexes and tools from these two categories are listed.

2.2.1 Continuous verification statistics

- *Mean Bias Error*

$$MBE = \frac{\sum_{i=1}^{n} \left(P_{obs}^{(i)} - P_{est}^{(i)} \right)}{n}$$

where $P_{obs}^{(i)}$ and $P_{est}^{(i)}$ are respectively the precipitation value provided by gauge data and the precipitation estimation provided by a satellite product for a single position/pixel, at the i-th time step.

- *Mean Square Error (MSE)*

$$MSE = \frac{\sum_{i=1}^{n} \left(P_{obs}^{(i)} - P_{est}^{(i)} \right)^2}{n}$$

The root of MSE (RMSE) is often used as it is dimensionally homogenous with the field considered.

- *Mean Absolute Error (MAE)*

$$MAE = \frac{\sum_{i=1}^{n} \left| P_{obs}^{(i)} - P_{est}^{(i)} \right|}{n}$$

- *Correlation Coefficient*

$$CC = \frac{cov\left(\mathbf{P}_{est}, \mathbf{P}_{obs}\right))}{\sigma(\mathbf{P}_{est}) \cdot \sigma(\mathbf{P}_{obs})}$$

where $\mathbf{P}_{est}$ and $\mathbf{P}_{obs}$ are respectively the gauge and satellite time series data for a single series of position/pixel.

- *Taylor diagram*
Taylor diagram (Taylor, 2001) is based on the geometrical relationship between correlation coefficient, series standard deviation and centered mean

square error as illustrated on figure 2.1. It is useful to summerize error statistical performances and it can be used to illustrate satellite precipitation products relative performances (e.g. see Ebert *et al.* (2007)).

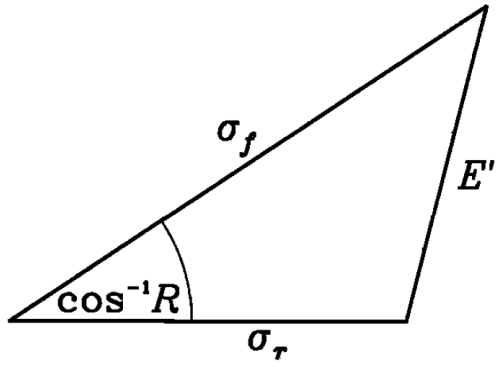

Figure 2.1: Geometric relationship between the correlation coefficient R, the centered pattern RMS error E', and the standard deviations σ_f and σ_r of the test and reference field respectively (Taylor, 2001).

2.2.2 Categorical verification statistics

Categorical indexes for measuring performance on detecting precipitation occurrences, are based on a contingency table that summarize correspondences between reference and validating dataset. In order to identify precipitation occurrences, a threshold value is considered. Therefore precipitation values below this threshold are not classified as occurrences.

Table 2.1: Contingency table used to classify precipitation occurrences and calculating categorical indexes

		Event Observed	
		Yes	*No*
Event Estimated	*Yes*	Hit (H)	False Alarm (FA)
	No	Miss (M)	Correct Rejection (CR)

Filling contingency table for a case study, that is classifying estimated precipitation occurrence based on simultaneous reference occurrence, can be referred

to a threshold value to separate positive and negative occurrences. From the contingency table reported on table 2.1 following categorical indexes can be computed.

- *Probability of detection*
$$POD = \frac{H}{H+M}$$
- *False alarm ration*
$$FAR = \frac{FA}{H+FA}$$
- *Success ratio*
$$SR = \frac{H}{H+FA}$$
- *Bias*
$$Bias = \frac{H+FA}{H+M}$$
- *Percent correct*
$$PC = \frac{H+CR}{n}$$
with $n = H + FA + M + CR$
- *Critical success index*
$$CSI = \frac{H}{H+FA+M}$$
- *Gilbert skill score*
$$GS = \frac{H-CH}{H+FA+M-CH}$$
where CH describes the hit due to chance: $CH = \frac{(H+FA)(H+M)}{n}$
- *True skill statistics*
$$TSS = \frac{H \cdot CR - FA \cdot M}{(H+M)(FA+CR)}$$
- *Heidke skill score*
$$HSS = \frac{H+CR-CRF}{H+FA+M+CR-CRF}$$
where CRF is the correct random forecast:
$CRF = \frac{(H+FA)(H+M)+(FA+CR)(M+CR)}{n}$

Interpreting results from several categorical indexes at the same time, can provide further insights. When categorical indexes computation are conducted considering several threshold values, a synthesis graphical representation, called, ROC (Relative Operating Characteristics) diagram, (Mason, 1982; Jolliffe and Stephenson, 2008) (figure 2.2) is useful to summarize performances. It is given by the cartesian representation of *Hit* rate against *False alarm* rate or by *POD* against *FAR*. Area below ROC curve, obtained e.g. considering several threshold values, represents the performance of the estimate considering that POD results close to 1 (all precipitation occurrences detected) and FAR results close to 0 (no false precipitation occurrence detected) give the best performance.

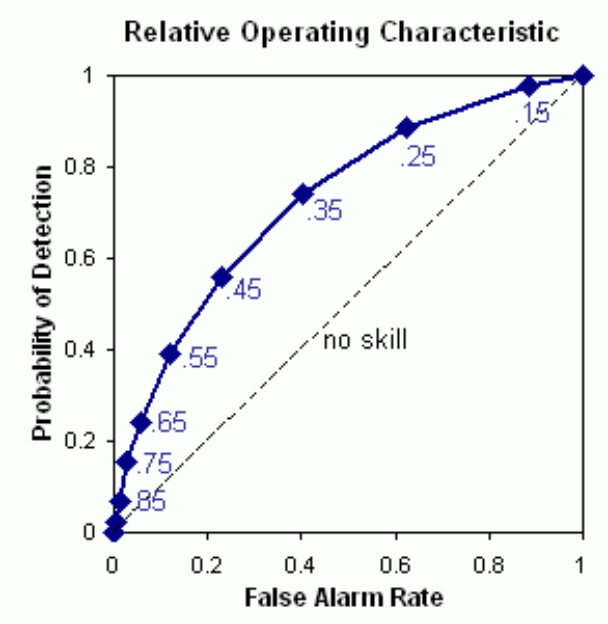

Figure 2.2: ROC diagram example. Points on the plot represents results obtained with different threshold values as indicated by values.

2.2.3 Alternative verification approaches

Some issues on evaluating estimate skills can arise from high resolutions data as they are characterized by high variability. Often the estimates or the

forecasts are able to capture the large-scale weather but small-scale error is still present and dominates the total error. It is typical the case of an occurrence being correctly detected but offset from the exact localization that results in a so called "double penalty" due both to the observed-but-not-forecast and the forecast-but-not-observed occurrences. Alternative approaches on measuring precipitation estimates data performances, have been proposed that make use of particular spatial considerations on precipitation patterns.

A *fuzzy verification* approach was proposed by Ebert (2008) for analysing gridded forecasts. Using this criterion, the overlapping requirement for relative occurrences is relaxed by using a window or a neighborhood surrounding the analysis point. The filtering operation can include averaging, thresholding or generation of a probability distribution function depending on the method used. Moreover the window size is based on the scale of analysis.

The *entity-based* approach (Ebert and McBride, 2000) is based on the identification of rain entities or contiguous rain areas (CRAs), whose properties from estimation data are verified against those from reference dataset. Verification are based on the computation of the position error, the difference between the estimated and observed rain area, volume, and mean and maximum rain rates, and the correlation between the position-corrected estimate and observations. Figure 2.3 shows a representation of CRAs. They are defined by a threshold isohyet that depends on precipitation magnitude. A position error can be determined by pattern matching. Possible best-fit criteria include minimization of the total-squared error, maximization of the spatial correlation coefficient, or maximum overlap. Then other features can be derived for corresponding entities and the total error can be decomposed into contributions from location, volume and pattern error. The weakness of *entity-based* approach is that, if estimated pattern does not sufficiently being similar to reference data, it may not be possible to reliably associate two entities objectively.

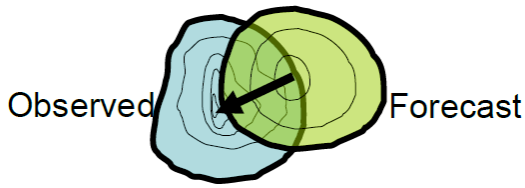

Figure 2.3: Contiguous rain area representation (Ebert and McBride, 2000)

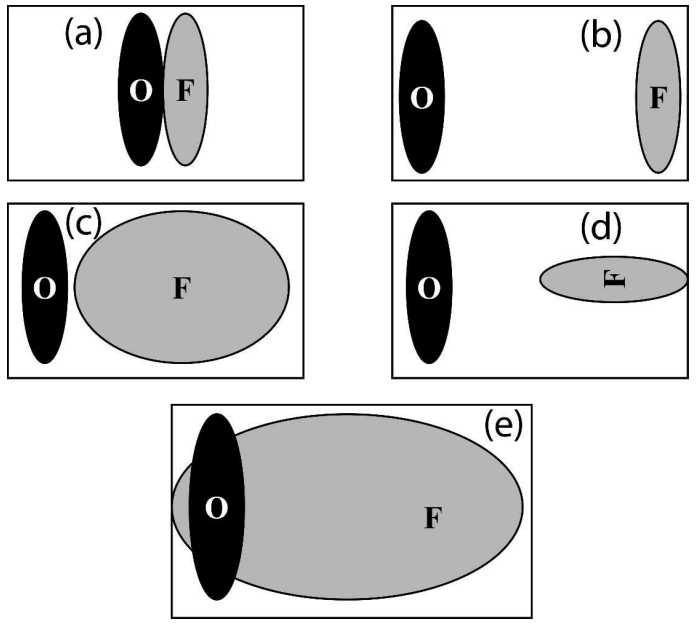

Figure 2.4: Representation of modeled and observed patterns. From (a) to (d) *Critical Success Index* CSI = 0, whereas for (e) is greater than zero but it does not represent a better estimate than all other cases. (Davis *et al.*, 2006).

Similar to the *entity-based* approach is the *object-based* (Davis *et al.*, 2006). Authors highlight that standard verification approaches often do not provide results similar to those that may come up from subjective perceptions (see figure 2.4).

The method is based on a preliminary object identification step given by a masking operation based on smoothing and thresholding analyses as shown in figure 2.5. Convolution and thresholding parameters depend on spatial and temporal scales. Then objects attributes, including centroid localization, size, orientation, curvature and intensity distribution are computed and a statistical comparison can be performed. Moreover modeled and reference objects are coupled by means of matching procedure based on displacement between centroids and objects size. Typical continuous and categorical indexes can then be computed considering matched objects.

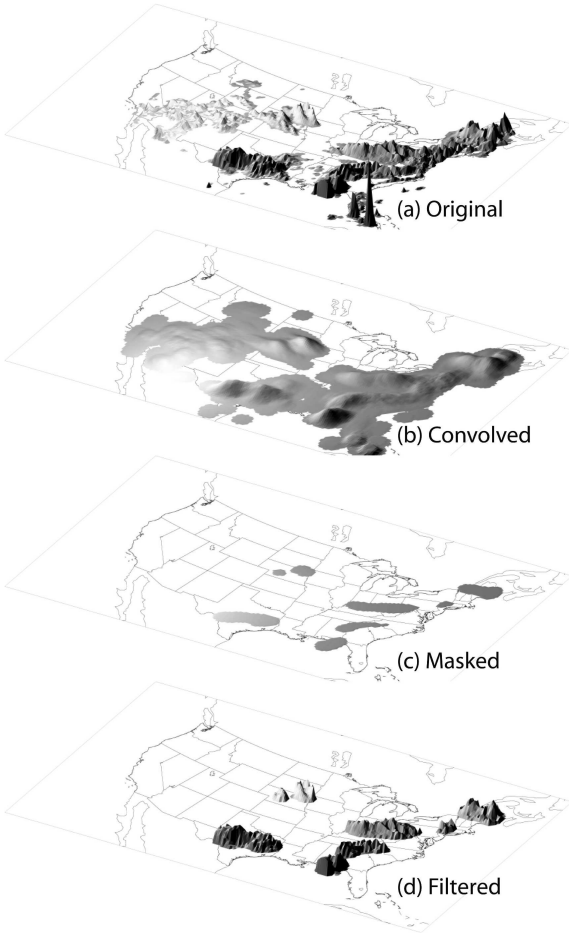

Figure 2.5: Example of object identification for the *object-based* method (Davis *et al.*, 2006).

2.2.4 Hydrological verification approaches

Given recent and foreseen improvements of satellite precipitation products, it is interesting testing the suitability of such datasets as input data in hydrological models. Output provided by hydrological models, such as the discharge simulated, can be used as validating information if a measured source is available, or as comparing information for satellite precipitation products.

Yilmaz *et al.* (2005) compared mean areal precipitation estimates derived from three sources: an operational rain gauge network, a radar/gauge multisensor product, and the PERSIANN satellite-based system for the time period from March 2000 to November 2003. The study area includes seven operational basins of varying size and location in the southeastern United States. The analysis indicates that agreements between the datasets vary considerably from basin to basin and also temporally within the basins. The analysis also includes evaluation of PERSIANN data in comparison with rain-gauge network data for use in flow forecasting with a lumped hydrologic model, the *Sacramento Soil Moisture Accounting Model* (SAC-SMA). The latter evaluation investigates two different parameter sets, the first obtained using manual calibration on historical rain-gauge network data, and the second obtained using automatic calibration on both satellite estimates and rain-gauge network data, but over a shorter time period (23 months). Results indicate that the overall performance of the model simulations using PERSIANN depends on both the bias in the precipitation estimates and the size of the basins, with poorer performance in basins of smaller size (large bias between rain-gauge network data and PERSIANN) and better performance in larger basins (less bias between rain-gauge network data and PERSIANN). When using PERSIANN, calibration of the parameters significantly improved the model performance. Figure 2.6 shows an example of results from validation by means of hydrological model extracted from this study.

Another study is proposed by Behrangi *et al.* (2011), that evaluated the effectiveness of using satellite-based precipitation products for streamflow simulation at catchment scale. Five satellite-based precipitation products (TMPA-RT, TMPA, CMORPH, PERSIANN, and PERSIANN-adj) are used as forcing data for streamflow simulations at 6-h and monthly time scales during the period of 2003-2008. SAC-SMA model is used again for streamflow simulation over the mid-size Illinois River basin. The results show that, by employing the satellite-based precipitation, the general streamflow pattern is well captured at both 6-h and monthly time scales. However, satellites products, with no bias-adjustment being employed, significantly overestimate both precipitation inputs

and simulated streamflows over warm months (spring and summer months). For cold season, on the other hand, the unadjusted precipitation products result in under-estimation of streamflow forecast. It was found that bias-adjustment of precipitation is critical and can yield to substantial improvement in capturing both streamflow pattern and magnitude. The results suggest that along with efforts to improve satellite-based precipitation estimation techniques, it is important to develop more effective near real-time precipitation bias adjustment techniques for hydrologic applications.

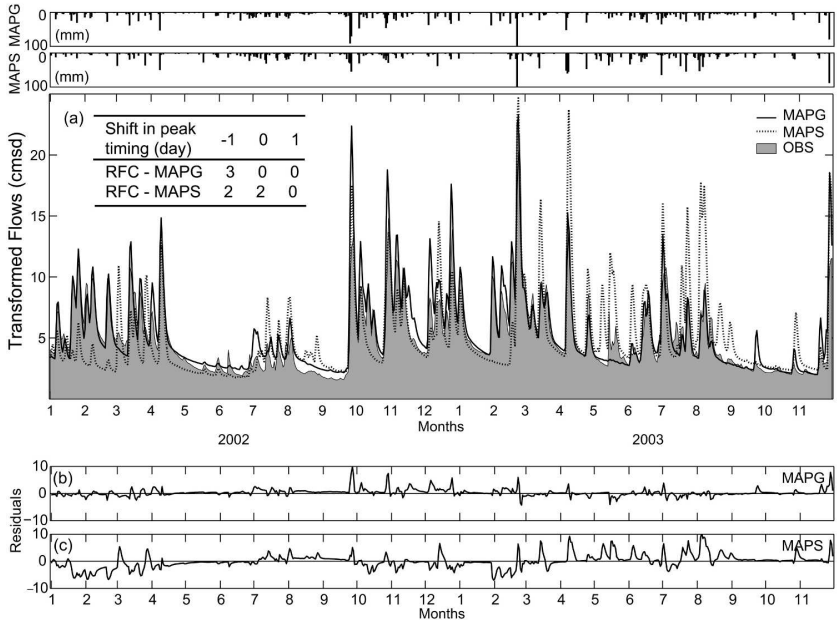

Figure 2.6: Example of precipitation data validation by means of a hydrological model (Yilmaz *et al.*, 2005). MAPG and MAPS indicate respectively the mean areal precipitation from gauge network and from satellite (PERSIANN); OBS is the observed flow.

2.2.5 Spatial and temporal analyses

The complexity of verifying estimates or forecasts precipitation, is not completely exploited by the large number of indexes and tools that can be adopted

on evaluating performances. Other issues arise from the investigation of feature related to spatial and temporal dynamics.

Spatial aspects, beyond the simple spatial distribution of considered field, include spatial variability, geographic characterization of feature, dependence and relationship with other variables, e.g. with the elevation.

Temporal considerations can arise from the detection of possible trends, the analysis of seasonality and that of the diurnal cycle.

Further insights can be derived from the analysis of verification indexes varying temporal and spatial resolutions. Specific graphical representations and maps are usually used to get supporting tool for these evaluations.

Chapter 3

Climatology of Sicilia

In order to be able to fully understand the outcomes from the analyses that will be exposed in the next chapters, it is useful to describe some climatological and meteorological features about the area of study. The Mediterranean climate, within which Sicilia is nested, represents a very complex system that needs to be described in order to have a general climatic framework. Therefore a general description of the Mediterranean climate is reported in the next section, followed by some more specific information about Sicilia.

3.1 The Mediterranean Climate

Mediterranean Sea is located in a transitional zone where mid-latitude and tropical features variability are both relevant. Thus, the Mediterranean climate region evolves on the north to the Marine West Coast Climate (from 40^o to sub-polar regions) and on the south to the Subtropical Desert Climate (southward of 30^o or 25^o). Further, the Mediterranean climate is exposed to the *South Asian Monsoon* (SAM) in summer and the Siberian high pressure system in winter. The southern part of the region is mostly under the influence of the descending branch of the Hadley cell, while the Northern part is more linked to the mid-latitude variability, characterized by the *North Atlantic Oscillation* (NAO) and other mid-latitude teleconnections patterns. However, the climate variability patterns present a large amount of synoptic to meso-scale spatial variability, inter-seasonal and multi-decadal to centennial time variability. An important consequence is that the analysis of the Mediterranean climate can be used to

identify changes in the intensity and extension of global scale climate pattern like NAO, ENSO (*El Niño Southern Oscillation*) and the monsoons and their region of influence.

However, the large-scale atmospheric circulation exerts a strong influence on the cold season temperature and precipitation over the Mediterranean, though the strength of the relation varies with region. The largest amount of studies on the effect of the mid-latitude variability refers to the role of NAO which determines a large and robust signal on winter precipitation, which is anti-correlated with NAO over most of the western Mediterranean region (Xoplaki, 2002). However, in its Eastern part the advection of moisture from the Mediterranean itself produces a more complicated situation, and eventually other large-scale patterns, like EA (*East Atlantic*), play an important role, and in the central Mediterranean the Scandinavian pattern has a strong influence (e.g. Xoplaki, 2002). This is superimposed with the effect of tropical variability, specifically with a reduction of cyclones in the Mediterranean area during La Niña events. Tropical variability events, like ENSO (Rodó, 2001; Mariotti *et al.*, 2002), can be important in the parts where NAO influence is weaker (Rodó *et al.*, 1997). There are evidences that ENSO is significantly correlated with winter rainfall in the Eastern Mediterranean (Yakir *et al.*, 1996; Price *et al.*, 1998) (Yakir et al., 1996 and Price et al., 1998). However it is still open for debate, what could be the physical mechanisms for these links. In summer, when the advection of moisture from the Atlantic is weaker and the Hadley cell moves northward and attenuates, there are evidences of connections with the Asian and the African monsoons (stronger in the eastern part).

The influence of NAO on the Mediterranean temperature is weaker than on precipitation and the observed correlation has been found to be non-linear and non-stationary (Pozo-Vázquez *et al.*, 2001). Mediterranean summer temperatures have no relation with the NAO, and they are not adequately linked to larger scale patterns. Rather, warm Mediterranean summers are connected with blocking conditions, subsidence, stability, a warm lower troposphere and positive Mediterranean sea surface temperature (Xoplaki *et al.*, 2003).

The analysis of teleconnection with global scale patterns is very important in a climate change perspective. During the second half of the 20th century, there is a well-documented trend showing the reduction of overall precipitation and its concentration in intense events, resulting in a progressively drier summer season and more dangerous floods. These trends can have large impacts on societies in the Mediterranean region. Because of the difficulty to resolve it in global climate simulations, the identification of teleconnections with large-scale patterns is a basic tool for the prediction of future climate conditions.

The variability of large and locale scale meteorological factors that arise around Mediterranean Sea, are reflected on the variegate climatology that is observable on related lands. In their updated world map of the *Köppen-Geiger climate classification*, Peel *et al.* (2007) classify the Mediterranean lands with several classes (see figure 3.1 and table 3.1). The western side of Africa coast is mostly classified as *warm desert climate*, while on the eastern side Algeria and Morocco coasts areas are classified as *warm Mediterranean* or *cold semi-arid climate* as well as part of Spanish coast, some Italian, Greek and Turkish, costs and islands (then comprising Sicilia). On the north *temperate Mediterranean*, *temperate oceanic* and *warm oceanic/humid subtropical climate* classes are attributed to French coasts, adjacent Spain and Italian lands and along the eastern Adriatic coast.

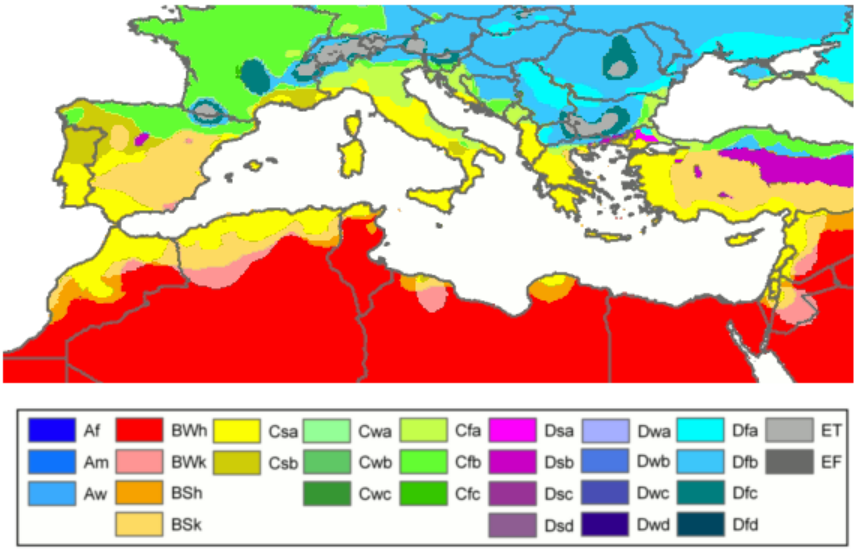

Figure 3.1: Köppen-Geiger classification map (Peel *et al.*, 2007)

Table 3.1: Köppen-Geiger classification legend table

Legend
Af: equatorial climate
Am: monsoon climate
Aw: tropical savanna climate
BWh: warm desert climate
Bwk: cold desert climate
Bsh: warm semi-arid climate
Bsk: cold semi-arid climate
Csa: warm mediterranean climate
Csb: temperate mediterranean climate
Cwa: humid subtropical climate
Cwb: humid subtropical climate/subtropical oceanic highland climate
Cwc: oceanic subpolar climate
Cfa: warm oceanic climate/humid subtropical climate
Cfb: temperate oceanic climate
Cfc: cool oceanic climate
Dsa: warm continental climate/mediterranean continental climate
Dsb: temperate continental climate/mediterranean continental climate
Dsc: cool continental climate
Dsd: cold continental climate
Dwa: warm continental climate/humid continental climate
Dwb: temperate continental climate/humid continental climate
Dwc: cool continental climate/subarctic climate
Dwd: cold continental climate/subarctic climate
Dfa: warm continental climate/humid continental climate
Dfb: temperate continental climate/humid continental climate
Dfc: cool continental climate/subarctic climate
Dfd: cold continental climate/subarctic climate
ET: tundra climate
EF: ice cap climate

3.2 Climatology of Sicilia

Sicilia is the larger island of Mediterranean Sea. Its surface is about 25.000 km^2 and its extension range from 36^o to 38^o North and from 12^o to 15^o East.

Even though the morphology is very complex, it is useful considering three sub-areas related to the three main sides of the island: the northern side, the south-western side and the eastern side. An important mountain range is present along the northern side facing the Tyrrhenian Sea that is considered the following of the Appenine mountains. The eastern side, exposed to the Ionian Sea, is characterized by the presence of the Etna volcano located on the plain of Catania while on the southern side is the hyblean plateau that shapes the morphology.

The mean annual precipitation over Sicilia is about 715 mm (period 1921-2004) with rainfall concentrated in the winter period. The July-August months are usually rainless. Considerable spatial variability of precipitation is observed, ranging from an average of 400 mm in the South-Eastern part to an average of 1300 mm in the Northern-Eastern part (Di Piazza *et al.*, 2011). Temperature range from 11 ^{o}C to 20 ^{o}C (Drago *et al.*, 2000). Specific precipitation (figure 3.2) and temperature (figure 3.3) maps have been elaborated respectively by Di Piazza *et al.* (2011) and Di Piazza (2011).

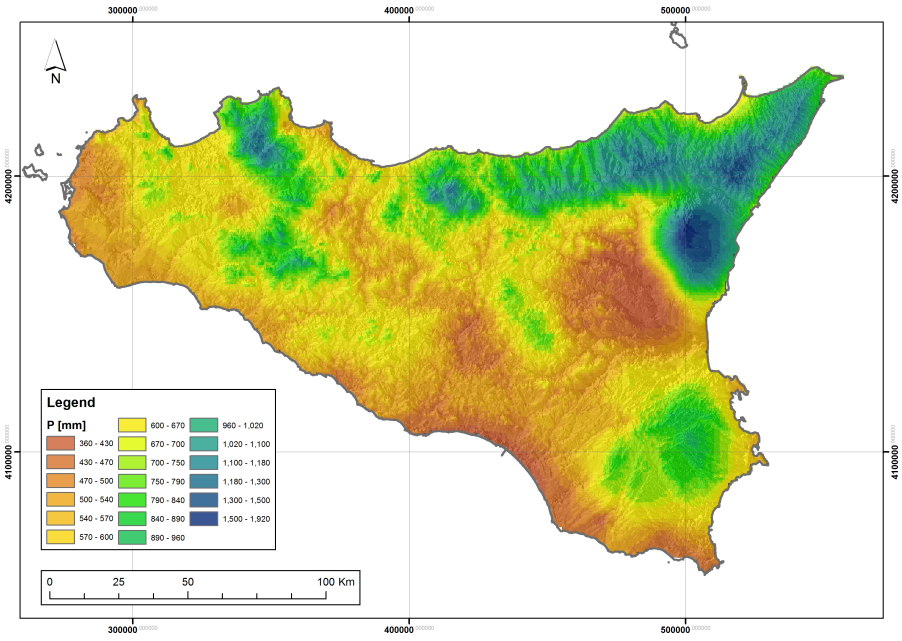

Figure 3.2: Mean precipitation map [mm/year] (Di Piazza *et al.*, 2011)

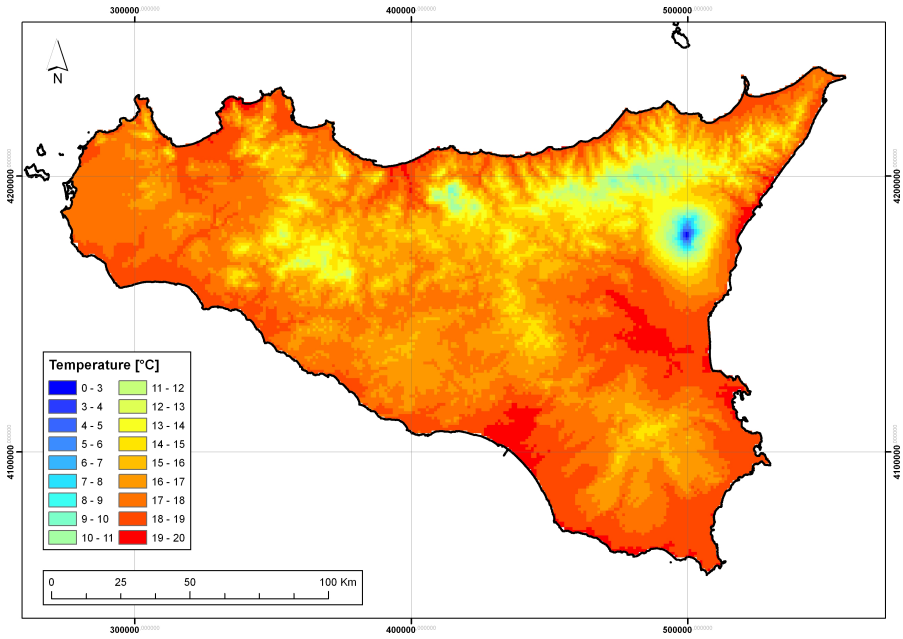

Figure 3.3: Mean temperature map [^{o}C] (Di Piazza, 2011)

Therefore, Sicilia and surrounding Mediterranean area is usually classified as *Csa* (dry-summer subtropical climates) on the Köppen climate classification. It is a climate characterized by colder monthly temperature greater than -3 ^{o}C and lower than 18 ^{o}C, dry summer with warmer monthly temperature greater than 22 ^{o}C. A study of the climatology of Sicilia is reported by Drago *et al.* (2000). Following the indication of the *World Meteorological Organization* (WMO) authors use precipitation and temperature data from 55 thermo-pluviometric and 127 rain-gauge stations related to the period 1965-1994.

The Peguy's (Péguy, 1961) climogram elaborated in this study are effective on describing the variety of climates present on the Island. These diagrams synthetically summarize thermo-pluviometric conditions at a given location. They are built from monthly mean precipitation and temperature data. Temperature and precipitation scales are reported respectively on the x and the y axis. Connecting twelve monthly points, a polygon is obtained whose shape and size represent climatic features for the considered location. On the diagram a triangular area is reported; it is considered as the frame where temperate conditions

are realized. Below this triangular area, arid conditions are described, while cold and warm climates are identified respectively on the left and on the right of the triangle. Peguy's climograms, elaborated for several location on Sicilia area (figure 3.4), show that given overall temperate conditions verified for many months, some locations present particular condition falling on various climatic conditions such as cold, warm and arid regions (respectively "Freddo", "Caldo" and "Arido" on figure 3.4).

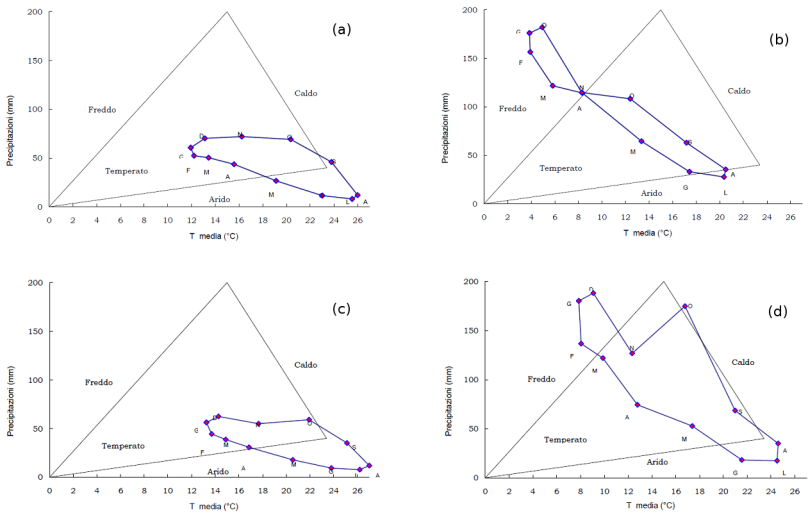

Figure 3.4: Peguy climate diagrams (Drago *et al.*, 2000). (a) Trapani (2 m a.s.l); (b) Floresta (1250 m a.s.l); (c) Gela (45 m a.s.l); (d) Nicolosi (698 m a.s.l)

3.3 Reference precipitation dataset

Rain-gauge dataset used in the evaluation analysis described on chapter 4 is furnished by SIAS (*Servizio Informativo Agrometeorologico Siciliano*) i.e. the agro-meteorological informative system of Sicilia that collects information and makes available a quality-controlled meteoclimatic dataset. It is constituted by 104 tipping bucket rain-gauges and, as shown in figure 3.5, spatial distribution is rather homogeneous in the territory with an average density equal to about 250 Km^2/gauge. Data are retrieved with high temporal resolution (10 minutes)

allowing time aggregation as necessary.

List of SIAS stations are provided on table 3.2 along with coordinates, elevation and activity period.

Table 3.2: SIAS network rain-gauges list with location and working period

Code	Location	North UTM ED50 (m)	East UTM ED50 (m)	Elevation (m)	Is active	Starting date	Ending date
[H] 201	Agrigento	4133668	371497	225	X	11/02/2002	
202	Agrigento	4122136	378997	40	X	29/03/2002	
203	Aragona	4146671	378326	305	X	01/01/2002	
204	Bivona	4162129	360110	350	X	01/01/2002	
206	Cammarata	4165750	388500	350	X	29/01/2002	
207	Cammarata	4164700	377200	1600		02/01/2002	20/07/2006
208	Canicattì	4135341	391378	475	X	20/03/2002	
209	Licata	4112719	401333	80	X	01/01/2002	
210	Sambuca di Sicilia	4169772	324977	300		01/01/2002	26/10/2004
211	Naro	4127486	392265	290		01/01/2002	28/10/2003
212	Ribera	4144951	346639	30	X	01/01/2002	
213	Sciacca	4162344	326937	90	X	13/08/2002	
214	Caltanissetta	4142950	415961	350	X	01/01/2002	
215	Delia	4134185	404850	360	X	01/01/2002	
216	Gela	4112703	440838	70	X	25/02/2002	
217	Butera	4110270	421268	54	X	24/11/2004	
218	Mazzarino	4128273	430320	480	X	01/01/2002	
219	Mussomeli	4157950	396800	650	X	01/01/2002	
220	Riesi	4125850	419244	300	X	29/01/2002	
221	S. Caterina Villermosa	4160218	420410	630		01/01/2002	23/05/2004
223	Adrano	4170704	483761	400		01/01/2002	13/06/2006
224	Bronte	4178677	481238	424	X	01/01/2002	
227	Caltagirone	4120652	462332	480	X	01/01/2002	
228	Catania	4144073	506089	10	X	01/01/2002	
229	Riposto	4170912	517486	50	X	01/01/2002	
230	Linguaglossa	4186715	511565	590	X	01/01/2002	

continued on next page

continued from previous page

231	Maletto	4186704	488838	1040	X	01/01/2002	
232	Mazzarrone	4105613	461052	300	X	01/01/2002	
233	Mineo	4130521	475760	200	X	01/01/2002	
234	Paternò	4152071	487181	100	X	01/01/2002	
235	Pedara	4166352	504345	810	X	01/01/2002	
236	Ramacca	4137201	482826	50		01/01/2002	23/01/2007
316	Ramacca Giumarra	4148383	467627	263	X	24/01/2007	
237	Randazzo	4193537	498224	680	X	01/01/2002	
312	Agira	4164155	456066	467	X	23/06/2006	
314	Calascibetta	4169633	431857	650	X	15/06/2006	
238	Enna	4152590	427200	350	X	01/01/2002	
239	Gagliano Castelferrato	4172361	456092	580		09/02/2002	30/05/2006
240	Leonforte	4162420	445113	340		01/01/2002	05/06/2006
241	Nicosia	4179735	449303	700	X	01/01/2002	
242	Piazza Armerina	4130260	443880	540	X	18/01/2002	
243	Aidone	4144990	452850	350	X	12/04/2002	
313	Antillo	4203520	522917	796	X	22/06/2006	
244	Caronia	4209150	455207	50	X	23/02/2002	
245	Caronia	4194487	454864	1470	X	21/09/2002	
246	Cesarò	4187970	471815	820	X	25/01/2002	
247	Cesarò	4198383	473142	1840	X	01/09/2002	
248	Fiumedinisi	4209767	532927	440	X	21/02/2002	
249	S. Pier Niceto	4220276	531566	460	X	01/01/2002	
250	Leni (Isola di Salina)	4268293	485566	315	X	18/10/2002	
251	Messina	4234667	549100	230	X	23/02/2002	
252	Militello Rosmarino	4210296	470802	460	X	28/01/2002	
309	Montalbano Elicona	4204279	497082	1250	X	24/09/2004	
253	Mistretta	4190807	441972	690	X	05/03/2002	
254	Naso	4217735	481277	480	X	01/01/2002	
256	Novara di Sicilia	4208750	512444	750	X	01/01/2002	
257	Patti	4221477	501713	70	X	02/03/2002	
258	Pettineo	4203210	437646	210	X	01/01/2002	
259	S. Fratello	4200929	466961	1040	X	01/01/2002	

continued on next page

continued from previous page

260	Taormina	4188911	519877	60		14/01/2002	20/06/2006
261	Torregrotta	4227100	531200	60	X	01/01/2002	
262	Alia	4177982	389507	560	X	01/01/2002	
263	Caltavuturo	4183408	404396	810		01/01/2002	08/11/2004
264	Camporeale	4197002	333044	460	X	01/01/2002	
265	Castelbuono	4203401	420047	430	X	01/01/2002	
267	Contessa Entellina	4177723	327586	200	X	11/02/2002	
268	Corleone	4185609	346000	450	X	02/01/2002	
269	Gangi	4185734	429078	830	X	01/01/2002	
310	Giuliana	4166605	343814	260	X	29/10/2004	
271	Lascari	4206383	405194	55	X	16/02/2002	
273	Mezzojuso	4190491	367634	390	X	01/01/2002	
274	Misilmeri	4210500	363375	160	X	01/01/2002	
315	Monreale	4193612	356465	730	X	29/06/2006	
275	Monreale	4210177	342278	630	X	01/02/2002	
276	Palermo	4221667	353448	50	X	01/01/2002	
277	Partinico	4214983	332863	120	X	01/01/2002	
278	Petralia Sottana	4165640	412795	720	X	11/05/2002	
279	Polizzi Generosa	4186883	411643	650	X	01/01/2002	
311	Prizzi	4176428	361237	990	X	25/11/2004	
222	Sclafani Bagni	4173822	398626	497	X	01/01/2002	
281	Termini Imerese	4203682	378151	350	X	01/01/2002	
282	Acate	4092281	446670	60	X	01/01/2002	
283	Comiso	4096752	463629	220	X	01/01/2002	
284	Ispica	4064910	499421	30	X	06/03/2002	
285	Modica	4081929	491280	300	X	20/12/2002	
286	Ragusa	4089982	471241	650	X	01/01/2002	
287	Santa Croce Camerina	4076830	455637	55	X	01/01/2002	
288	Scicli	4068435	471153	30	X	01/01/2002	
289	Augusta	4126276	513303	60	X	01/01/2002	
290	Siracusa	4101770	514148	90	X	07/01/2002	
291	Francofonte	4122166	490607	100	X	01/01/2002	
292	Lentini	4132840	493420	50	X	25/01/2002	

continued on next page

continued from previous page

293	Noto	4077815	505127	30	X	17/04/2002	
297	Pachino	4059653	508512	50	X	04/01/2002	
298	Palazzolo Acreide	4101771	488592	640	X	13/01/2002	
299	Alcamo	4204926	324113	230		28/03/2002	15/11/2002
300	Calatafimi	4192052	313693	310	X	17/03/2002	
301	Castellammare del Golfo	4209531	314734	90	X	01/01/2002	
302	Castelvetrano	4168921	310591	120	X	01/01/2002	
303	Erice	4212219	288088	590	X	11/01/2002	
304	Marsala	4186611	285975	120	X	15/01/2002	
305	Mazara del Vallo	4172830	294987	30	X	01/01/2002	
306	Salemi	4188232	299335	280	X	07/02/2002	
307	Trapani	4202386	285021	50	X	29/01/2002	
308	Trapani	4202573	294518	180	X	23/02/2002	

In this study, precipitation information measured by these stations, are used as reference data source to perform the evaluation analysis of satellite precipitation products. A data representativeness problem then arises since rain-gauges measures are point representative, while satellite precipitations represent surface estimates. This issue regards the uncertainty of each source and on that of results obtained from comparison.

Here the problem has been addressed interpolating point rain-gauges network at the same resolution provided by satellite precipitation products, that for those used in the evaluation analysis described on chapter 4 is equal to 0.25^o. Therefore it has been assumed that, given the large pixel size of satellite products, the error and related uncertainty component from rain-gauges data interpolation, can be neglected, then assuming that such an interpolated dataset is suitable for conducting the evaluation study.

A comparative evaluation of different interpolation methods referred to this specific application would be necessary to select the most suitable one. Hofstra *et al.* (2008) compared six different interpolation procedures to produce daily gridded surface of European climate data. These methods varied from simpler algorithms like IDW (*Inverse Distance Weighting*) and NN (*Natural Neighbor*) methods, to kriging based methods. They found that as the density of ground point measurement increases, performances of all methods improve and tend to converge, so even simple methods like IDW or NN methods produce good results. A simple interpolation method is applied even by Sohn *et al.* (2010); it uses a weighted average of gauges based on successive neighboring zones to get grid surfaces for a comparison study.

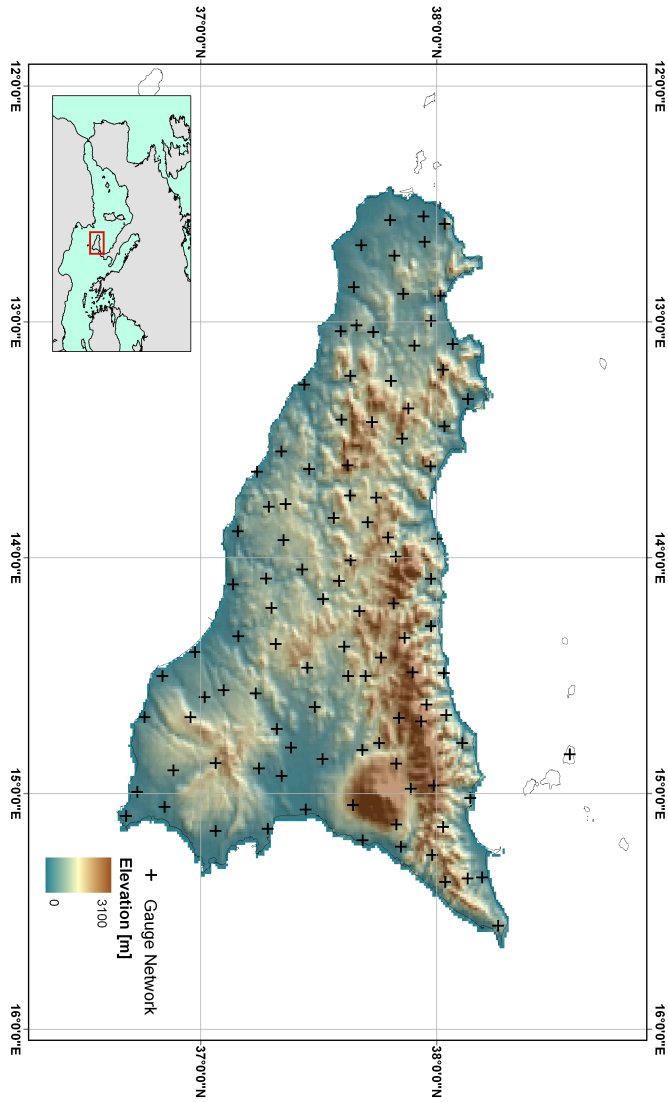

Figure 3.5: Study area location with digital elevation model and rain-gauges distribution

Considering the large number of maps that could be necessary in order to evaluate a long period of satellite estimates (e.g. consider that at the typical 3 hours time resolution, 2920 maps are to be produced for a one year analysis), and the low spatial resolution of maps output, a simple method that does not need parameter selection has been preferred in this study. Natural Neighbor (NN) interpolation method (Sibson, 1981) has been selected since it represents a simple procedure that implicitly accounts for proximity and direction of measurements. NN method is based on the spatial intersection between Thiessen polygons obtained considering only sampled points, and that related to the estimation point, in order to derive weights related to sampled surrounding values, for a linear estimate. Using traditional NN to produce grid estimates, corresponds to the point estimate related to the centroid of each pixel. This could result either in an estimation that does not correspond to the entire pixel block, in case of relative high density, or corresponds to a greater area when rain-gauge network is characterized by relative low density. Therefore a modified version of Natural Neighbor procedure has been adopted where instead of considering Thiessen polygon of grid center in the intersection, grid box is considered (as illustrated in figure 3.6). It is assumed that this procedure is suitable for the purposes of this study, where much emphasis has been paid to considerations about precipitation magnitude rather than spatial distribution.

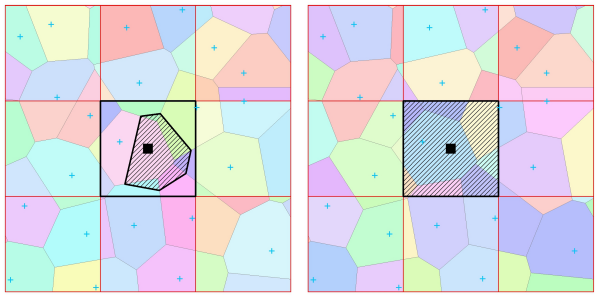

Figure 3.6: Traditional NN intersection and modified procedure used in this study

A procedure that automatically produces interpolated maps has been built. It selects available stations from table 3.2 on the basis of an input period. Only stations available for the entire year are used to produce a unique weights layer that have to be multiplied to the gauge precipitation values at each time step

in order to obtain the related map (figure 3.7). Since the spatial intersection between Thiessen polygons and output grid reticulate is performed once, such a procedure is effective on elaborating long series of maps when only the common stations available for the entire period have to be used, allowing for saving computing resources.

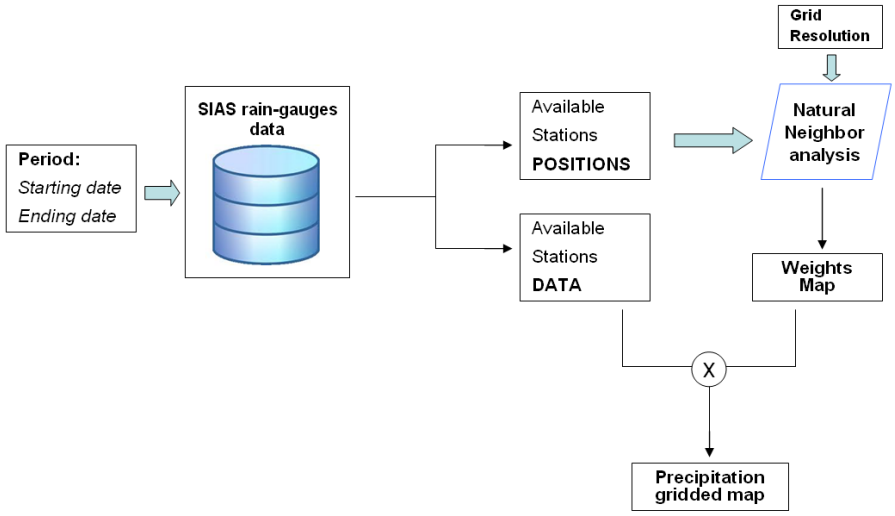

Figure 3.7: Scheme of the elaboration procedure adopted to interpolate long time series data. Here the Natural Neighbor analysis is intended as the only spatial intersection between Thiessen polygons and grid reticulate.

Chapter 4

Analysis of satellite precipitation products with reference to Sicilia

4.1 Datasets and methodology outline

The main aim of the evaluation analysis is exploring potentialities offered by precipitation estimates from satellites referred to typical rain-gauges measurements. As it has been widely described on previous chapters, algorithms share a number of features as well as data sources, namely sensors considered to retrieve precipitation information. Then it does not result being useful to consider a complete list of satellite precipitation products available from literature, since a selection of the more important can be considered fully representative of the entire class of algorithms.

In this study, six among more representative products have been selected (see table 4.1). As it has been described on section 1.4, CMORPH, PERSIANN and TMPA-RT represent three different approaches for blending PMW and IR data (figure 4.1). CMORPH uses IR information to infer hydrometeor movements; PERSIANN uses PMW precipitation estimates to calibrate IR-Rainfall relationship by means of an artificial neural network; TMPA-RT uses calibrated IR precipitation estimates to infill gaps on precipitation estimates provided by PMW data.

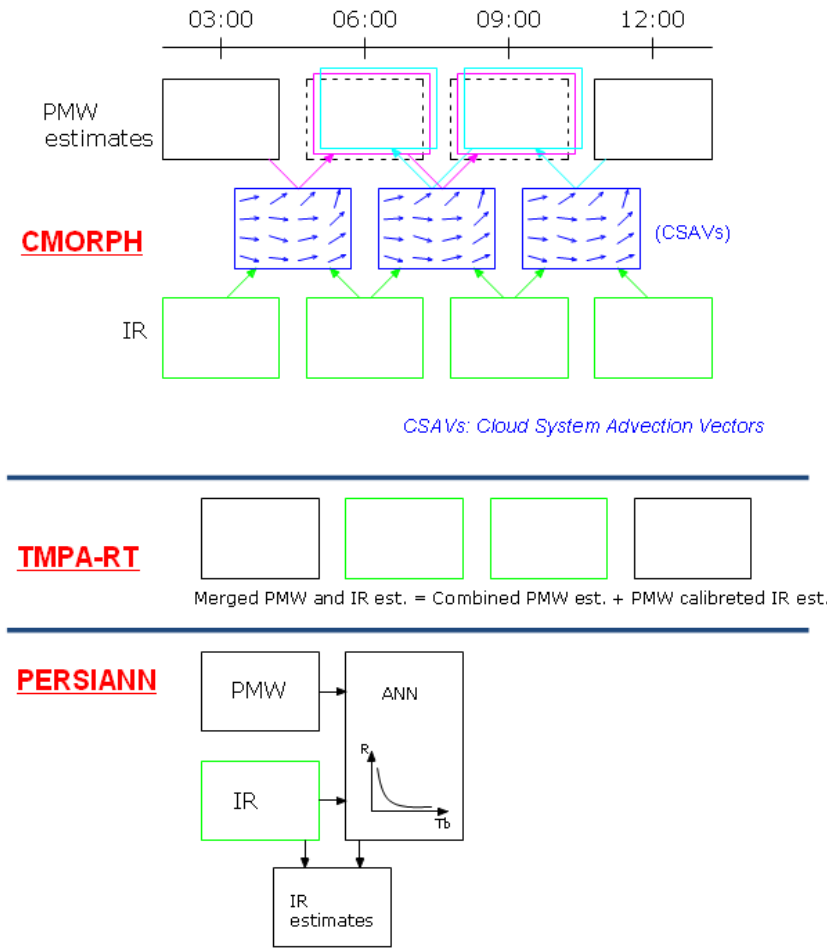

Figure 4.1: Schematic representation of CMORPH, TMPA-RT and PERSIANN IR and PMW blending approaches.

Table 4.1: Satellite precipitation products information.

Product Name	Developer	Domain	Period of record	Bias Adjusted
CMORPH	NOAA CPC	Global (60N-60S)	2003 to present	-
PERSIANN	CHRS (UC Irvine)	Global (50N-50S)	2000 to present	-
TMPA-RT	NASA-GSFC	Global (50N-50S)	1998 to present	-
PERSIANN-CCS	CHRS (UC Irvine)	Global (50N-50S)	2000 to present	-
PERSIANN Adjusted	CHRS (UC Irvine)	Global (50N-50S)	2000 to present	Yes (from PERSIANN, based on GPCP)
TMPA	NASA-GSFC	Global (50N-50S)	1998 to present	Yes (from TMPA-RT, based on GPCP)

Moreover PERSIANN-CCS has been added to the evaluated satellite products since it provides an estimate that is more related to IR data, than allowing for getting further information about its potentialities. Finally two adjusted products, the PERSIANN adjusted and the TMPA, have been compared to evaluate the effectiveness of adjusting procedures on satellite precipitation estimates.

While detailed algorithms descriptions can be found on chapter 1, some useful technical and operative characteristics are reported on table 4.1.

In order to obtain information about general performances of selected satellite products, a long reference period has been chosen than allowing to obtain information about both average features presented by satellite products and those related to seasonality and eventually on particular events. Considering the starting time of this study, the most recent available two years period has been selected, i.e. 2007-2008. Still such a two years period could not give a full depiction of performances behavior of satellite products, since some trend variability, perhaps related to climate changes, may not being captured, but this is out the scope of this study and the representativeness of the selected study period is assumed.

Gridded reference data, for this selected time period, from SIAS rain-gauge network has been prepared using an interpolation procedure as described on section 3.3. The availability checking procedure returned 93 and 94 stations respectively for 2007 and 2008. Beyond the spatial framework of the analysis, in order to be able to compare estimates from different sources, it is necessary

considering the same temporal framework. The reference temporal resolution considered is 3 hours that can be considered the typical resolution of most operational satellite products that are nowdays available. Therefore the SIAS gridded data has been opportunely aggregated. Figure 4.2 reports a summarizing scheme of the analysis with satellite products considered and spatio-temporal framework used.

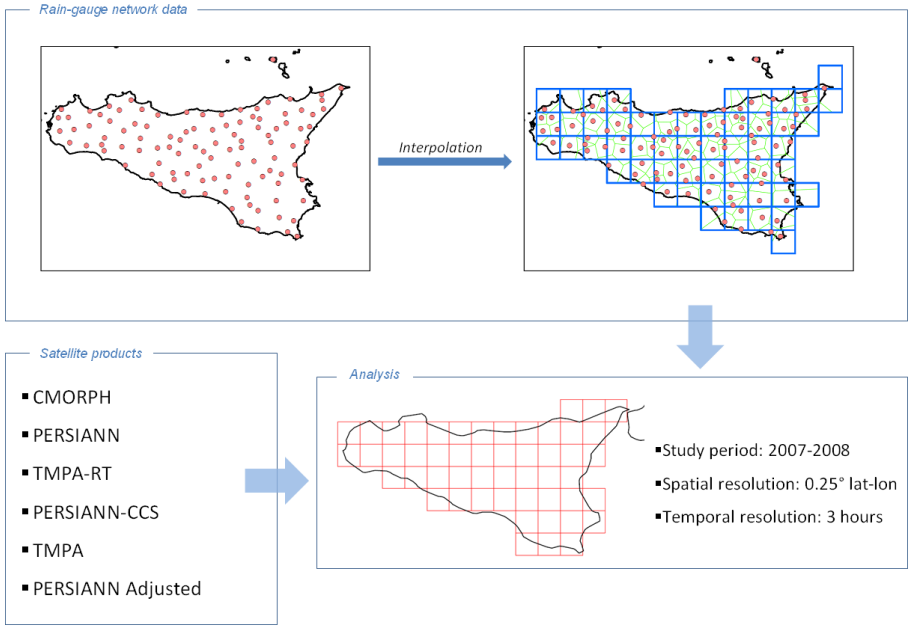

Figure 4.2: Scheme of evaluation framework.

In this study, satellite products performances have been first evaluated on the basis of a selection of evaluation indexes, considering their spatial distribution as well. Then some graphical analyses have been performed to summarize further insights. Finally some considerations about global scale have been reported to understand and consolidate some results coming from previous analyses.

4.2 Spatial analysis

The availability of a long observation period, allows to make some general considerations about satellite precipitation products performances. In order to retrieve and display information about evaluation indexes spatial distribution, temporal series analysis has been performed for each grid cell within the study area.

Temporal mean and standard deviation maps, obtained considering temporal series for each grid, are shown in figure 4.3 and summary mean statistics, corresponding to spatial averaged values, are reported in table 4.2. These results show great differences between magnitude of precipitation estimated by satellite products and reference data, resulting in a strong underestimation by satellite products. In particular only-satellite PMW mainly based products, (CMORPH, PERSIANN and TMPA-RT) underestimate more than 50% of gauge mean value whereas PERSIANN-CCS does not seem reproducing the same behavior reporting only a 20% underestimation probably because of its more IR-based derivation.

Table 4.2: Mean value and coefficient of variation (CV) from mean maps and mean values from standard deviation (STD) maps. Values in brackets represent the variation, as percentage ratio, of satellite product performances with respect to gauge performance.

	Mean map		STD map
Dataset	Mean (mm/3hr)	CV	Mean (mm/3hr)
Gauge	0.229	0.288	1.299
CMORPH	0.093 (-59%)	0.215 (-25%)	0.772 (-41%)
PERSIANN	0.084 (-63%)	0.167 (-42%)	0.628 (-52%)
TMPA-RT	0.115 (-50%)	0.243 (-16%)	0.933 (-28%)
PERSIANN-CCS	0.186 (-19%)	0.204 (-29%)	1.017 (-22%)
PERSIANN Adj.	0.140 (-39%)	0.179 (-38%)	1.055 (-19%)
TMPA	0.178 (-22%)	0.135 (-53%)	1.395 (7%)

Such an underestimation bias is still detectable on the scatterplots in figure 4.4 between reference data and satellite products data where the angular amplitude between lines represents the bias magnitude.

The mean gauge precipitation map on fig 4.3 appears related to the morphology of the area, with higher mean precipitation values in the high elevation areas (where even snow precipitation occurs), as it is observable comparing mean maps

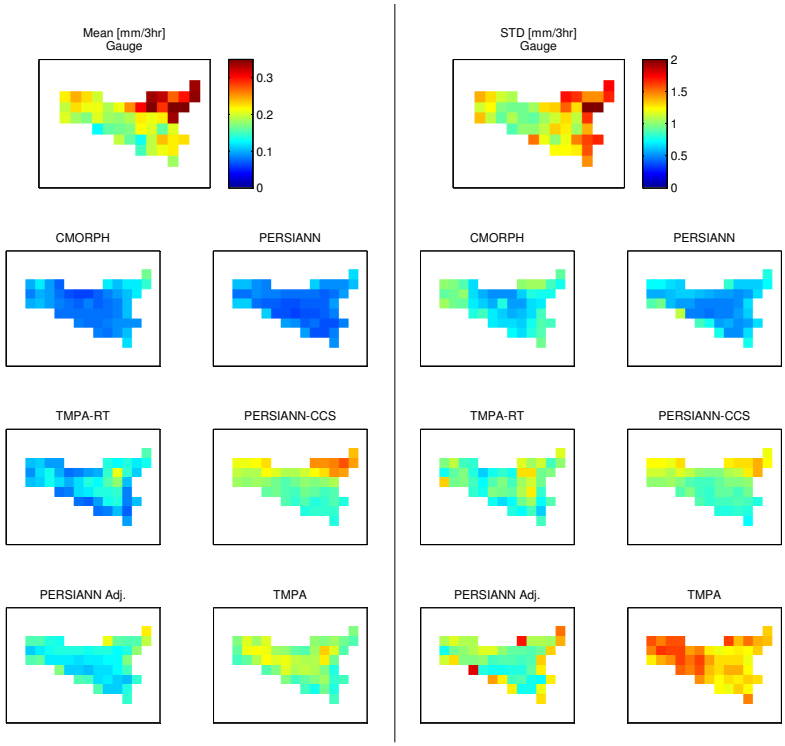

Figure 4.3: Temporal mean and standard deviation (STD) maps of precipitation obtained from rain-gauges data and satellite products (mm/3hr).

with elevation pattern (see figure 3.5). Underestimation is reduced for adjusted products (PERSIANN Adj. and TMPA) but it remains still relevant in spite of the GPCP correction. To address this latter issue, further analysis are needed particularly on the suitability of GPCP dataset for precipitation depiction at local scale.

Coefficient of variation (CV) values from the temporal mean maps (table 4.2) give a measure of spatial variability of the average precipitation that is still underestimated by all satellite products, particularly by PERSIANN (with CV=0.167 against 0.288 from gauge) and TMPA (CV=0.135) in spite of its bias adjustment that probably leads to a flattening of spatial distribution in the

study area.

Temporal variability, observed by means of standard deviation (STD) maps (figure 4.3) and related mean values (table 4.2), is even underestimated by CMORPH, PERSIANN and TMPA-RT (underestimation between 51%-28%), while PERSIANN-CCS shows a closer level to gauge reference data, but this result is related to the less biased distribution that is detected on mean values. Coherently with this observation, adjusted products report STD values closer to reference dataset level with TMPA even greater than it.

The frequency plots reported on figure 4.5, computed considering only non-zero reference dataset occurrences, show as all satellite products differ from reference dataset as they report a higher percentage of low values occurrences that leads to the mean underestimation. TMPA displays a particular behavior as it starts particularly above the gauge reference line and goes below that after a value around 10 mm/3hr, leading to a mean overestimation for high values. Therefore it turns out that adjustment procedures report some issues about frequency distribution representation since the correction procedure seems producing an overall bias reduction by overestimating high values and keeping on underestimating a wide range of low and medium values. The displacements between reference dataset and products for rain-rate equal to zero, suggests that an important component of the error is given by false rain occurrences registered by satellite products. Particularly TMPA, shows higher values than other dataset, indicating that the related correction procedure leads to the distribution of rain amount on non-precipitating areas.

In order to have a quantitative and comparative estimation of satellite-product performances, indexes spatial distributions have been computed (figure 4.6). Threshold value adopted for categorical indexes is fixed equal to 0.125 mm/3hr according to Ebert *et al.* (2007).

MBE maps confirm that higher bias occur on more elevated areas, where mean rainfall magnitude is greater, and highlight the underestimation reduction by adjusted products.

PERSIANN-CCS, even if not adjusted, displays low bias levels probably because of its estimation structure based on a stronger IR relationship. RMSE maps display the elevation pattern already observed in the mean maps and do not show large differences among different satellite-products. The greater values on the east side could be due to both the high-elevation area with related greater precipitation magnitude and based on different mechanism of precipitation (i.e. orographic rather than cyclonic).

Correlation coefficient (CC) maps report a slightly better performance of CMORPH compared to others products. One can observe that these maps

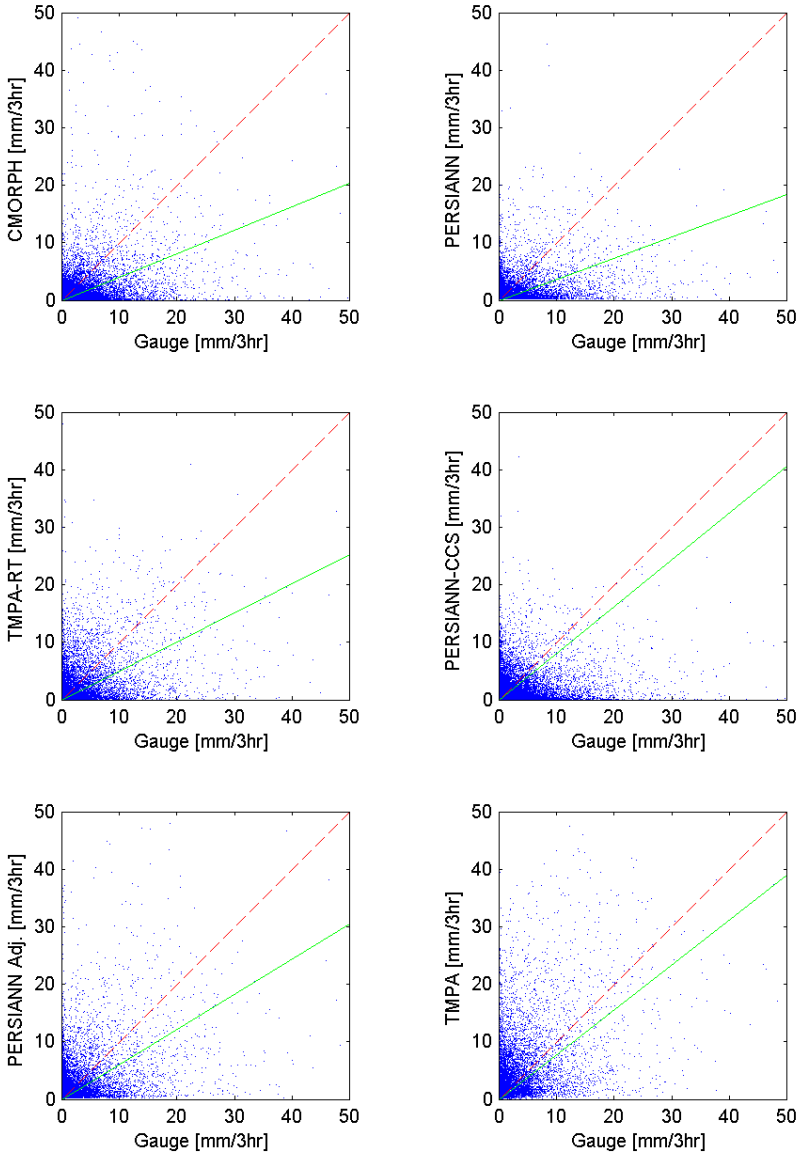

Figure 4.4: Scatterplots from reference gauge dataset and satellite products.

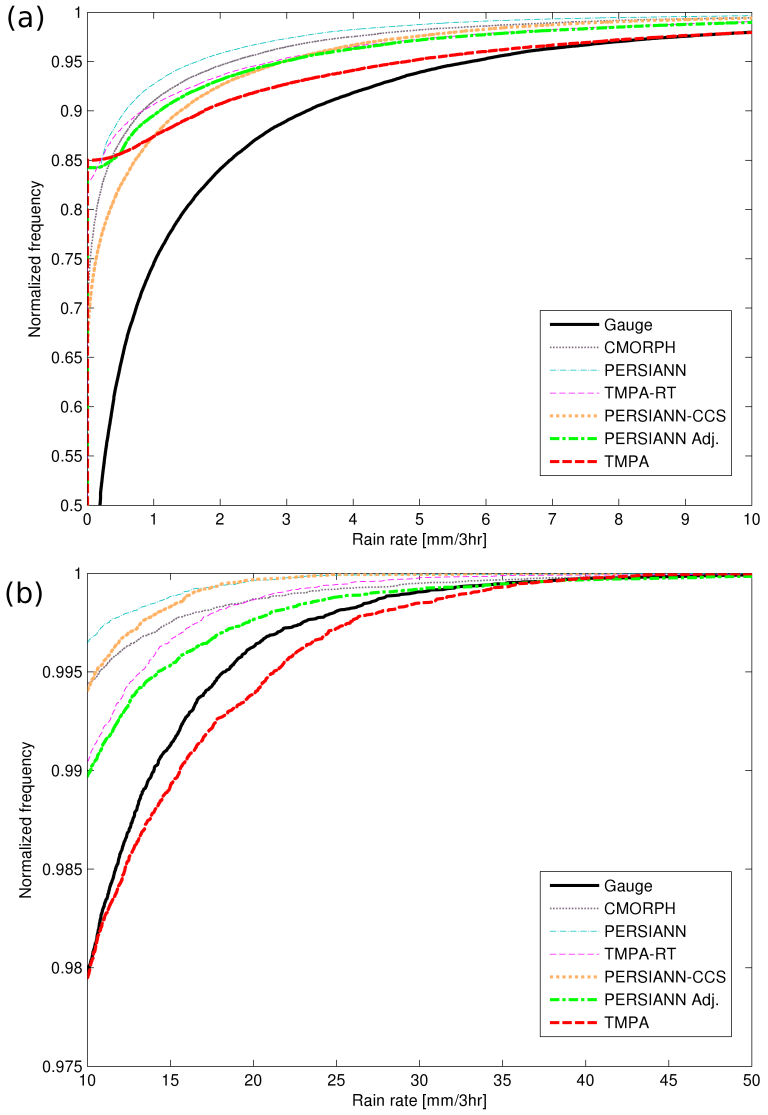

Figure 4.5: Normalized frequency distribution plots considering (a) 0-10 mm/3hr range and (b) 10-50 mm/3hr range.

indicate the best performing area in the center of the island. This could be due to a problem arising from coastal treatment since PMW retrieval algorithms suffer for some weaknesses due to different radiative properties of hydrometeors respectively over the land and over the ocean (Kummerow *et al.*, 2001).

POD and FAR mean levels are related to the time scale considered (3 hours) where it is challenging, for satellite estimates, achieving good results. For this time scale low values are expected, however plots allow to compare products performance levels. In particular PERSIANN-CCS and CMORPH report relatively good results. In the TMPA-RT and TMPA POD maps, central area displays better results than coastal pixels confirming the existence of problems for coastal areas. TMPA-RT and TMPA turn out being the best FAR performing. They show even some issues with pixels on the eastern high-area. From performance maps on figure 4.3 one can conclude that the adjustment procedures, although allow for the bias reduction, do not achieve relavant improvements on other skills represented by RMSE, CC and categorical indexes.

Table 4.3: Mean and standard deviation (STD) of the evaluation indexes maps.

	Mean					STD				
Dataset	MBE (mm/3hr)	RMSE (mm/3hr)	CC	POD	FAR	MBE (mm/3hr)	RMSE (mm/3hr)	CC	POD	FAR
CMORPH	0.136	1.189	0.465	0.318	0.473	0.057	0.285	0.074	0.058	0.117
PERSIANN	0.145	1.253	0.350	0.233	0.544	0.064	0.278	0.05	0.038	0.047
TMPA-RT	0.114	1.287	0.395	0.238	0.450	0.061	0.282	0.085	0.058	0.073
PERSIANN-CCS	0.043	1.456	0.246	0.348	0.633	0.045	0.284	0.046	0.03	0.040
PERSIANN Adj.	0.089	1.331	0.404	0.233	0.544	0.058	0.293	0.070	0.038	0.047
TMPA	0.051	1.442	0.456	0.225	0.428	0.069	0.238	0.089	0.054	0.089

Taylor diagram realized considering mean correlation coefficient and standard deviation values from map distributions is reported in figure 4.7.

As described in the indexes description, Taylor diagram summarizes relationship between testing and reference series standard deviations, correlation coefficient and RMSD (root mean square difference) between series centered pattern by means of a trigonometric similitude. Taylor diagram indicates that error performance, measured by means of RMSD centered pattern, is given by a combination of correlation coefficient and standard deviations.

Since reducing underestimation bias, overall precipitation variance increases along with its magnitude, adjusted products (PERSIANN-Adj. and TMPA)

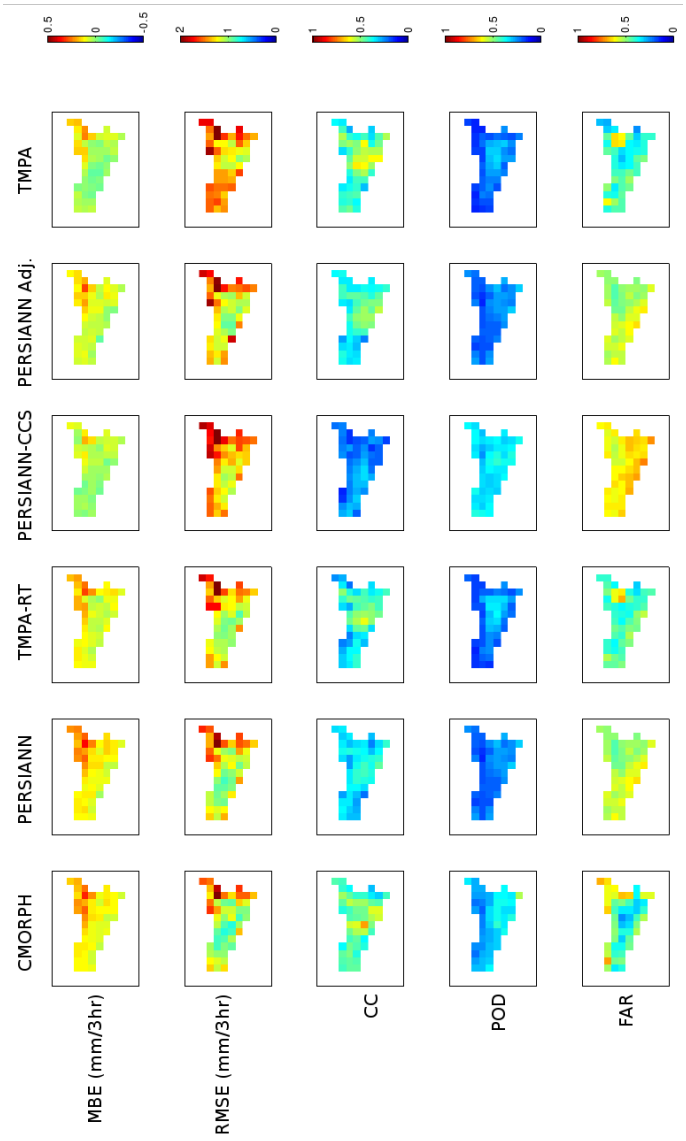

Figure 4.6: Evaluation indexes maps.

result performing worse, in terms of RMSD centered pattern, than most of not adjusted (CMORPH, PERSIANN and TMPA-RT). This effect affects the mean RMSE values (table 4.3) as well.

Such a result highlights that for this area, and generally where an underestimation bias is observed, an adjustment procedure that reduces underestimation not producing a significant increase of correlation features, may lead to worse performances in terms of root mean square error.

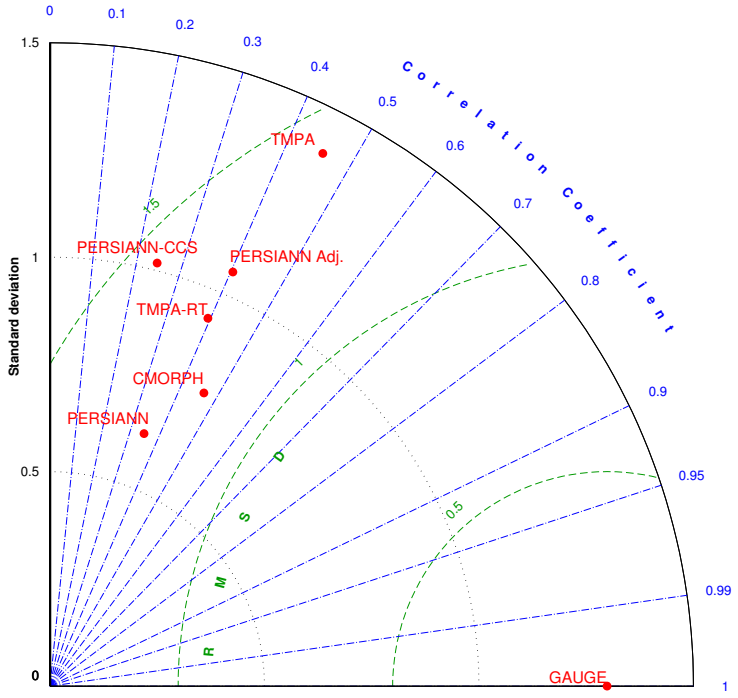

Figure 4.7: Taylor diagram from averaged values. Points are represented by means of polar coordinates with standard deviation as radius and $cos^{-1}(Corr)$ as angle. Distances from Gauge point give the centered pattern Root Mean Square Error (indicated as RMSD) assumed as performance index.

4.3 Time aggregation and temporal trend analysis

In order to evaluate how the capability of satellite-products improve as the temporal resolution considered in the estimation increases, mean values of statistics have been evaluated considering different time resolution ranging from original 3 hours to one month. Precipitation maps have been first temporally aggregated at the new time resolution by summation, and then the evaluation analysis has been performed. In order to summarize results, spatial averaged results for each time resolution analysis have been computed and are represented on figure 4.8. RMSE and MBE were rescaled to the same time unit (3hr) to have comparable values along time aggregated series. Threshold values adopted for categorical indexes have been calculated proportionally to time intervals from the value considered for first analysis (e.g. for the last time resolution equal to one month, threshold value is $0.125 \cdot (24/3 \cdot 30)\, mm/(time\ resolution)$).

In figure 4.8, which shows results of this analysis, the comparative performances observed on the maps in figure 4.3 are generally maintained and indexes describe an improvement of results as time aggregation increases confirming similar results obtained by Sohn *et al.* (2010).

MBE levels do not change with the aggregation since this does not affect the ratio between mean bias and mean precipitation. PERSIANN-CCS is confirmed being the less biased product followed by the adjusted products (PERSIANN-Adjusted and TMPA) and other only satellite products while CMORPH presents the highest bias.

RMSE decreases as time aggregation interval increases without relevant differences among products. In the CC subplot PERSIANN and PERSIANN-CCS are particularly under the average performance level described by the others products.

POD and FAR performances improve substantially in the first time intervals and then tend to stabilize. This behavior is observable even for RMSE and CC and 5 days time aggregation interval can be identified and considered as a time scale where performances tend to remain constant.

Finally the computation and representation of spatial averaged time series for the evaluation indexes has been carried out over the study area. Figure 4.9 shows spatial averaged evaluation indexes values for each month, computed considering time resolution equal to 5 days.

MBE analysis confirms that underestimation is concentrated on the precipitation months, then showing a clear seasonal trend.

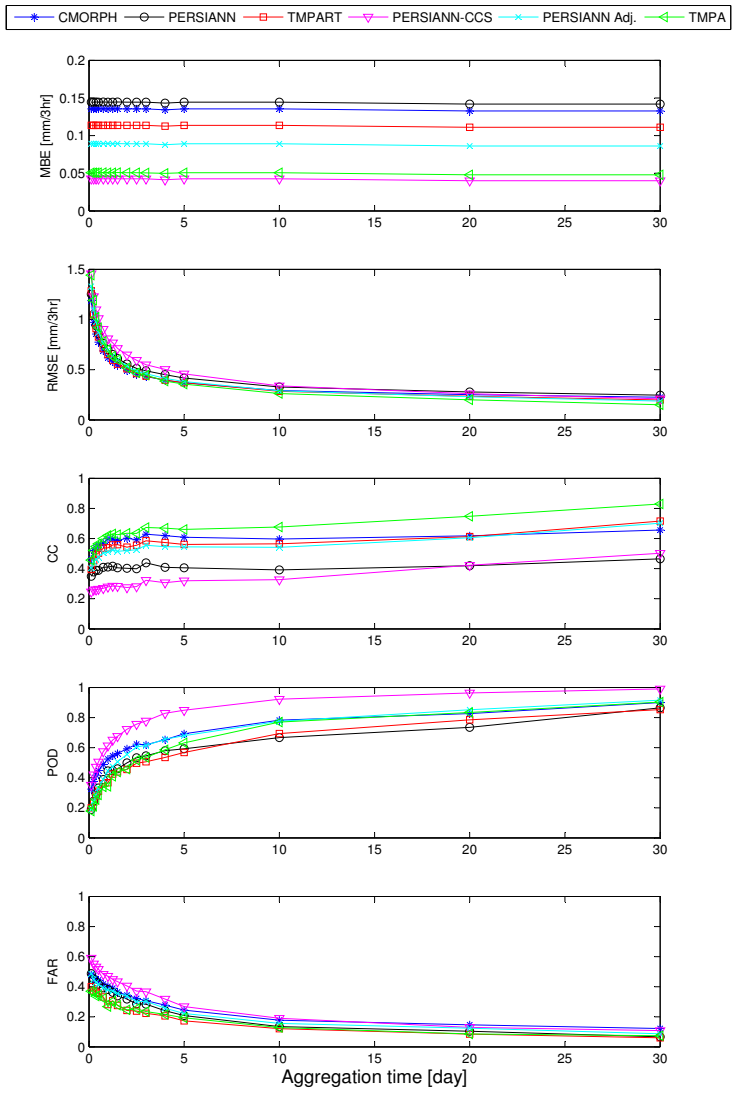

Figure 4.8: Relationship between mean evaluation indexes and time aggregation.

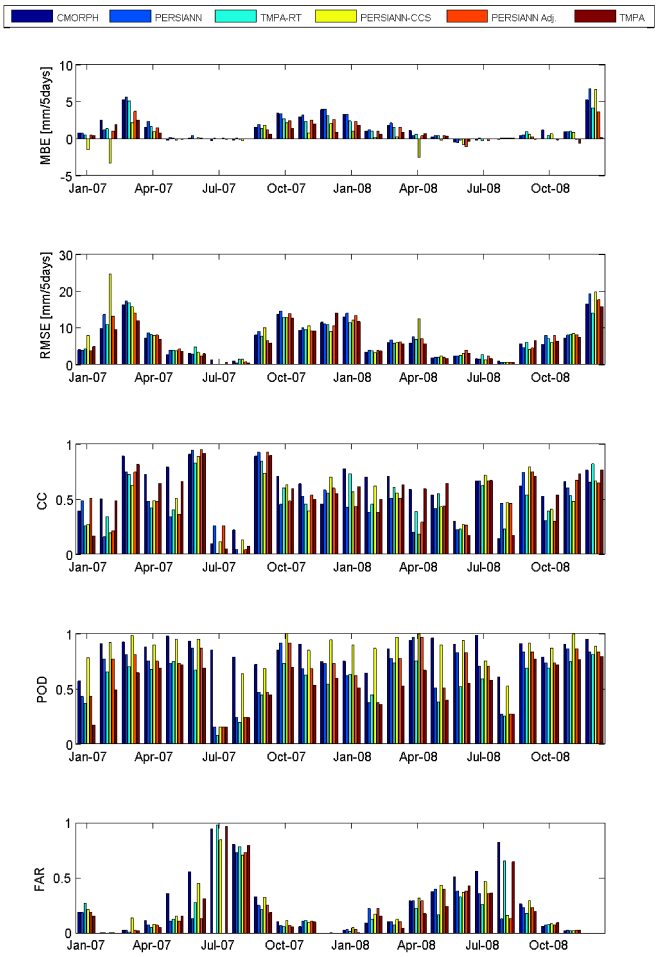

Figure 4.9: Evaluation indexes monthly values.

PERSIANN-CCS is the only product that shows some overestimation occurrences. A seasonal trend is even shown by RMSE values. CC and POD figures show particular low performances for July and August 2007, indicating that much of the few precipitation occurrences have not been detected. Finally FAR values present a seasonal trend with higher values (lower performances) on summer period when many occurrences registered by satellite products do not correspond to true events. Results follow seasonality with greater errors in the winter period (see in particular RMSE and MBE) while a clear and systematic differences among products is not observed.

4.4 Large scale considerations

The issue of the relevant bias in all the satellite products, need to be addressed trying to understand the nature of this inconsistence. As a first step it has been investigated whether it is a problem for the particular study area or it involves a wider area.

In order to address this question the accumulated monthly rainfall global data from GPCP version 2.1 with spatial resolution equal to 2.5^o has been retrieved and compared to similar maps obtained from CMORPH, PERSIANN, TMPA-RT, PERSIANN-Adjusted and TMPA datasets (see figure 4.10) referring to an extension ranging from northern Africa coast to mid-Europe (30^o-50^o latitude).

From a simple observation of these maps it seems that the passage from north Africa climatic regime to the continental European, characterized by a greater amount of annual rain, is to not well captured by satellite products.

Such a result is congruent with Tian and Peters-Lidard (2010) findings that, in a study on the uncertainties of satellite precipitation, observed that they are more reliable over tropical oceans and flat surfaces while complex terrains, coastlines and water bodies, high latitudes and light precipitation show larger measurement uncertainties. In their analysis Europe and Mediterranean area result being characterized by high uncertainty especially during winter. Issues on Europe area have been recently addressed as well by Kidd *et al.* (2012) that reported the overall underestimation by satellite products and addressed some difficulties arising on mid and high latitude such as those related to low intensities, frozen precipitation occurrences and issues with the surface backgrounds. Therefore, weaknesses on the precipitation retrieval process and related improvements, are to be pursued reviewing retrieval algorithms structure and implementation, that is one of the most addressed open issue about satellite precipitation.

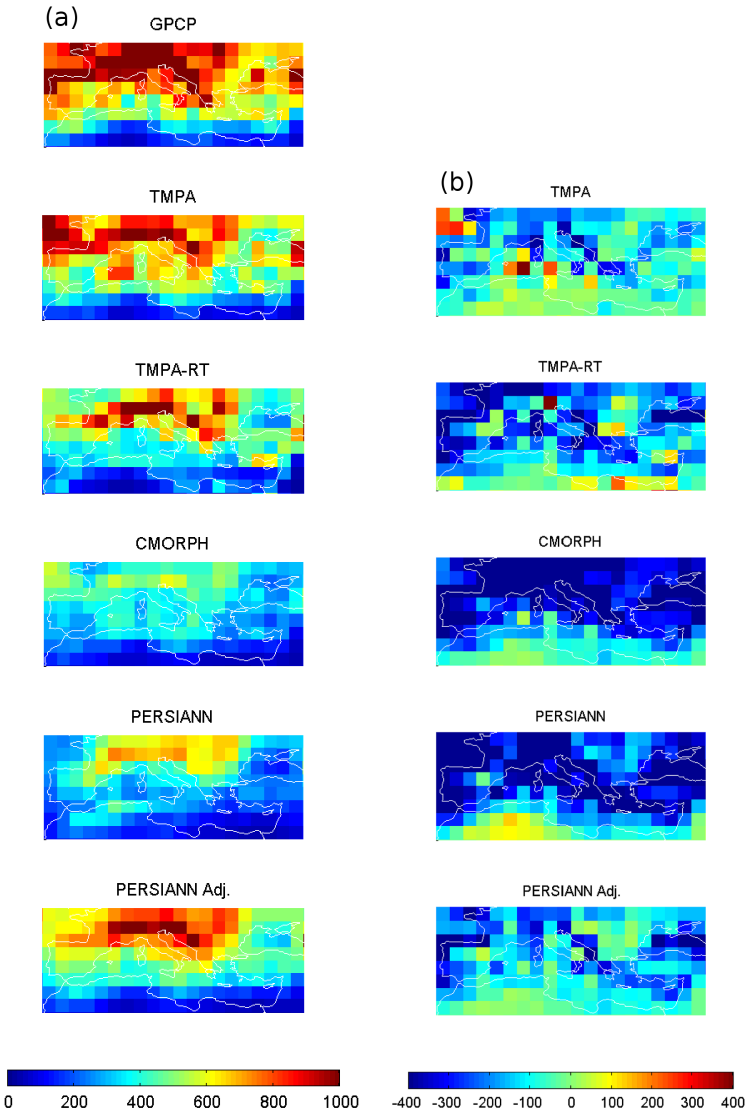

Figure 4.10: Cumulated rainfall maps (a) and annual bias maps (b) (2007-2008) - [mm/year].

As described by the developers of the GPROF algorithm (*Goddard Profiling algorithm*) (Kummerow *et al.*, 2001), retrieval inconsistencies could be due to the PMW algorithm as the meteorological model simulations, currently used in the database feeding the algorithm, are tropical in nature and probably it results in a poor representation of extratropical zones. Panegrossi *et al.* (1998) and Kummerow *et al.* (2006) showed that bayesian PMW retrieval algorithm approaches are characterized by errors due to lack of accuracy of the microphysical details provided by the CRM in the *a priori* database, the completeness of the CRM database and its suitability to represents differences in climate regimes. Even Mugnai *et al.* (2008) pointed out how effective upwelling PMW brightness temperatures and associated radiances profile from CRMs may differ because of uncertainty in microphysical parameterizations. Ryu *et al.* (2010) observed some differences among PMW radiances captured by TMI and those obtained from GPROF for the characteristics of rain systems over the Korean Peninsula. The authors introduced some customization on the CRM simulations that lead to quality results improvement, therefore demonstrating weaknesses of the general algorithm at the local scale. Another case of considerable satellite products biased estimates is reported by Sohn *et al.* (2010) for the Korean Peninsula. Authors highlight that a general underestimation pattern is described by several products due to shared PMW precipitation algorithms and related weaknesses. Moreover they show that even though the gauge-adjusted TMPA seems to have less bias and shows a similar pattern to climatology, it reports increased RMSE values. Therefore authors suggest that TMPA works best when correlation between preadjusted values and gauge measurements is high because adjustments can be made homogeneously throghout the rainfall range.

4.5 GPCC suitability analysis

The evaluation analysis of satellite products, has led to two issues related to estimates bias: the first concerns a systematic underestimation, reported by satellite precipitation, that can be observed on a larger area in the Mediterranean area. Referring to the evaluation literature, this issue is to be studied considering the geographic performances of precipitation retrieval algorithms and their capability to reproduce appropriate meteorological features. The second issue regards the bias reported by adjusted products that are computed incorporating ground-based information by means of GPCP data. Indeed, adjusted products, even though able to reduce the underestimation bias displayed by corresponding only-satellite product, still show a considerable gap referred

to the reference rain-gauge data used in the analysis. This discrepancy could be attributed to different performances between SIAS and the GPCC ground data used by GPCP. Since introducing adjustment procedures is considered as the main direction on reaching reliable estimates, understanding this discrepancy is a key activity on characterizing the potentiality on using GPCP data as reference ground data. In particular the illustrated case study, points out potential weaknesses related to local scales of observation. Here a direct comparison between SIAS dataset used in the evaluation, and the GPCC dataset that provides the rain-gauge information to GPCP (then in turn to the adjusted satellite precipitation products) is performed.

The GPCC *Full Data Reanalysis* monthly dataset with spatial resolution equal to 0.5^o has been retrieved from the web-based delivering service made available by the DWD German meteorological service for the period 2003-2009. These data are analyzed in comparison with the SIAS data for the same period, interpolated at the same spatial and time resolution according with the Natural Neighbor method as previously described. Figure 4.11 shows the monthly spatial averaged precipitation from both datasets. The two series generally show a good agreement. About 80% of occurrences differ less than 20 mm/month and particular strong differences can be observed for specific months. Both underestimation and overestimation by GPCC with respect to SIAS are observed with a prevalence of underestimation occurrences (about 70%).

The MBE, calculated as difference between SIAS and GPCC data, is equal to 6.25 mm/month. Referring to the same time period of the evaluation analysis, that is the 2007-2008 period, the mean bias between GPCC and SIAS is 9.31 mm/month. This value can be compared with the corresponding values reported by PERSIANN Adjusted and TMPA, respectively equal to 21.36 and 12.24 mm/month. This difference is to be attributed to the use of the GPCC *monitoring product* by GPCP whereas here the *Full data reanalysis* has been used, and on the adjusting algorithms used by precipitation products. Figure 4.12 displays the scatterplot of the same spatial averaged series represented on figure 4.11 that still highlights the overall underestimation by GPCC for several months and the general agreement measured by the coefficient of determination.

Figure 4.13 (a) displays the averaged annual values from spatial averaged time series again. It is confirmed the general underestimation presented by GPCC, with 2006 being the only year showing GPCC values greater than SIAS. Figure 4.13 (b), with mean monthly values, shows that the GPCC underestimation is distributed along all the year with the exception of July and October.

Figure 4.14 shows that correlation coefficient values between SIAS and GPCC spatial averaged monthly estimates aggregated by year, keep always

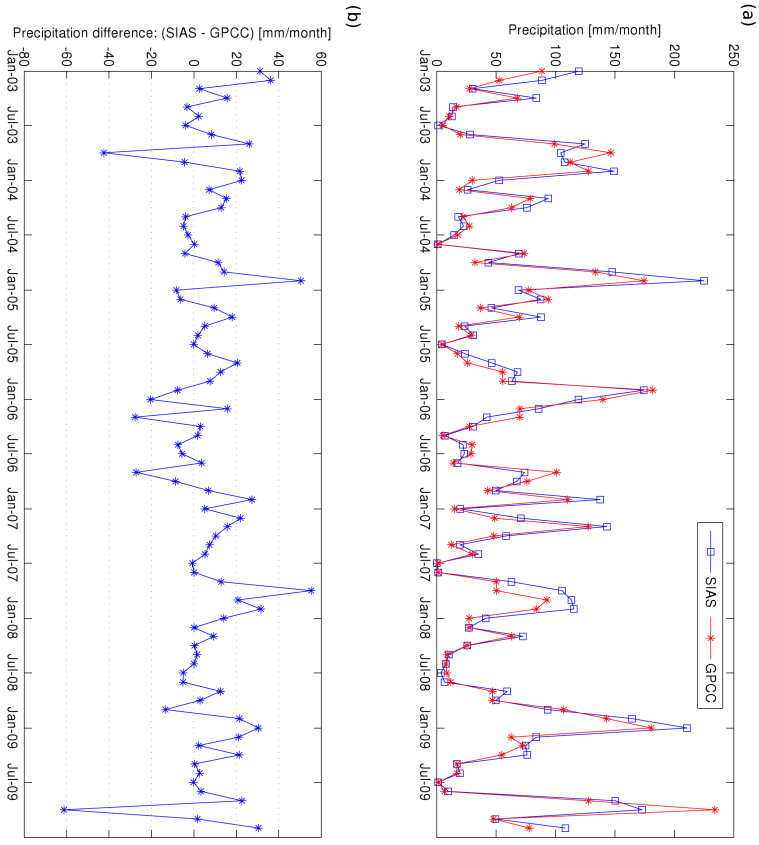

Figure 4.11: Precipitation series from GPCC and SIAS data (a); differences between datasets (b).

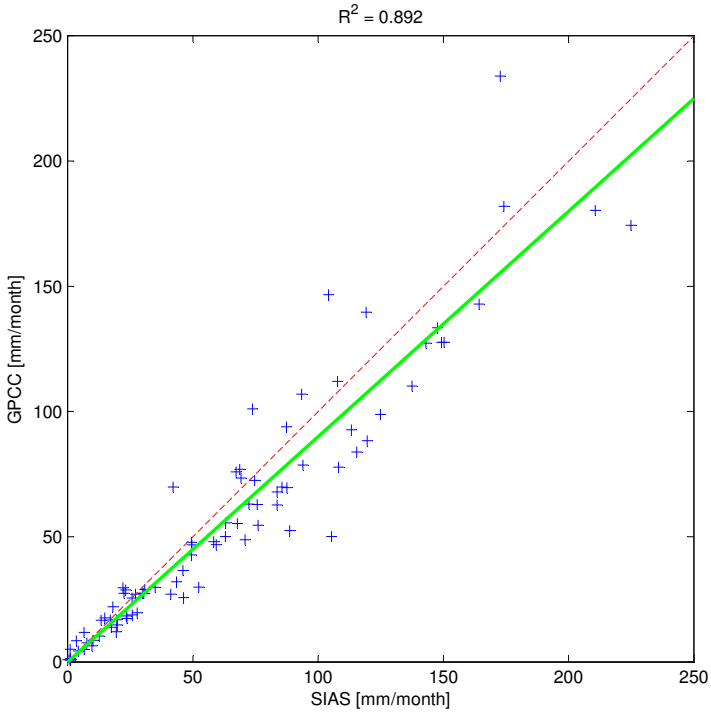

Figure 4.12: Scatterplot of precipitation data for the period 2003-2009.

values up to 0.9. Spatial distribution maps of CC, MBE and RMSE, reported on figures 4.15, indicate that the high elevation area on the eastern, shows low performances for all the indexes. Even for some pixels on western side lower values than those on central area are observed. However CC map displays values always greater than 0.6. MBE map, reports values greater than 40 mm/month for a couple of pixel on the eastern area, where evidently particular issues due to poor sampling on high elevation area are observed. Other underestimation occurrences of GPCC respect to SIAS are observed on the eastern side while some overestimation occurrences are observed, up to about 10 mm/month, in the central area. On the RMSE map, particular high values are observed on the same western pixels where high MBE was detected, while a few poor performing values can be identified on the eastern side and the best performing pixels can be localized on the central area.

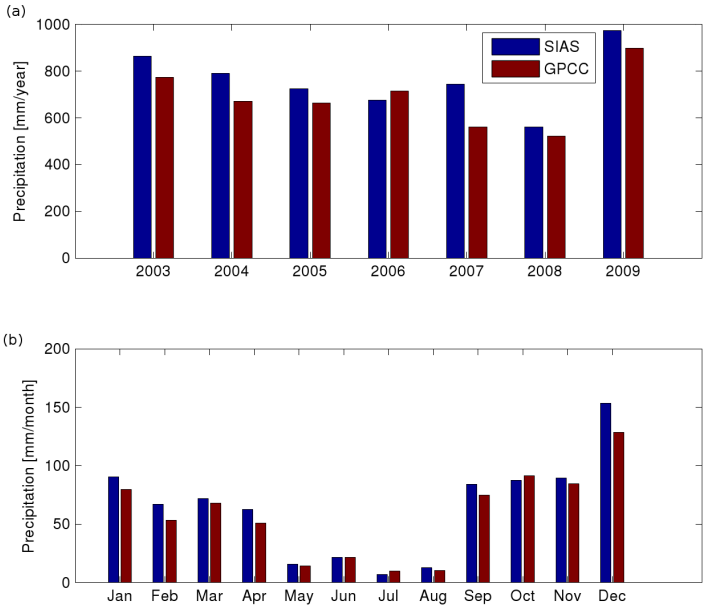

Figure 4.13: Total annual precipitation (a) and mean monthly contribution (b).

In order to understand real capabilities on reproducing precipitation pattern by GPCC, it is useful to observe particular cases where notable average bias is

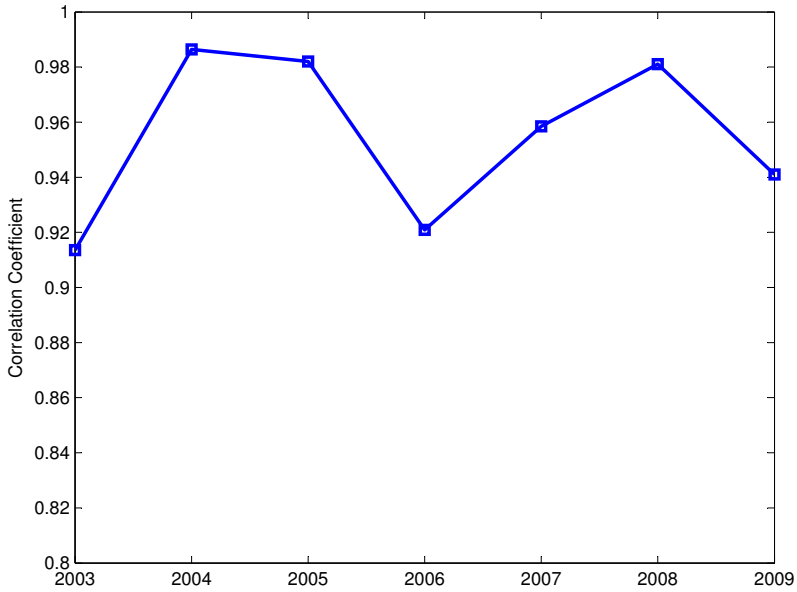

Figure 4.14: Correlation coefficient between SIAS and GPCC spatial averaged monthly values for each year.

reported by GPCC data. A box-plot diagram of spatial averaged differences between SIAS and GPCC maps, built considering distribution within each month (see figure 4.16 (a)), has been used as supporting diagnostic tool, coupled with comparative trend on figure 4.11, to identify such cases. Boxplot on figure 4.16 (b), reporting standardized values of the same values, is even useful on finding out occurrence whit relevant bias respect to the mean value for that month.

Selected observation months are reported on figures 4.17, 4.18, 4.19 and 4.20. As can be inferred from these maps, bias is often due to local strong differences observed in a few pixels. It seems that particular areas show regular bias, such as the Etna volcano corresponding pixel and those related to the Peloritan mountains range as can be observed on the maps for December 2004, September 2005, September 2006 and October 2007. Even western pixels report considerable differences for many occurrences, such as those observed on December 2004 and October 2009 maps. Bias on March 2006 appears equally distributed on

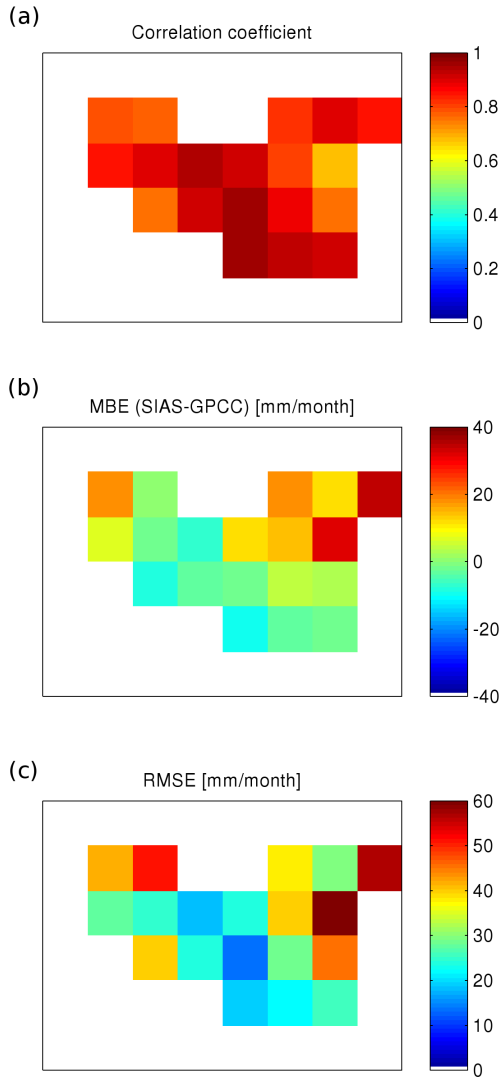

Figure 4.15: Correlation coefficient, MBE and RMSE maps.

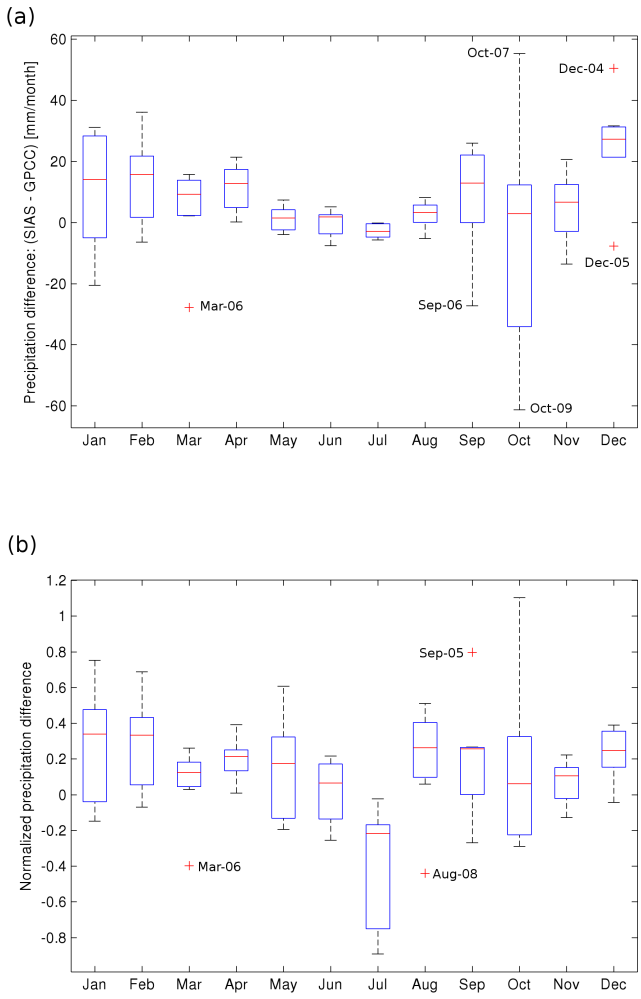

Figure 4.16: Box-plot diagrams of spatial averaged differences (SIAS-GPCC) (a) and normalized values (b). The box has lines at the lower quartile, median, and upper quartile values. Whiskers extend from each end of the box to the most extreme values within 1.5 times the interquartile range from the ends of the box. Outliers (data with values beyond the ends of the whiskers) are displayed with a + sign. Selected relevant extreme occurrences are highlighted with indication of time reference.

the entire area. These cases concerns both underestimation and overestimation occurrences and the main insight is the identification of some pixels regularly concerned by bias issues such as the high elevation areas that are the Etna volcano and the Peloritan mountains range. Moreover a less pronounced trend of lower bias performances can be observed for the coastal pixels.

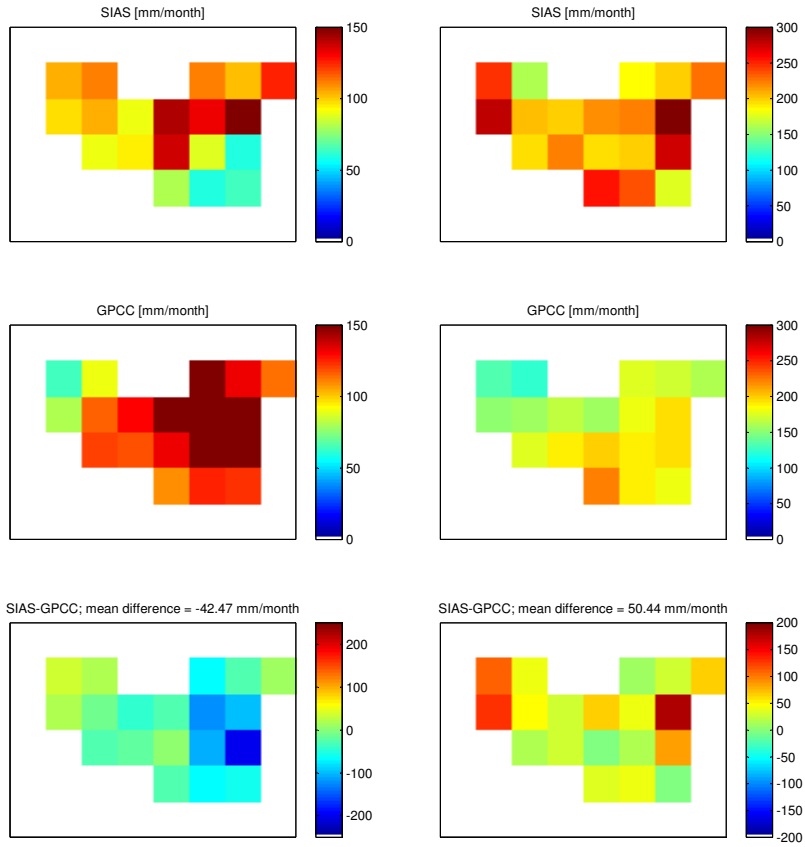

(a) October 2003 (b) December 2004

Figure 4.17: Comparison between SIAS and GPCC data on particular cases.

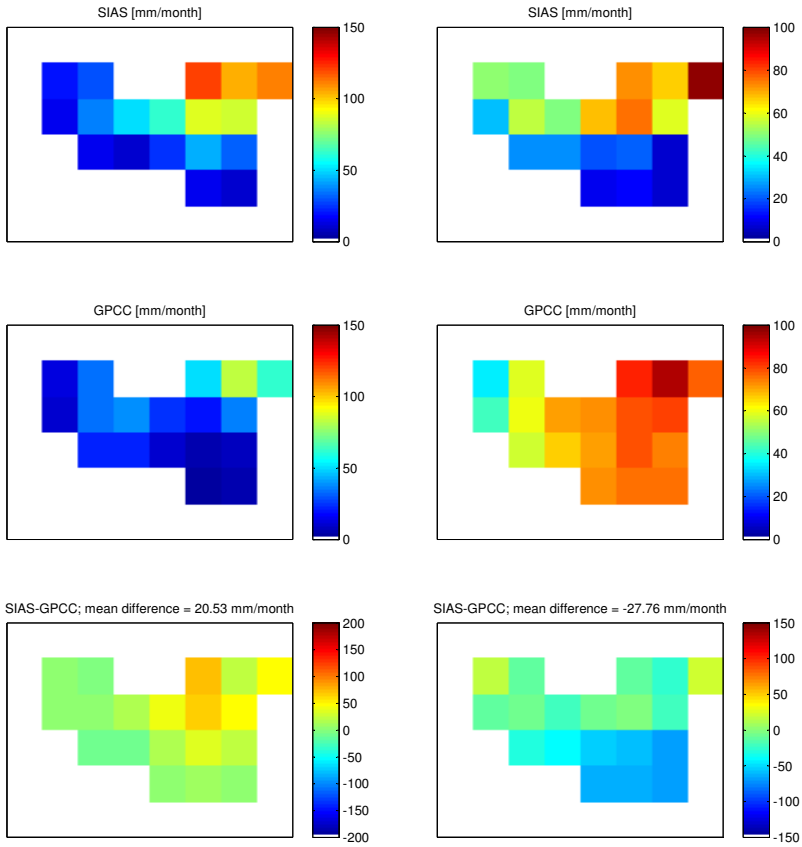

(a) September 2005 (b) March 2006

Figure 4.18: Comparison between SIAS and GPCC data on particular cases.

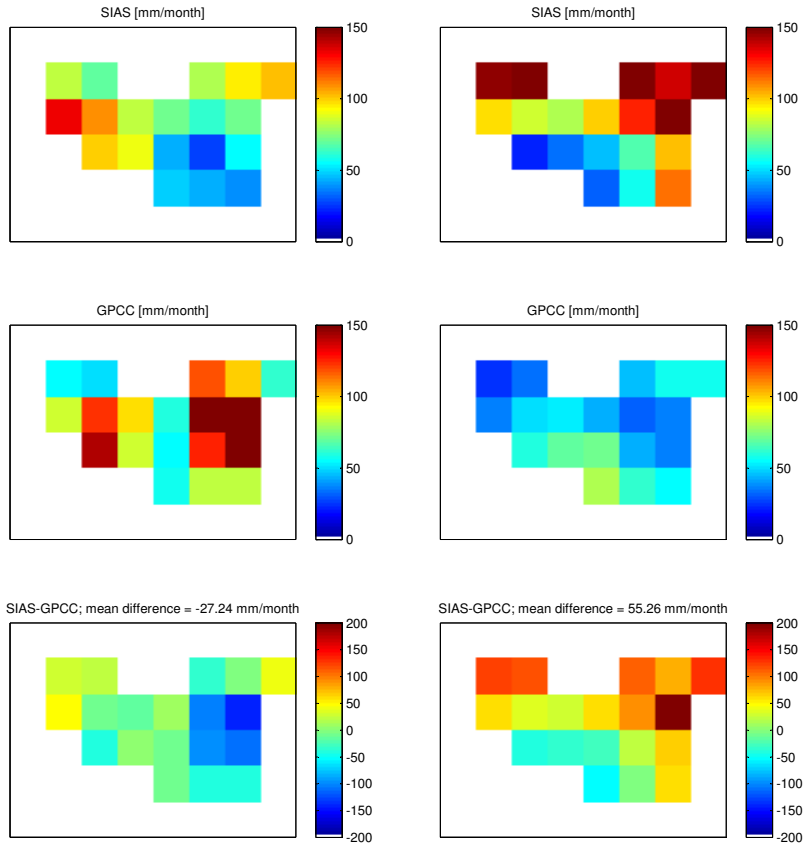

(a) September 2006 (b) October 2007

Figure 4.19: Comparison between SIAS and GPCC data on particular cases.

Given these considerations, it can be supposed that an imperfect depiction of precipitation spatial dynamics, may origin from a poor sampling of average precipitation amounts within each of these large pixels. Both SIAS and GPCC gridded estimates used so far, origin from rain-gauges placed on different positions around the study area. Obviously spatial sampling can affect the statistics

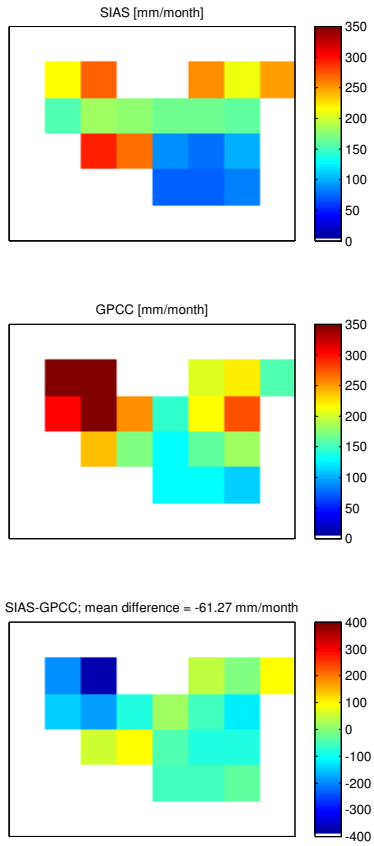

Figure 4.20: Comparison between SIAS and GPCC data on particular cases (October 2009).

of precipitation derived from the same events. GPCC online delivering service, makes available an informative layer with stations density for pixels used on each analysis (see figure 4.21). The low network density can be inferred from this map, but still it is little informative about the relationship between precipitation distribution and sampling performed by stations. Then location of stations used in the GPCC analysis have been requested to the DWD office that made these data available. Figure 4.22 displays positions of stations over Sicilia used in GPCC procedures, SIAS network and a mean annual precipitation map elaborated according to Di Piazza *et al.* (2011).

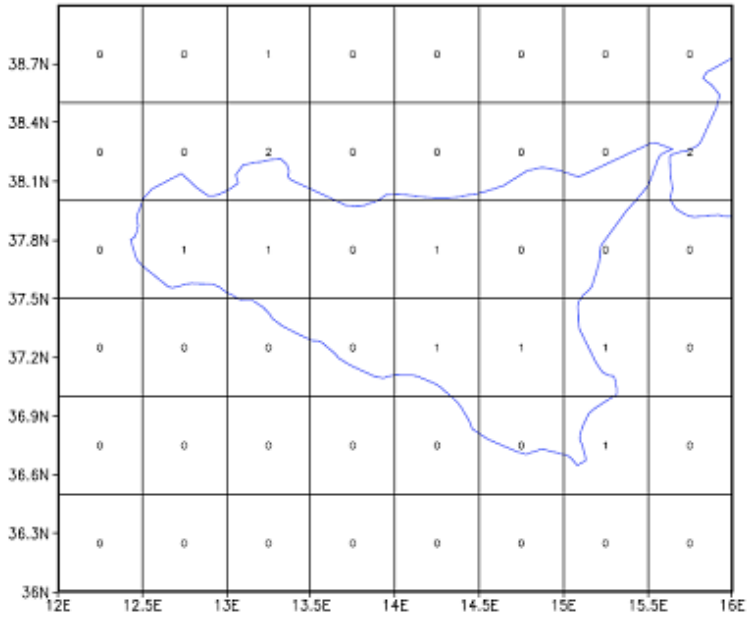

Figure 4.21: GPCC stations density referred to Full product 5, January 2003.

Some GPCC stations are labeled as WMO stations, so it has been supposed that these are characterized by different managing procedures and that the different number of station available for different periods may in part be attributed to the different network sources. One can observe that location of GPCC stations miss a large high precipitation area around Etna volcano and Peloritan mountains range. On figure 4.15 (a) the correlation coefficient map

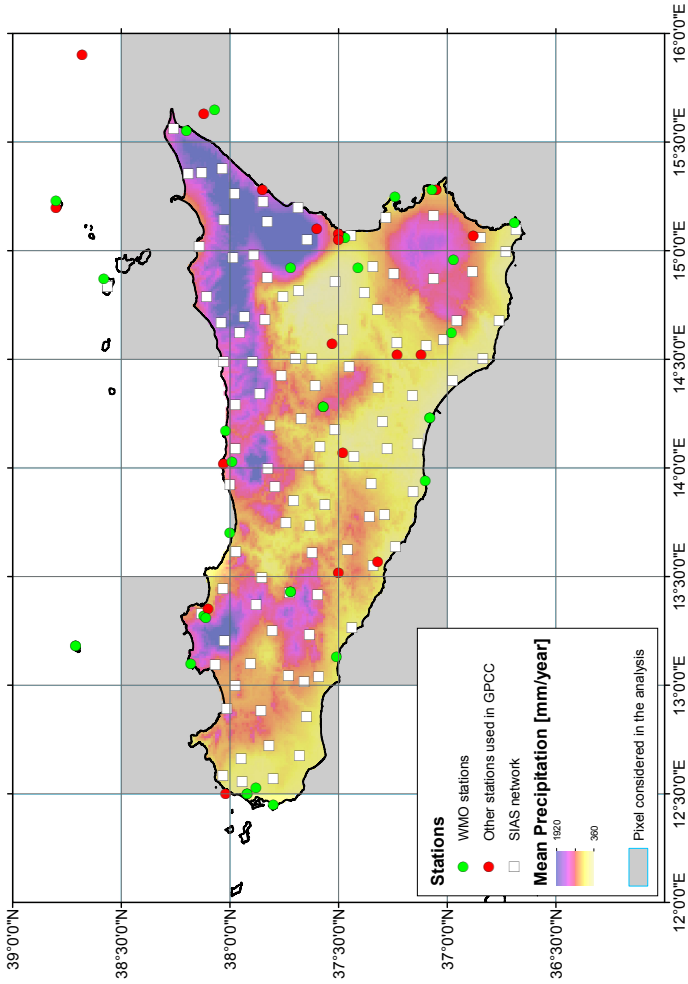

Figure 4.22: GPCC and SIAS stations locations.

obtained from the temporal series for each pixel, reveals that the area around Etna volcano is characterized by a very low level of agreement between SIAS and GPCC. In order to investigate the dependence of network sampling on long term statistics, the mean precipitation map from Di Piazza *et al.* (2011) here considered as the true precipitation distribution on Sicilia, has been sampled using three different network position schemes: the SIAS network, the GPCC stations network and the only WMO GPCC stations. Samples have than been spatially interpolated at the GPCC resolution using Natural Neighbor method as described for the previous analysis. It does not correspond to the interpolation method used by GPCC, but here the objective is not to reconstruct the exact GPCC estimate, but to obtain and compare spatial estimates from different sampling schemes. Mean annual precipitation maps, corresponding to each scheme, are reported in figure 4.23.

Both GPCC and GPCC-WMO schemes report average mean value lower then SIAS that in turn is lower than that provided by the reference map equal to 680 mm/year. Underestimations can be attributed to the sampling gap on the high-precipitation rate area on the Etna volcano and Peloritan mountain range at high elevations. Mean and standard deviation of maps values reported on table 4.4 show that the missed sampling on areas with high mean precipitation leads to the underestimation of both spatial averaged mean and spatial variability of precipitation in the area.

Table 4.4: Mean and standard deviation of precipitation maps obtained according to Di Piazza *et al.* (2011), and considering three sampling schemes corresponding to SIAS network, GPCC stations and GPCC-only WMO stations.

	Mean [mm/year]	STD [mm/year]
Di Piazza *et al.* (2011)	678.79	189.94
SIAS	665.64	147.50
GPCC	617.56	112.04
GPCC-WMO	636.60	117.73

Finally the empirical cumulative distribution functions of these maps, reported in figure 4.24, clearly highlight the missing sampling of higher rate by all schemes and remarkably by the GPCC's schemes.

This analysis confirms the influence of sampling and network density on the capability of precipitation networks to be suited for describing climatological features. In particular the low network density of stations used by GPCC and

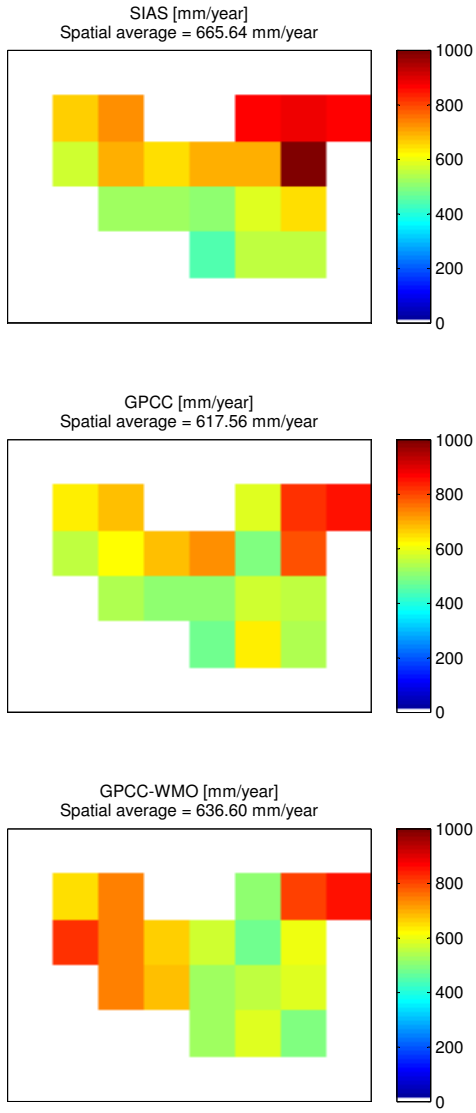

Figure 4.23: Mean annual precipitation maps at 0.5^o spatial resolution by means of sampling using the SIAS network scheme (SIAS), the GPCC stations scheme (GPCC), the only WMO GPCC stations (GPCC-WMO).

in turn by GPCP and satellite adjusted products, affects the effectiveness of achieving an unbiased estimation. Therefore, even though the large temporal resolution on which GPCC data are elaborated, allows for reducing the resources needed to retrieve precipitation information, such a low sampling results being inadequate on given areas and, consequently, leads on an overall underestimation behavior.

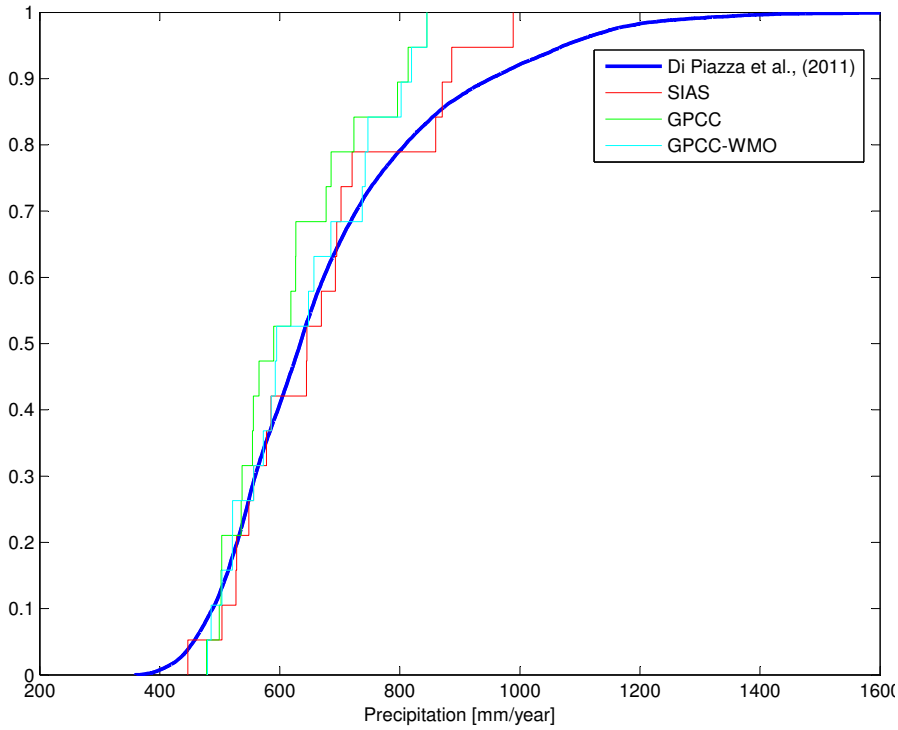

Figure 4.24: Empirical cumulative distributions of reference mean precipitation map (Di Piazza *et al.*, 2011), obtained interpolating samples on the basis of SIAS network positions, GPCC and only WMO GPCC stations positions (GPCC-WMO).

Chapter 5

A post-retrieval enhancement procedure for satellite precipitation estimates

5.1 Precipitation applications and related satellite data suitability

As described on the previous chapters, satellite precipitation estimates show some features that make their usage attractive for several application in many fields. The initial motivation on developing the capability to depict the precipitation distribution on global scale mainly for climatological purposes, has been exploited in a number of possibilities that range from those related to meteorology and NWP prediction models, by means of data assimilation nesting procedures, hydrology models as precipitation input variable, land modeling, hydraulic and hydrologic risk assessment and management, etc. However, the effective usability of main satellite precipitation products, still presents some weaknesses that makes data not suitable for most of hydrological, weather monitoring and meteorology applications. In order to identify potentialities and weaknesses about the practical usage of satellite estimates, an analysis of appli-

cation requirements and corresponding suitability of satellite estimates feature, is needed. Here this analysis has been performed considering main features that result being of interest on evaluating the suitability of a precipitation dataset for a set of typical application fields. These are the data coverage, the temporal and spatial resolutions, the quality assessment by means of evaluation indexes and the availability readiness of data. In order to characterize potential suitability and performance of satellite precipitation estimates, a qualitative analysis of comparison between requested features by each application, and capability of satellite estimates to provide such performances, has been carried out and is summarized on table 5.1 where three application classes (climatology, meteorology and hydrology) have been considered, and colors represent the suitability level for the requested level of performance for the given feature as indicated within corresponding cell. The same analysis has been repeated for weather radar and rain-gauge networks in order to understand relative strengths and weaknesses (tables 5.2 and 5.3).

Satellite precipitation estimates provide a unique possibility of supporting climatology on global scale with the only disadvantages of being a relatively "young" data source, then not allowing to be applied on long time series, and some bias issue that can be observed on the mesoscale and local scale as those highlighted in the evaluation study reported on the previous chapter. These two aspects do not compromise the usage of satellite data for climatological applications since the time length of dataset is nowdays sufficient to most application of interest and however they are usually coupled with other data sources when at time period older than that of satellite data availability is investigated. Bias issues do not affect application at very large scale and maybe they have not been sufficiently highlighted and considered by users community. Meteorology applications require strict performance features in terms of categorical indexes since the exact identification and localization of rain occurrence is essential for providing feasible weather monitoring and forecasting information. For the same reasons, the readiness of precipitation data, that means the availability of precipitation information with a short latency time, or in real time when possible, results being very important and satellite data are nowdays close to be suitable for such a requirement. Hydrology applications, substantially represented by hydrological models, require to estimate rain volume for the investigated event or analysis period, as exactly as possible in order to not affect other variables estimated by modeling hydrological system. Therefore performance indexes are required to be sufficient well performing and, in particular, having an unbiased estimate results being essential.

Radar analysis reported on table 5.2 highlights the good suitability of radar

Table 5.1: Precipitation potential applications and related required features; colours relate to the suitability of satellite precipitation products for each feature: green means that satellite precipitation estimates are suitable for that feature; yellow means that improving that feature is preferably; red means that improving the feature is essential for the usability of that application.

Application	Coverage		Resolution		Performance			Readiness
	Temporal	Spatial	Temporal	Spatial	Unbiasness	Correlation and square error	Categorical indexes	
Climatology	Long	Global-Synoptic	Low	Low	Important	Relevant	Not important	Not important
Meteorology	Short; Event-scale	Mesoscale-Local	High	High	Not important	Important	Important	Important
Hydrology	Event-scale	Local	High	High	Important	Important	Relevant	Relevant

Table 5.2: Precipitation potential applications and related required features with reference to radar suitability.

Application	Coverage		Resolution		Performance			Readiness
	Temporal	Spatial	Temporal	Spatial	Unbiasness	Correlation and square error	Categorical indexes	
Climatology	Long	Global. Synoptic	Low	Low	Important	Relevant	Not important	Not important
Meteorology	Short: Event-scale	Mesoscale-Local	High	High	Not important	Important	Important	Important
Hydrology	Event-scale	Local	High	High	Important	Important	Relevant	Relevant

Table 5.3: Precipitation potential applications and related required features with reference to rain-gauge networks suitability.

Application	Coverage		Resolution		Performance			Readiness
	Temporal	Spatial	Temporal	Spatial	Unbiasness	Correlation and square error	Categorical indexes	
Climatology	Long	Global-Synoptic	Low	Low	Important	Relevant	Not important	Not important
Meteorology	Short: Event-scale	Mesoscale-Local	High	High	Not important	Important	Important	Important
Hydrology	Event-scale	Local	High	High	Important	Important	Relevant	Relevant

data for meteorological applications given its capability of providing precipitation in real time, feasible rain detection that results in a good categorical indexes performances, and suitable spatial and temporal scales. While its usage for climatological application usually is not considered because of reduced spatial and temporal coverage (even though collection of radar information can be considered for some climatological considerations), the hydrological suitability is affected only by possible bias issues. When such an aspect can be addressed by means of rain-gauge availability, it is possible to fully exploit radar potentialities. Obviously radar usage is subject to the presence of an installation and typical related issues, have to not affect the measurement.

Rain-gauge networks provide the time longest available precipitation data source, then they are considered the reference dataset for climatological analyses involving older periods. From a climatological point of view, a fundamental limitation of rain-gauge network arise from the missing observation on the oceans being such a source limited on land areas. Meteorological potentialities of rain-gauge networks are strongly limited by their spatial representativeness given by point measurements and readiness performances since often the availability of ground data is subject to delay due to collection and managing of data. Finally using rain-gauge network data for hydrological applications, even though that is the traditional way of introducing precipitation data into models, suffers for point representativeness issues, intended both in terms of spatial coverage and resolution. Beyond application specific potentialities, rain-gauge network data are fundamental as coupled reference information for correcting and adjusting other sources.

Therefore satellite estimates, radar and rain-gauge network measurement, complement each other on several aspects related to performances requested by the simplified application framework considered. Many possibilities on coupling different sources have been exploited by each application family, and in particular the usage of rain-gauge data, as reference source for both satellite estimates and radar measurements, is ordinary applied. Weather radar have introduced a new way on retrieving precipitation information that fills the spatial representativeness and resolution weaknesses of rain-gauge networks. However the sparse distribution and the missed sampling over the sea, leave feature gaps for large scale climatological applications and usage on areas uncovered.

Finally satellite precipitation estimates set a new era on the knowledge of precipitation, since they allow for having spatial global complete estimates all world around. Such a potentiality, that typically is of climatological interest, is supported by efficient retrieving, elaboration and delivering systems that makes these estimates available with a short latency time, and are experiencing in-

creasing performance levels due to sensors and algorithms improvements.

In particular, potentialities on using satellite estimates for hydrological applications, may be highlighted, motivated by their coverage that ensure the presence of such an estimate almost everywhere and can results being the only available data source when radar and rain-gauge networks are not available.

Given this "depiction" of satellite precipitation potentialities referred to applications, it is useful considering possible improvement procedures that can increase their suitability once they are retrieved. Some of the most important procedures that can be considered are the following:

- spatial and temporal downscaling;
- bias adjustment and correction procedures using ground data;
- improvement of sensors and satellite missions;
- improvement of precipitation retrieval algorithms;
- improvement of data elaboration and delivering services.

Bias adjustment and spatial downscaling result being particularly interesting because of their practicability on satellite estimates and the strong impact on feature improvements. Moreover a bias adjustment procedure results being essential for the Mediterranean area given the results from the evaluation analysis presented in the previous chapter. Therefore a coupled bias adjustment and spatial downscaling procedure has been studied and realized for the study area of Sicilia starting from the SIAS rain-gauge network and meteorological information provided by a re-analysis dataset.

5.2 Bias adjustment procedures

Blended approaches of LEO and GEO satellites information provide precipitation estimates that keep the strength from each system. But without referencing to the ground measurement, still these precipitation estimates may be biased from surface rainfall. Additional measurement from gauges helps to reduce bias from satellite measurement. Although improvement has been made from merging satellite and gauge measurements at monthly scale or even for providing adjustment at daily scale based on global monthly gauge measurement (Xie and Arkin, 1997; Huffman *et al.*, 2001), a fine-scale precipitation measurement at sub-daily scale is needed for many hydrologic applications. Currently

the most practical approach to reduce these errors is to merge ground-based measurements from rain gauges or radar networks. A leading example is the TMPA (TRMM research product 3B42 version 6) (Huffman *et al.*, 2007, 2010) produced at the NASA-GSFC. After merging intercalibrated PMW retrievals from multiple space-borne sensors, and filling PMW coverage gaps with IR-based estimates, TMPA uses the monthly accumulation of global surface gauge measurements to rescale the satellite-based estimates in post-real time. This procedure results in estimates with substantially reduced biases, especially on the time scales of a month or longer. Smith *et al.* (2006) used the median of the long-term mean values from an ensemble of satellite-based products as the reference value, to estimate and then reduce biases in satellite-based estimates, especially over the ocean when gauge data do not exist. This method works best when the errors in different satellite-based estimates are independent, but this condition is usually not satisfied. The *Air Force Weather Agency* (AFWA) has produced a real-time global precipitation analysis, based on PMW and IR retrievals, superseded by gauge reports from the WMO's GTS. But the gauge reports available from GTS in real time are rather sparse in space, and this approach leaves some artifacts that result from the disparity between satellite-based estimates and isolated gauge reports (Tian *et al.*, 2009). Recently Xiong *et al.* (2008) and Janowiak *et al.* (2009) proposed a procedure to correct the CMORPH data in real time. This procedure first performs bias correction for CMORPH with the PDF-matching technique against real-time global daily rain gauge data. Then it combines the corrected CMORPH with the gauge analysis itself with the *optimal interpolation* (OI) technique. Their test results over China showed substantial improvements in the merged CMORPH analysis. Over continental US (CONUS), Boushaki *et al.* (2009) used the real-time CPC daily gauge analysis (Higgins *et al.*, 2000) to correct the PERSIANN-CCS data, and the corrected data show dramatic improvements over test areas in the southwestern United States. A critical requirement in the existing gauge-correction schemes is the availability of gauge data as timely as that of the satellite-based estimates. Otherwise, gauge correction in real time is not possible; one has to resort to an approach similar to TMPA with a monthly scale correction, at the price of a latency in the availability of such data products. However, the number of gauge reports available in real time over the globe is rather limited; a significant number of gauge reports, such as those within the WMO's GTS, are issued with various delays. In addition, many regions over the world, including the United States, are seeing many weather stations disappear recently (Stokstad, 1999), leaving only historical data available. For example, there were over 18,000 daily gauge reports over United States before 2004, but

there have been less than 10,000 since 2004 (Chen *et al.*, 2008). In China, there had been around 700 hydrological stations before they ceased to operate in 1997 (Xie *et al.*, 2007). Finally, collecting, processing, and quality-controlling real-time gauge reports are logistically tedious and complex. Therefore, it is highly desirable to explore a new approach to reduce the biases in the satellite-based estimates in real time, without depending on the timely availability of surface gauge observations. Tian *et al.* (2010) proposed a scheme to explore this possibility. This new scheme is based on the observation that the error characteristics in satellite-based estimates are remarkably consistent. For example, over CONUS, estimates for summer show regularly positive biases (overestimates), while those for winter suffer negative biases (i.e. underestimates) (Tian *et al.*, 2010). In addition, most of the errors are caused by hit biases, meaning the satellite-based estimates have sufficient capability in detecting precipitation events, but are short in determining the correct rate rates of the events. Therefore, authors developed a Bayesian approach to "train" an algorithm with the coincidental satellite and gauge data within a recent historical period. This algorithm essentially establishes a statistical relationship between coincidental gauge measurements and satellite estimates. Then this "learned" relationship is applied to real-time satellite estimates, when gauge data are not available, to derive the mostly likely values of gauge measurements as the corrected satellite estimates.

5.2.1 Local bias adjustment for Sicilia

The procedure proposed here as bias adjustment correction step, is based on that described by Tian *et al.* (2010). Authors developed a Bayesian approach to "train" an algorithm with the coincidental satellite and gauge data within a recent historical period. This algorithm essentially establishes a statistical relationship between coincidental gauge measurements and satellite estimates. Then this "learned" relationship is applied to real-time satellite estimate, without using time-corresponding gauge data, to derive mostly likely values of gauge measurements as the corrected satellite estimate.

In order to achieve a more robust procedure, it has been decided to apply the bias estimation on spatially averaged values and successively distributing this estimated bias on pixels.

Correction is based on the following Bayesian relationship between spatial average satellite estimate and timing corresponding spatial average rain-gauge value, denoted respectively as $\bar{G}_i$ and $\bar{S}_j$ (note that here indices i and j are used

just to identify different values on precipitation intensity range):

$$p\left(\bar{G}_i|\bar{S}_j\right) = \frac{p\left(\bar{G}_i, \bar{S}_j\right)}{p\left(\bar{S}_j\right)}$$

Conditional probability $p\left(\bar{G}_i|\bar{S}_j\right)$ gives the likelihood of a gauge spatial average measurement $\bar{G}_i$ when a satellite-based estimate has the value $\bar{S}_j$, and it is calculated by means of Bayes's theorem, using joint probability $p\left(\bar{G}_i, \bar{S}_j\right)$ and satellite estimates probability $p\left(\bar{S}_j\right)$ empirical estimates. Since all the terms on the right-hand side of this equation can be computed from a training gauge-satellite precipitation dataset, most probable value of the gauge measurement can be calculated given any $\bar{S}^*$ from the probability distribution $p\left(\bar{G}_i, \bar{S}^*\right)$ e.g. as that corresponding to the maximum probability value.

As highlighted by authors, this approach is effective when error characteristics are remarkably consistent (i.e. seasonality of errors is systematically reproduced) and are mainly caused by hit biases, meaning that satellite estimates succeed on detecting precipitation occurrences, but provide a biased estimate. Here such assumptions are not checked for the study area and considered datasets; moreover from the evaluation study exposed on the previous chapter, it can be stated that bias is due to both missed occurrences detection and biased values.

Nevertheless, in this study emphasis is put on achieving a first satellite bias-corrected estimate in real-time with respect to the satellite retrieving time. Furthermore, such a procedure will result more well performing as improvements on estimating precipitation using satellite data, in particular in terms of detection capabilities, will be achieved by algorithms. Therefore it has been reputed useful exploring potentialities of such a procedure in order to have a tool to perform bias adjustment as satellite data become available.

Implementation of this method requires a training dataset with both a satellite precipitation product data (S) and a reference dataset (G), in order to estimate the conditional distribution $p\left(\bar{G}_i|\bar{S}_j\right)$. Such a procedure has been carried out in this study using CMORPH data and interpolated SIAS rain-gauge network data (as used on the evaluation analysis), for the period 2003-2009.

Given satellite and reference data, joint probability distribution $p\left(\bar{G}_i, \bar{S}_j\right)$ has been estimated as their empirical bivariate frequency distribution and $p\left(\bar{S}_j\right)$ as empirical frequency distribution for the satellite data. In order to increase the number of samples for more stable statistics, rain-rate values have been discretized into logarithmic bins, to keep the number of strong events sufficiently large, and the events distribution closer to normal distribution.

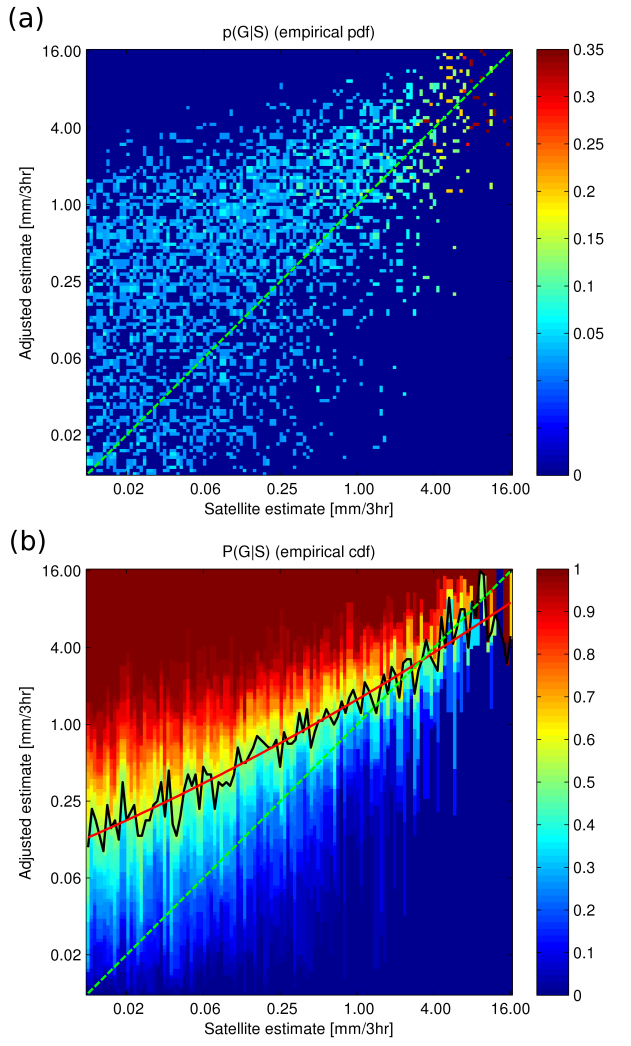

Figure 5.1: (a) Representation of $p\left(\bar{G}_i|\bar{S}_j\right)$; (b) Representation of $P\left(\bar{G}_i|\bar{S}_j\right)$ (empirical cumulative distribution function) along with empirical median values and corresponding second order polynomial approximation function (on log-log space).

Conditional distribution $p\left(\bar{G}_i|\bar{S}_j\right)$ obtained is represented on figure 5.1 (a). It has been decided to estimate adjusted satellite value $\bar{S}^{adj}$ corresponding to an input value $\bar{S}^*$, as the median of the probability distribution $p\left(\bar{G}_i|\bar{S}^*\right)$. The following second order polynomial approximation, that constitutes the final bias adjustment relationship, has been fitted to empirical median values obtained from $p\left(\bar{G}_i|\bar{S}^*\right)$ for the entire range of $\bar{S}$ values:

$$\bar{S}^{adj} = exp\left(0.0156 \cdot log\left(\bar{S}\right)^2 + 0.5886 \cdot log\left(\bar{S}\right) + 0.4490\right)$$

Figure 5.1 (b) reports *cdf* of conditional distribution along with median values and adopted polynomial approximation. On both figures 5.1 underestimation of satellite products respect to SIAS reference data can be observed.

Once the spatial average bias is estimated for the entire area, it is spatially partitioned proportionally on pixels based on their precipitation value using the following expression:

$$S_k^c = S_k + \left(\bar{S}^{adj} - \bar{S}\right)\frac{S_k}{\bar{S}}$$

where S_k identify the satellite estimate on the *k-th* pixel and S_k^c the related corrected value.

5.3 Spatial downscaling procedures

The need for developing downscaling methods derives mainly from the gap existing between the precipitation forecast needed to support particular hydrological application, such as forecasting of flood events even in small mountain catchments and urban areas, and those provided by *limited-area meteorological models* (LAMs). Such meteorological models are numerical limited-area models based on parameterizations of turbulent convection and of cloud microphysics, that are routinely employed for regional meteorological forecasts and are usually nested into the output of *General Circulation Models* (GCM). Cloud-resolving models, on the other hand, deal explicitly with turbulence and microphysics and they can reach much smaller scales, but cannot run over large domains due to computational constraints. Indeed floods forecasting applications usually require knowledge of the precipitation field down to scales of a few square kilometers and tens of minutes (Castelli, 1995; Ferraris *et al.*, 2002), whereas LAMs are able to provide precipitation forecasts on scales of about 100 km^2 and a few hours. One option to fill the scale gap and to obtain small-scale rainfall estimates is based on the use of stochastic models for rainfall downscaling. A

typical downscaling procedure is based on the implementation of a stochastic disaggregation algorithm that is capable of generating a small-scale fluctuating field from a smoother rainfall distribution on larger scales. In principle, this approach provides random precipitation fields that should simultaneously satisfy the large-scale constraints imposed by meteorological forecasts (e.g. the expected average rainfall intensity) and are consistent with the known statistical properties of the small-scale rainfall distribution. For example, the power spectrum of a precipitation field produced by a downscaling procedure should smoothly merge, at low wave numbers, with that predicted by meteorological models on larger scales, and it should reproduce, at high wave numbers, the power spectra of rainfall fields measured under similar circumstances. Note, also, that a rainfall field produced by a downscaling procedure should never be taken as the rainfall distribution that is to be expected but rather as one possible realization of it. Repeated application of the downscaling procedure naturally leads to an ensemble of possible realizations of the small-scale rainfall field and to the concept of ensemble rainfall prediction (Ferraris *et al.*, 2002). Clearly, stochastic disaggregation is not a substitute for a physically based dynamical model, but it can be seen as a way to resolve variability at scales smaller than those currently resolved by physical models. In past years, several stochastic models for rainfall downscaling have been proposed. In particular, disaggregation models can be grouped into three main categories:

1. point processes based on the random positioning of a given number of rainfall cells (Waymire *et al.*, 1984; Rodriguez-Iturbe *et al.*, 1986; Eagleson *et al.*, 1987; Northrop, 1998; Wheater *et al.*, 2000; Willems, 2001)

2. simple autoregressive processes (Mejia and Rodriguez-Iturbe, 1974; Bell, 1987; Guillot and Lebel, 1999) sometimes called "meta-Gaussian" models;

3. fractal cascades (Lovejoy and Mandelbrot, 1985; Schertzer and Lovejoy, 1987; Gupta and Waymire, 1993; Over and Gupta, 1996; Perica and Foufoula-Georgiou, 1996a; Menabde *et al.*, 1997a,b, 1999; Deidda *et al.*, 1999).

Mixed models, combining some of the above approaches, have also been proposed (Veneziano *et al.*, 1996; Veneziano and Iacobellis, 2002).

5.3.1 Spatial downscaling procedure for Sicilia

Downscaling procedure used in this study is based on that proposed by Perica and Foufoula-Georgiou (1996a,b). Authors define multiscale rainfall fluctua-

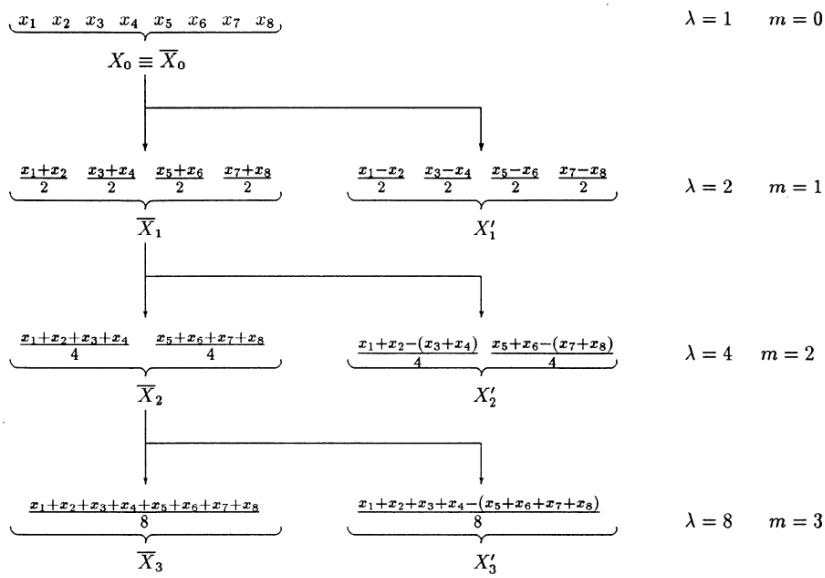

Figure 5.2: Schematic representation showing the concept of fluctuations for a discrete one-dimensional process. Relative scales λ and scale indices m ($\lambda = 2^m$) are also indicated in the figure (Perica and Foufoula-Georgiou, 1996a).

tions considering successive aggregations of a process at different spatial scales. With reference to a discrete one-dimensional process, figure 5.2 reports a representation of such a multiscale process, and derivation of average values and fluctuations for each scale.

Following this model, precipitation data from different spatial scales, can be related each other by means of a statistical model where parameters can be estimated using meteorological characterization. The variable on which the statistical characterization is applied is the standardized precipitation fluctuations:

$$\xi_{m,i} = \frac{X'_{m,i}}{\overline{X}_m}$$

where m is the scale index, i a direction parameter equal to 1, 2 or 3 respectively for horizontal, vertical and diagonal fluctuations, $X'_{m,i}$ is the precipitation fluctuation at scale m and direction i, while $\overline{X}_m$ is mean value of precipitation

field X. Hypotheses of gaussianity and presence of dynamic scaling are verified for standardized fluctuations on the spatial range 4-64 km. Therefore parameters of this gaussian distribution, μ and $\sigma_{m,i}$ are evaluated using the following expressions:

$$\mu = 0$$
$$\sigma_{m,i} = 2^{(m-1)H_i}\sigma_{1,i}$$

where H_i and $\sigma_{1,i}$ are model parameters relatively to the i-th direction. Authors verified that directionality can be neglected, since results corresponding to different directions do not significantly differ each other, and that parameters are related to a meteorological variable named CAPE (*Convective Available Potential Energy*) referred to the pre-event time. This relationship allows for estimating model parameters by means of empirical expressions:

$$H = 0.0516 + 0.9646\left(CAPE \cdot 10^{-4}\right)$$

$$\sigma_1 = 0.5390 - 0.8526\left(CAPE \cdot 10^{-4}\right)$$

Authors verified these relationships for values of CAPE between 1000 and 3000 J/kg. Note that in these equations spatial scale $m = 1$ corresponds to $L = 4$ km, and than other scales are obtained for aggregation, leading to $m = 4$ corresponding to $L = 64$ km that roughly approximates the spatial resolution of satellite data, i.e. 0.25^o. Such references are maintained hereafter.

As highlighted by Perica and Foufoula-Georgiou (1996a) positive correlation between CAPE and H and negative correlations between CAPE and σ_1 are explained based on physical and statistical arguments. It is known, for instance, that there are positive correlations among the maximum and mean rainfall rates and the corresponding measures of convective energy (Zawadzki and Ro, 1978; Zawadzki *et al.*, 1981). In general, high CAPE values coincide with high observed rainfall intensities. It is also well known that there exists a strong spatial dependence in observed rainfall rates, i.e. high rainfall intensities are more likely to occur in the neighborhood of pixels with high rainfall intensity, which implies relatively small gradients (fluctuations) of the field. In general, this results in small variability of the rainfall fluctuations and, since the fluctuations are symmetric around zero mean, in small absolute values of the fluctuation processes $X'_{m,i}$ relative to the variability of the corresponding process $\overline{X}_m$ at the same scale. This difference is much more pronounced for storms with high intensities than for the low-intensity storms. Having in mind that the standardized fluctuations are defined as the ratios between the fluctuations and the corresponding average field, and that these fields are highly

dependent, the variability of the standardized fluctuations at scale $m = 1$ described through parameter σ_1 is in general lower for higher-intensity storms. Therefore, since storms with high rainfall rates have smaller σ_1 estimates and higher CAPE estimates, it follows directly that the correlation between CAPE and σ_1 values is negative. As we proceed with averaging of the rainfall process at larger scales $m > 1$, the differences between the average $\overline{X}_m$ and gradients $X'_{m,i}$ at the same scale decrease. Accordingly, that implies higher dispersion in the probability density functions of the standardized fluctuations and higher σ_m estimates. Differences in σ_m estimates between storms with different intensities become less and less noticeable as the scales becomes larger and larger. This implies weaker correlation between σ_m and CAPE for $m > 1$.

In order to study the applicability of such a formulation for downscaling of satellite precipitation data with reference to Sicilia area, CAPE data have been retrieved and examined from the ERA40 Re-analysis dataset (*European Centre for Medium-Range Weather Forecasts, ECMWF 40 Year Re-Analysis*) for the period 2003-2009. Figure 5.3 (a) shows mean precipitation and CAPE values at monthly scale. Seasonality can be observed on both the series, but it results being opposed displaying high precipitation and low CAPE values in winter and low precipitation and high CAPE in summer. Moreover figure 5.3 (b), reporting the correlation coefficient within each month, show that during winter months, precipitation and CAPE estimates result being considerably correlated.

This relationship is confirmed on figure 5.4 where values for January 2007 are reported. At this scale a diurnal cycle is revealed by CAPE that is not reproduced by precipitation values. Interpretation of this relationship is not trivial since an accurate investigation of meteorological dynamics would be necessary. In particular winter CAPE values result being too low to be considered representative of convective events. CAPE values shown by ERA40 dataset do not fall into the range on which Perica and Foufoula-Georgiou (1996a) verified relationships for estimating H and σ_1. Figure 5.5 gives a representation of these relationships and the approximate indication of CAPE range observed in Sicilia according to ERA40 dataset.

Therefore, another way to estimate H and σ_1 has been investigated. Considering that CAPE results being strongly related to precipitation magnitude and that probably convective precipitation rarely occurs particularly during winter season, new formulation is searched considering precipitation at pre-event time instead of CAPE. Such a formulation would allow for providing a real-time downscaling operation. The characterization of σ_1 would requires the knowledge of precipitation rain-rate at that scale (about 4 km). Here such an information is not available, and only the rain-rate at scale $m = 4$ (about 64 km) can be

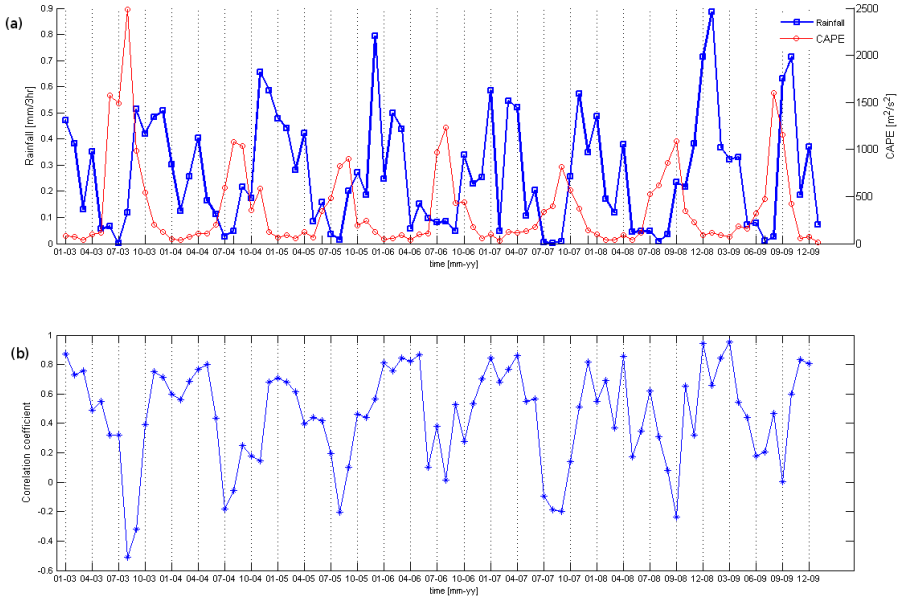

Figure 5.3: Monthly precipitation (interpolated SIAS data) and CAPE estimates (ERA40) temporal series for Sicilia (top) and correlation within each month (bottom)

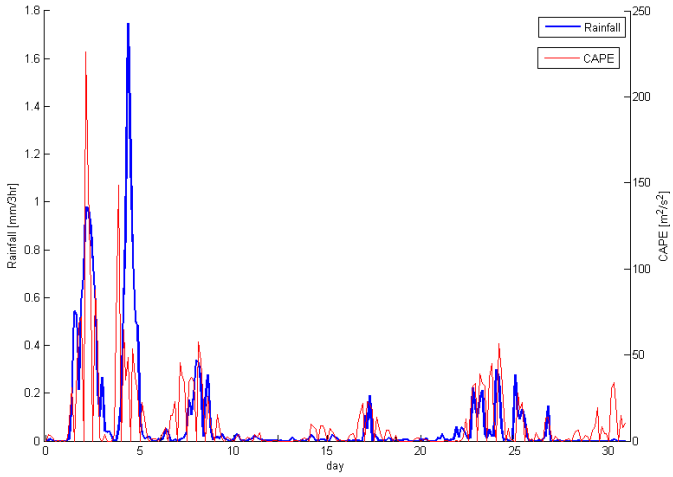

Figure 5.4: Precipitation and CAPE values for January 2007

analyzed. For this reason the dynamic scaling property is considered in order to derive a formulation that uses σ_4 in place of σ_1 as reference value to estimate other σ_m:

$$\sigma_m = 2^{(m-4)H}\sigma_4$$

The existence of a relationship between precipitation rain-rate and standard deviation referred to spatial distribution of standardized precipitation fluctuations, has been investigated. Such values have been computed for the entire period of data availability. Figure 5.6 displays spatial averaged σ_4 values obtained from each temporal step, with reference to corresponding log-scaled spatial averaged pre-event precipitation rain-rate. The presence of a relationship that describes decreasing σ_4 values for lower precipitation rain-rate can be observed. The following second-order polynomial approximation has been estimated and represented on figure 5.6 above empirical points:

$$\sigma_{m=4} = 0.0211 \cdot [logP]^2 - 0.1573 \cdot [logP] + 0.7889.$$

Exploring a relationship between H and precipitation rain-rate, requires the knowledge of σ_m at two different spatial scale, in order to estimate empirical H

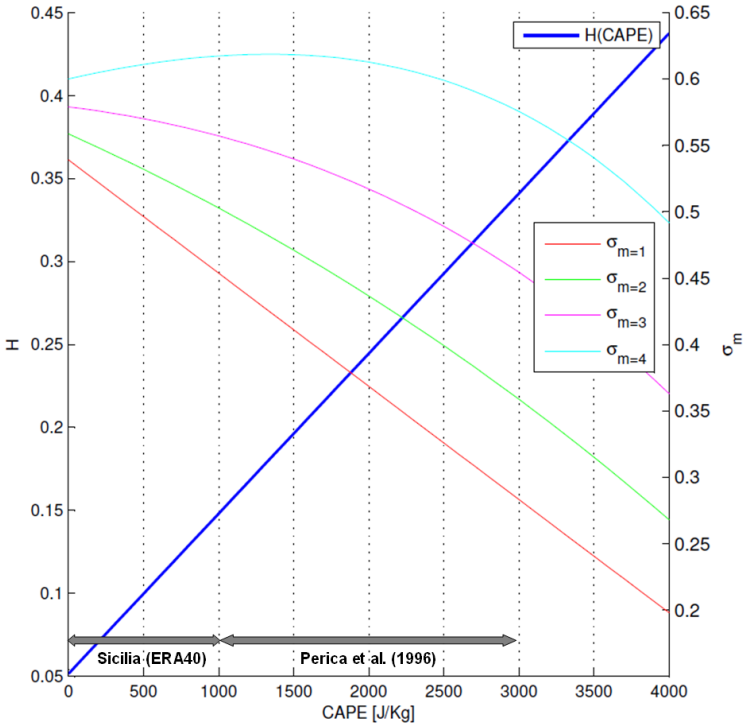

Figure 5.5: Relationships between CAPE and H and σ_m according to Perica and Foufoula-Georgiou (1996a) with indication of applicability range and that of CAPE values observed in Sicilia according to ERA40 dataset.

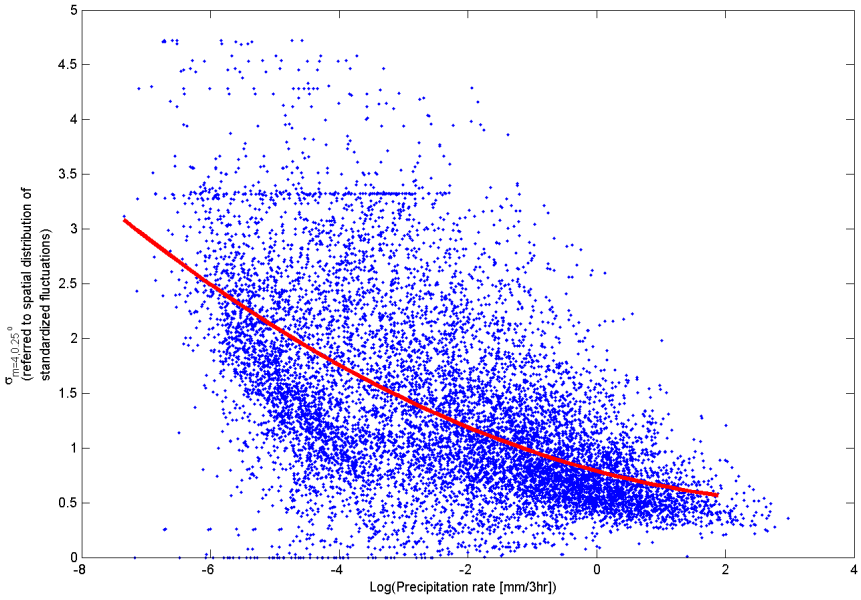

Figure 5.6: Standard deviation of standardized fluctuation spatial distribution and precipitation values. Available data on period 2003-2009 at 3-hour time resolution and 0.25^o spatial aggregation has been used. Adopted approximation relationship is indicated.

using dynamic scaling formulation:

$$H = log_2 \left(\frac{\sigma_m}{\sigma_{m-1}} \right).$$

Studying precipitation spatial process at scales lower than $m = 4$ would require a more dense rain-gauge network. Therefore here is not possible to estimate H parameter as function of precipitation intensity. Actually interpolating rain-gauge data at lower resolution could provide supporting data for this analysis, but network density suitability to describe spatial variability of precipitation, need to be carefully checked. Moreover possible availability of weather radar in the future for the study area, could be useful for performing such an analysis.

Considering such a missed updating formulation for H parameter, it has been preferred to adopt the original formulation of Perica and Foufoula-Georgiou (1996a) with related relationships for estimating σ_1 and H based on CAPE, that is obtained from ERA40 dataset, even though such expressions are verified for CAPE values higher than those retrieved for Sicilia.

5.4 Coupled bias-adjustment and spatial downscaling application

The bias adjustment procedure and the spatial downscaling, are combined in sequence to produce a unique post-retrieval tool for satellite precipitation estimates. As exposed on the previous paragraphs, emphasis has been put on the possibility of using such a tool in real-time with the retrieving of satellite estimates, that nowdays are often available with a latency time smaller than that of corresponding ground-based measurements. Such a feature has been achieved developing a bias adjustment procedure that does not need real-time rain-gauge measurements and a spatial downscaling procedure that makes use of a simplified parametrization based uniquely on a value of pre-event CAPE. This post-retrieval tool is not expected to provide high performance since it has been designed to readily provide precipitation maps with reduced bias level and at different spatial scales that can be considered as first-guess estimates. It has been specifically designed for the local area of interest for this study, that is the Sicilia island.

Procedure steps, namely the bias adjustment and the spatial downscaling, have been described respectively on subsection 5.2.1 and 5.3.1. On figure 5.7

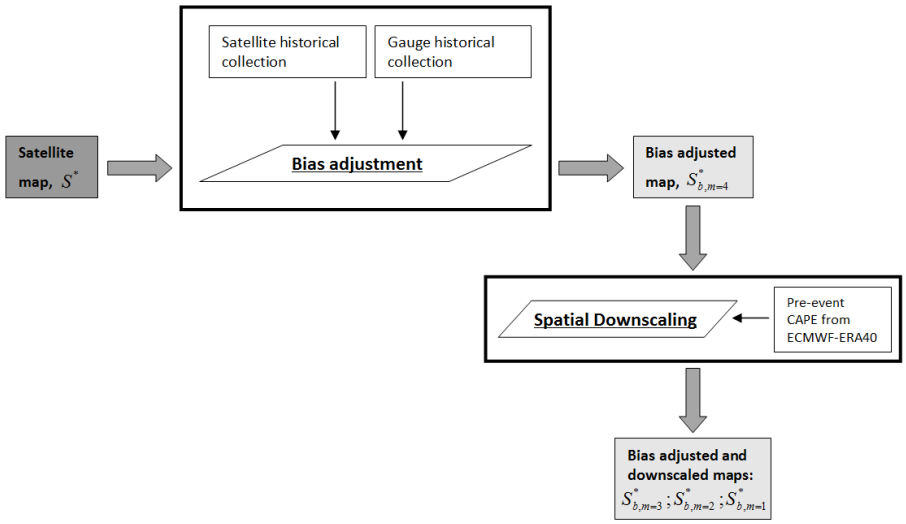

Figure 5.7: Post-retrieval procedure scheme

the complete framework is illustrated. The retrieved map from a satellite product (S^*) is introduced as input data for the bias adjustment procedure. This procedure is previously trained on the basis of historical data from the same satellite product being used, and timing corresponding ground data. Then the bias adjusted map $S^*_{b,m=4}$ is obtained that is in turn introduced on the spatial downscaling procedure. Then the bias adjusted and spatially downscaled maps at three scales are derived.

Two examples of applying the post-retrieval tool are reported on figures 5.8 and 5.9, where the input CMORPH maps, reported on the top of each figure, have been introduced as input and a bias adjusted map and three downscaled maps at different spatial scales are produced as output.

Since the post-retrieval procedure has not been developed for producing well-performing results, no validation procedure has been carried out. Of course it is expected the results showing lower bias levels because of the bias-adjustment procedure. But it is possible that the simplified method proposed here may produce erroneous correction where satellite estimation is reporting an opposite bias respect that modeled by the bias correction expression. Therefore there is still room for improvements that arise from the opportunity of accounting for underestimation/overestimation local trend. Even the spatial downscaling

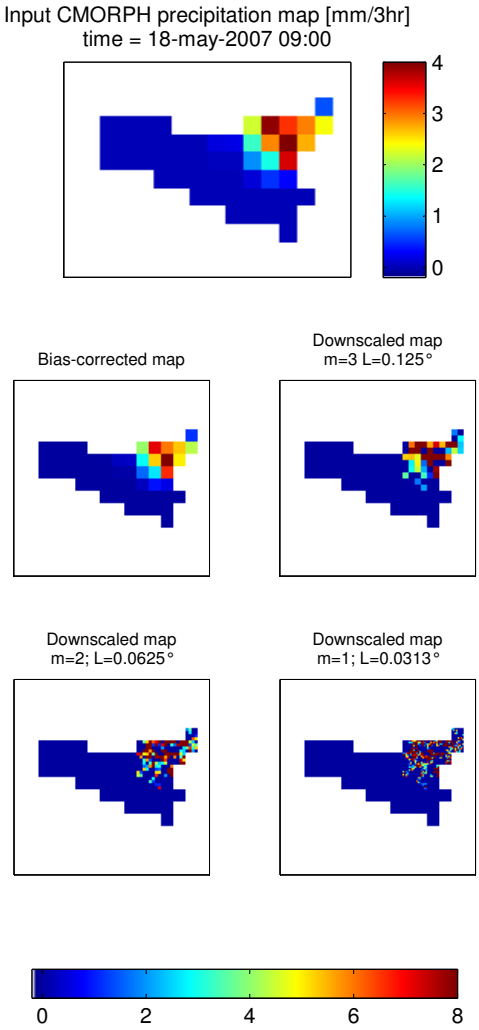

Figure 5.8: Post-retrieval procedure example; CMORPH estimate, 18-may-2007 09:00

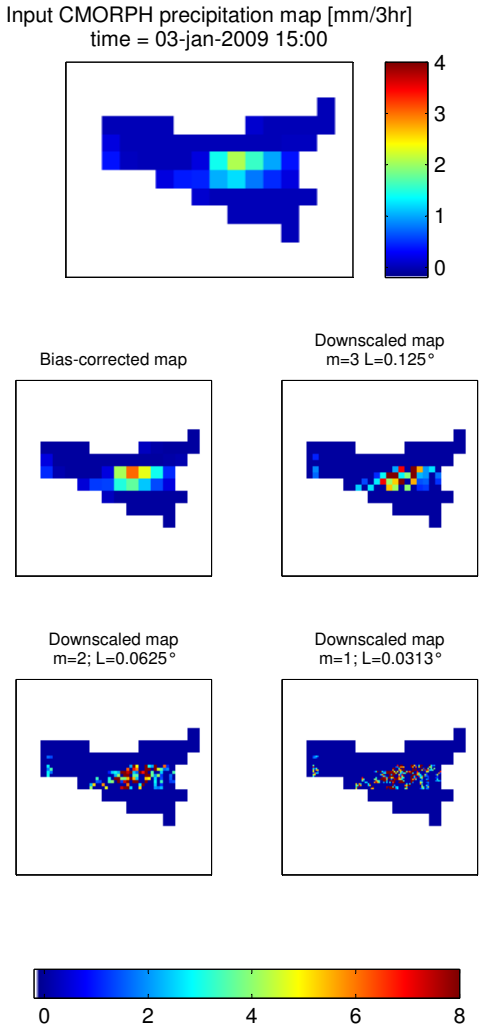

Figure 5.9: Post-retrieval procedure example; CMORPH estimate, 03-jan-2009 15:00

needs further work as some assumptions should be better verified and empirical expressions improved. In particular the spatial variability estimation should be characterized at fine scale ($m = 1$) and the dynamic scale hypothesis, along with the coefficient H, has to be verified from the study of a relationship between spatial variability of standardized fluctuations at different scales. Then more robust empirical relationships between downscaling parameters and an explanation field (i.e. the pre-event precipitation intensity) may be derived. Furthermore, other spatial downscaling approaches could be considered and evaluated.

Finally, it has to be highlighted the nature of the entire developed post-retrieval tool that aims on achieving first-guess estimates of precipitation field at different spatial resolutions on near real-time, not making use of timely available ground precipitation information.

Conclusions

Satellite precipitation products estimates promise to be useful for a wide application range. As the products development is continuously going on extending data source and improving algorithms, performance evaluation studies have to be carried out in order to assess their usability. Evaluation study activity can be explored and summarized by features and requisites for given applications and geographic area. A consolidated evaluation literature describes satellite estimates potential suitability for several fields, and a number of issues that require further improvements, differentiating geographically performances features. In this study some major precipitation products developed during last years, have been evaluated and compared against rain-gauge network for the area of Sicilia, placed in the Mediterranean Sea for the period 2007-2008. The main issue emerging from the analysis is a systematic underestimation shown by each satellite product. Obviously ground-adjusted product are able to reduce the gap as the GPCP data is considered into the algorithms. But still a certain and important underestimation level is displayed by adjusted products indicating the reduced reliability of GPCP data to represent local precipitation features.

Evaluation analysis has been carried out performing a series of spatial analyses based on selected performance indexes. Even if the adjusted products considered in the analysis are effective on reducing bias, they present some weaknesses that deserve further analyses. In particular, discrepancies between frequency distributions and low performing RMSE values due to risen precipitation magnitude without any correlation coefficient improvement, give interesting insight for future development of adjusting procedures.

PERSIANN-CCS displays the best bias level among only-satellite data products, but it still shows low correlation coefficient and false alarm ratio performances probably due to a not accurate description of the precipitation process. On the other hand, other only satellite products (CMORPH, PERSIANN,

TMPA-RT) are more correlated to the reference data even if characterized by high bias as already highlighted.

An analysis with spatial averaged values aggregated at different time scales, indicates that performances improve as the temporal resolution increases and a strategic value, where a stable performance is reached, is equal to 5 days, that can be considered as the minimum value where satellite estimates keep a feasible level. Moreover relationships between temporal evaluation indexes mean trends and precipitation seasonality is observed with larger errors concentrated on the winter season.

From a wider spatial perspective, a large scale annual underestimation is observed for the Mediterranean area indicating that satellite estimates are unsuitable to represent the corresponding climate. The bias issue needs further analyses and PMW retrieval algorithms structure and implementation is a field to be investigated since many authors highlight how these algorithms still present several weaknesses that can compromise estimation and impact climatic features derived by satellite products. Some major issues are related to their difficulties to represent mid-latitude precipitation systems due to unsuitability of CRM simulations and their poor microphysical parameterization. Moreover a more complex ground-atmosphere representation, due to possible non-liquid precipitation occurrences and coastlines retrieval uncertainties, can lead to incorrect estimates.

The bias level shown by adjusted products (PERSIANN adjusted and TMPA) has been pointed out examining GPCC ground-based dataset that is introduced by means of GPCP within these products. GPCC data has been compared with SIAS information for the period 2003-2009. In order to perform direct comparison, SIAS data has been reduced to the same spatial and temporal scales of GPCC. Datasets resulted being in general good agreement, with GPCC showing mean values generally lower than SIAS, then confirming the bias level observed on the previous evaluation analysis. Elaborations shown that particular lower performances resulted localized on high elevation areas. Therefore it has been formulated the hypothesis of an inadequate spatial sampling of precipitation with missing measurements on such areas and producing the observed bias level. In order to confirm such a hypothesis, positions of GPCC stations within the study area have been obtained and used to compare spatial sampling schemes from GPCC and SIAS. A mean annual precipitation map has been used as background field for sampling. This analysis confirmed the missed sampling by GPCC dataset around high elevation areas therefore related to high precipitation rates, resulting in the underestimation level observed on previous analyses.

In order to identify and apply possible improving tasks on satellite precipitation products, an analysis of suitability between a general precipitation concerned application framework (including climatological, weather and meteorological, and hydrological applications) and precipitation sources (rain-gauge networks, weather radars and satellite estimates) has been performed. It resulted that spatial coverage features able satellite estimates to be considered by the entire application range, but still some features need to be addressed in order to effectively make them suitable for such applications. In particular, given the consolidated role on climatological fields of satellite precipitation estimates, and looking at the possible other applications in which they can be involved, a challenge arise from the opportunity to adopt these dataset for hydrological applications and other fields that typically make use of ground-data measurements. This possibility leads to the necessity to improve some features such as the unbiasness performance and the spatial resolution. While the bias adjustment procedures have been pointed out from the satellite precipitation retrieval community itself, as this is a well known issue, the downscaling approaches have been mainly applied to resolve the finee scale fields from GCMs and LAMs. Here a bias adjustment procedure has been developed that make use of local information and does not need simultaneous external information resulting in a real-time tool to bias-adjust satellite estimates. This procedure is constituted by a relationship between precipitation estimates from satellite products and corresponding adjusted values, whose design was achieved from a training dataset including both spatial averaged rain-gauge and satellite estimates by means of a Bayesian expression. The downscaling step is based on a multiscale approach that link spatial statistics of precipitation fields to meteorological condition by means of CAPE variable obtained from ERA40 Re-analysis dataset. Hypothesis of dynamic scaling that allow for linking statistics of precipitation spatial variability at different scales is introduced on this approach . The variable for which such hypothesis is adopted, is the standardized fluctuation of precipitation and empirical expression for deriving distributions parameters using CAPE are available. It has been seen that these relationships may result inadequate for the Sicilia case study, since related range of occurred CAPE values, is lower than that for which such relationships were developed. Then it has been explored the possibility to achieve modified expression starting from spatial averaged pre-event precipitation intensity. However it has been preferred using original expression for this study just highlighting their potential limit for this area. Even though the tool has not been validated, it is possible to list main strength and weaknesses of this procedure. Such an information provided by satellite precipitation product data and successively elaborated by means of the

proposed post-retrieval tool, is available with the same time latency of satellite products that, for operative algorithm, is almost the same of remote sensing data. This latency time is often shorter than rain-gauge network data availability, then allowing for using precipitation data on application with restrictive data readiness requirements. The downscaled maps, even though are to be considered as a statistical realization of the precipitation process described on the larger spatial scale, can be used for hydrological applications since they are able to reproduce consistent statistical properties. Improvements of the downscaling procedure are related to a more exhaustive understanding of meteorological features on the study area that would allow for a better parametrization of the same downscaling procedure, while bias adjustment procedure will benefit of improvements on satellite retrieval algorithms.

Appendix A

Acronyms

AGPI Adjusted GOES Precipitation Index

AIP Algorithms Intercomparison Program

AMSR-E Advanced Microwave Scanning Radiometer

AMSU-B Advanced Microwave Sounding Unit-B

ANN Artificial Neural Network

AVHRR Advanced Very High Resolution Radiometer

CAMS Climate Assessment and Monitoring System

CAPE Convective Available Potential Energy

CC Correlation coefficient

CLW Column Liquid Water

CMA China Meteorological Administration

CMORPH CPC Morphing tecnique

CPC Climate Prediction Center

CPR Cloud Profiling Radar

CRA Contiguous Rain Area

CRM Cloud Resolving Model

CSAV Cloud System Advection Vectors

CSI Critical success index

DMSP Defense Meteorological Satellite Program

DSD Drop Size Distribution

DWD Deutscher Wetterdienst

ECMWF European Centre for Medium-Range Weather Forecasts

ENSO El Niño Southern Oscillation

EOS Earth Observing System

ERA40 ECMWF 40 Year Re-Analysis

EUMETSAT European Organization for the Exploitation of Meteorological Satellites

FAR False alarm ratio

FOV Field Of View

FY-2 Feng-Yun-2

GEWEX Global Energy and Water Cycle Experiment

GCM General Circulation Models

GEO Geostationary Earth Orbiting

GHCN Global Historical Climate Network

GOES Geostationary Operational Environmental Satellites

GOS Global Observing System

GPCC Global Precipitation Climatology Centre

GPCP Global Precipitation Climatology Project

GPCP Global Precipitation Climatology Project

GPI GOES Precipitation Index

GPM Global Precipitation Mission

GPROF Goddard Profiling Algorithm

GS Gilbert skill score

GSFC Goddard Space Flight Center

GSMaP Global Satellite Mapping of Precipitation

GTS Global Telecommunication System

HRIS Human Resource Information System

HRPP High Resolution Precipitation Products

HSS Heidke skill score

IPWG International Precipitation Working Group

IR Infrared wavelength

JAXA Japan Aerospace Exploration Agency

JMA Japan Meteorological Agency

LAM Limited-Area Meteorological Model

LEO Low Earth Orbiting

MAE Mean Absolute Error

MBE Mean Bias Error

MICRA Microwave Infrared Combined Rainfall Algorithm

MIRA Microwave/Infrared Rainfall Algorithm

MM5 Fifthgeneration Mesoscale Model

MPM Multivariate Probability Matching

MSE Mean Square Error

MSG Meteosat Second Generation

MTG Meteosat Third Generation

MTSAT Multifunctional Transport Satellites

NAME North American Monsoon Experiment

NAO North Atlantic Oscillation

NASA National Aeronautics and Space Administration

NESDIS National Environmental Satellite, Data, and Information Service

NCDC National Climate Data Center

NCEP National Centers for Environmental Prediction

NERN NAME Event Rain Gauge Network

NESDIS National Environmental Satellite, Data, and Information Service

NN Natural Neighbor

NOAA National Oceanic and Atmospheric Administration

NRL Naval Research Laboratory

NSMC National Satellite Meteorological Center

NWP Numerical Weather Prediction

NWS National Weather Service

OLR Outgoing Longwave Radiation

PC Percent correct

PEHRPP Pilot Evaluation of High Resolution Precipitation Products

PERSIANN Precipitation Estimation from Remotely Sensed Information using Artificial Neural Networks

PERSIANN-adj PERSIANN Adjusted

PERSIANN-CCS PERSIANN Cloud-patch Classification System

PIP Precipitation Intercomparison Program

PMIR Passive Microwave-InfraRed tecnique

PMW Passive microwave wavelength

POD Probability of Detection

PR Precipitation Radar

QPE Quantitative Precipitation Estimates

QPF Quantitative Precipitation Forecast

RMSE Root Mean Square Error

ROC Relative Operating Characteristics

SAC-SMA Sacramento Soil Moisture Accounting Model

SAM South Asian Monsoon

SCaMPR Self-Calibrating Multivariate Precipitation Retrieval

SCE-UA Shuffled Complex Evolution-University of Arizona

SEVIRI Spinning Enhanced Visible and InfraRed Imager

SOFM Self-Organizing Feature Map

SR Success ratio

SSM/I Special Sensor Microwave/Imager

$\mathbf{T}_b$ Temperature of brillance

TIROS-1 Television InfraRed Observing Satellite-1

TMI TRMM Microwave Imager

TMPA TRMM Multitemporal Precipitation Analysis

TOVS TIROS Operational Vertical Sounder

TPW Total Precipitable Water

TRMM Tropical Rainfall Measuring Mission

TSDIS TRMM Science Data and Information System

TSS True skill statistics

VIRS Visible and Infrared Scanner

VIS Visible wavelength

VISSR Visible and Infrared Spin-Scan Radiometer

WCRP World Climate Research Programme

WMO World Meteorological Organization

Bibliography

R. F. Adler, G. J. Huffman, and P. R. Keehn. Global tropical rain estimates from microwave-adjusted geosynchronous ir data. *Remote Sensing Reviews*, 11:125–152, 1994.

R.F. Adler, C. Kidd, G. Petty, M. Morrissey, and H.M. Goodman. Intercomparison of global precipitation products: the third precipitation intercomparison project (pip-3). *Bulletin of the American Meteorological Society*, 82:1377–1396, 2001.

R.F. Adler, G.J. Huffman, A. Chang, R. Ferraro, P.P. Xie, J. Janowiak, B. Rudolf, U. Schneider, S. Curtis, D. Bolvin, A. Gruber, J. Susskind, P. Arkin, and E. Nelkin. The version-2 global precipitation climatology project (GPCP) monthly precipitation analysis (1979-present). *Journal of Hydrometeorology*, 4(6):1147–1167, 2003.

K. Aonashi and G. Liu. Passive microwave precipitation retrievals using tmi during the baiu period of 1998. part i: Algorithm description and validation. *Journal of Applied Meteorology*, 39:2024–2037, 2000.

P.A. Arkin and B.N. Meisner. The relationship between large-scale convective rainfall and cold cloud over the western hemisphere during 1982-84. *Monthly Weather Review*, 115:51–74, 1987.

P.A. Arkin and P. Xie. The global precipitation climatology project: first algorithm intercomparison project. *Bulletin of the American Meteorological Society*, 75:401–419, 1994.

D. Atlas, D. Rosenfeld, and D. Short. The estimation of convective rainfall by area integrals. 1. the theoretical and empirical basis. *Journal of Geophysical Research*, 95:2153–2160, 1990.

E.C. Barrett, J. Dodge, H.M. Goodman, J. Janowiak, C. Kidd, and E.A. Smith. The first wetnet precipitation intercomparison project. *Remote Sensing Reviews*, 11:49–60, 1994.

P. Bauer. Over-ocean rainfall retrieval from multisensor data of the tropical rainfall measuring mission. part i: Design and evaluation of inversion databases. *Journal of Atmospheric and Oceanic Technology*, 18:1315–1330, 2001.

P. Bauer and P. Schlnessel. Rainfall, total water, ice water and water vapor over the sea from polarized microwave simulations and ssmb data. *Journal of Geophysical Research*, 98:20737–20759, 1993.

A. Behrangi, B. Khakbaz, T.C. Jaw, A. AghaKouchak, K.-L. Hsu, and S. Sorooshian. Hydrologic evaluation of satellite precipitation products over a mid-size basin. *Journal of Hydrology*, 397:225–237, 2011.

T. L. Bell. A space-time stochastic model of rainfall for satellite remote sensing studies. *Journal of Geophysical Research*, 92:9631–9643, 1987.

T. Bellerby, K.-L. Hsu, and S. Sorooshian. Lmodel: A satellite precipitation methodology using cloud development modeling. part i: Algorithm construction and calibration. *Journal of Hydrometeorology*, 10:1081–1095, 2009.

R. Bennartz. Passive microwave remote sensing of precipitation at high latitudes. In Vincenzo Levizzani, J. Turk, and P. Bauer, editors, *Measuring Precipitation from Space - EURAINSAT and the future*, chapter 13, pages 165–178. Springer, 2007.

F. I. Boushaki, K. L. Hsu, S. Sorooshian, G. H. Park, S. Mahani, and W. Shi. Bias adjustment of satellite precipitation estimation using ground-based measurement: A case study evaluation over the southwestern united states. *Journal of Hydrometeorology*, 10:1231–1242, 2009.

F. Castelli. Atmosphere modelling and hydrology prediction uncertainty, paper presented at workshop on hydrometeorology: Impacts and management of extreme floods, italian res. counc., la colombella, perugia, italy,. 1995.

A. T. C. Chang, L. S. Chiu, C. Kummerow, and J. Meng. First results of the trmm microwave imager (tmi) monthly oceanic rain rate: Comparison with ssm/i. *Geophysical Research Letters*, 26:2379–2382, 1999.

M. Chen, P. Shi, W. Xie, V.B.S Silva, V. E. Kousky, R. W. Higgins, and J. E. Janowiak. Assessing objective techniques for gauge-based analyses of global daily precipitation. *Journal of Geophysical Research*, 113:D04110, 2008.

C. Davis, B. Brown, and R. Bullock. Object-based verification of precipitation forecasts. part i: Methodology and application to mesoscale rain areas. *Monthly Weather Review*, 134:1772–1784, 2006.

R. Deidda, R. Benzi, and F. Siccardi. Multifractal modeling of anomalous scaling laws in rainfall. *Water Resources Research*, 35:1853–1867, 1999.

A. Di Piazza. *The problem of missing data in hydroclimatic time series. Application of spaztial interpolation tecniques to construct a comprehensive archive of hydroclimatic data in Sicily, Italy.* PhD thesis, Università degli Studi di Palermo, Dipartimento di Ingegneria Civile, Ambientale e Aerospaziale, 2011.

A. Di Piazza, F. Lo Conti, L.V. Noto, F. Viola, and G. La Loggia. Comparative analysis of different techniques for spatial interpolation of rainfall data to create a serially complete monthly time series of precipitation for sicily, italy. *International Journal of Applied Earth Observation and Geoinformation*, 13 (3):396–408, 2011.

P. N. Dills and S. B. Smith. Comparison of profiler and satellite cloud tracked winds. In *Prepr. 6th Conf. Satellite Meteor. and Ocean., 5-10 January, Atlanta, GA, Amer. Meteor. Soc., 155-158*, 1992.

A. Drago, D. Cartabellotta, B. Lo Bianco, and M. Lombardo. Atlante climatologico della sicilia. Technical report, Regione Siciliana, Assessorato Agricoltura e Foreste, Palermo., 2000.

Q. Duan, S. Sorooshian, and V.K. Gupta. Effective and efficient global optimization for conceptual rainfall-runoff model. *Water Resources Research*, 28: 1015–1031, 1992.

P. S. Eagleson, N. M. Fenessey, W. E. Quiliang, and I. Rodriguez-Iturbe. Application of spatial poisson models to airmass thunderstorm rainfall. *Journal of Geophysical Research*, 92:9961– 9978, 1987.

E.E. Ebert. Fuzzy verification of high resolution gridded forecasts: A review and proposed framework. *Meteorological Applications*, 15:51–64, 2008.

E.E. Ebert and J.L. McBride. Verification of precipitation in weather systems: determination of systematic errors. *Journal of Hydrology*, 239:179–202, 2000.

E.E. Ebert, M.J. Manton, P.A. Arkin, R.J. Allam, C.E. Holpin, and A. Gruber. Results from the gpcp algorithm intercomparison programme. *Bulletin of the American Meteorological Society*, 77:2875–2887, 1996.

E.E. Ebert, J.E. Janowiak, and C. Kidd. Comparison of near-real-time precipitation estimates from satellite observations and numerical models. *Bulletin of the American Meteorological Society*, 88(1):47+, 2007.

L. Ferraris, R. Rudari, and F. Siccardi. The uncertainty in the prediction of flash floods in the northern mediterranean environment. *Journal of Hydrometeorology*, 3:714–727, 2002.

R.R. Ferraro and G.F. Marks. The development of ssm/i rain-rate retrieval algorithms using ground-based radar measurements. *Journal of Atmospheric and Oceanic Technology*, 12:755–770, 1995.

J. Gottschalck, J. Meng, M. Rodell, and P. Houser. Analysis of multiple precipitation products and preliminary assessment of their impact on global land data assimilation system land surface states. *Journal of Hydrometeorology*, 6 (5):573–598, 2005.

N. C. Grody. Classification of snow cover and precipitation using the special sensor microwave imager. *Journal of Geophysical Research*, 96:7423–7435, 1991.

A. Gruber and V. Levizzani. Assessment of global precipitation products - wcrp report. Technical report, World Climate Research Programme (WCRP) - Global Energy and Water Cycle Experiment (GEWEX) Radiation Panel, 2008.

G. Guillot and T. Lebel. Disaggregation of sahelian mesoscale convective system rain fields: Further developments and validation. *Journal of Geophysical Research*, 104:31,533– 31,551, 1999.

V. K. Gupta and E. C. Waymire. A statistical analysis of mesoscale rainfall as a random cascade. *Journal of Applied Meteorology*, 32:251– 267, 1993.

E. Habib, A. Henschke, and R.F. Adler. Evaluation of TMPA satellite-based research and real-time rainfall estimates during six tropical-related heavy rainfall events over Louisiana, USA. *Atmospheric Research*, 94(3):373–388, 2009.

Z. S. Haddad, D. A. Short, S. L. Durden, E. Im, S. Hensley, M. B. Grable, and R. A. Black. A new parameterization of the rain drop size distribution. *IEEE Transactions on Geoscience and Remote Sensing*, 35:532–539, 1997a.

Z. S. Haddad, E.A. Smith, C.D. Kummerow, M. Iguchi, S.L. Farrar, S. L. Durden, M. Alves, and W.S. Olson. The trmm day-1 radar/radiometer combined rain-profiling algorithm. *Journal of the Meteorological Society of Japan*, 75: 799–809, 1997b.

L. D. Herman. Obtaining cloud motion vectors from polar orbiting satellites. In *Prepr. 6th Conf. Satellite Meteor. and Ocean., 5-10 January, Atlanta, GA, Amer. Meteor. Soc., 110-113*, 1992.

R. W. Higgins, W. Shi, and E. Yarosh. Improved united states precipitation quality control system and analysis. Technical report, NCEP/Climate Prediction Center Atlas 7, 2000.

N. Hofstra, M. Haylock, M. New, P. Jones, and C. Frei. Comparison of six methods for the interpolation of daily, European climate data. *Journal of Geophysical Research-Atmospheres*, 113(D21), 2008.

Y. Hong, K.-L. Hsu, S. Sorooshian, and X. Gao. Precipitation Estimation from Remotely Sensed Imagery using an Artificial Neural Network Cloud Classification System. *Journal of Applied Meteorology*, 43(12):1834–1852, 2004.

Y. Hong, D. Gochis, J.-T. Cheng, K.-L. Hsu, and S. Sorooshian. Evaluation of PERSIANN-CCS rainfall measurement using the NAME Event Rain Gauge Network. *Journal of Hydrometeorology*, 8(3):469–482, 2007.

K. Hsu, H. V. Gupta, X. Gao, and S. Sorooshian. Estimation of physical variables from multichannel remotely sensed imagery using a neural networks: application to rainfall estimation. *Water Resources Research*, 35:1605–1618, 1999.

K.-L. Hsu and S. Sorooshian. Satellite-based precipitation measurement using persiann system. In S. Sorooshian, K.-L. Hsu, E. Coppola, B. Tomassetti, M. Verdecchia, and G. Visconti, editors, *Hydrological Modelling and the Water Cycle*, volume Water Science and Technology Library, 2008, 63, pages 27–48. Springer, 2008.

K.-L. Hsu, X. Gao, S. Sorooshian, and H.V. Gupta. Precipitation estimation from remotely sensed information using artificial neural networks. *Journal of Applied Meteorology*, 36(9):1176–1190, 1997.

G. J. Huffman, R. F. Adler, D. T. Bolvin, and E. J. Nelkin. The trmm multi-satellite precipitation analysis (tmpa). In F. Hossain and M. Gebremichael, editors, *Satellite Applications for Surface Hydrology*, pages 3–22. Springer, 2010.

G.J. Huffman, R.F. Adler, B. Rudolf, U. Schneider, and P.R. Keehn. Global precipitation estimates based on a technique for combining satellite-based estimates, rain gauge analysis, and nwp model precipitation information. *Journal of Climate*, 8:1284–1295, 1995.

G.J. Huffman, R.F. Adler, P. Arkin, A. Chang, R. Ferraro, A. Gruber, J. Janowiak, A. McNab, B. Rudolf, and U. Schneider. The global precipitation climatology project (gpcp) combined precipitation dataset. *Bulletin of the American Meteorological Society*, 78:5–20, 1997.

G.J. Huffman, R.F. Adler, M. Morrissey, D.T. Bolvin, S. Curtis, R. Joyce, B. McGavock, and J. Susskind. Global precipitation at one-degree daily resolution from multisatellite observations. *Journal of Hydrometeorology*, 2:36–50, 2001.

G.J. Huffman, R.F. Adler, D.T. Bolvin, G. Gu, E.J. Nelkin, K.P. Bowman, Y. Hong, E.F. Stocker, and D.B. Wolff. The TRMM multisatellite precipitation analysis (TMPA): Quasi-global, multiyear, combined-sensor precipitation estimates at fine scales. *Journal of Hydrometeorology*, 8(1):38–55, 2007.

T. Iguchi, T. Kozu, R. Meneghini, J. Awaka, and K. Okamoto. Rain profiling algorithm for the trmm precipitation radar. *Journal of Applied Meteorology*, 39:2038–2052, 2000.

J. Janowiak, R. Joyce, and P. Xie. Cmorph improvements: A kalman filter approach to blend various satellite rainfall estimate inputs and rain gauge data integration. *Geophysical Research Abstracts*, 11:EGU2009–9810, 2009.

J.E. Janowiak, R.J. Joyce, and Y. Yarosh. A real-time global half-hourly pixel-resolution infrared dataset and its applications. *Bulletin of the American Meteorological Society*, 82:205–217, 2001.

I.T. Jolliffe and D.B. Stephenson. Proper scores for probability forecasts can never be equitable. *Monthly Weather Review*, 136:1505–1510, 2008.

R. J. Joyce and R.R. Ferraro. Improvements of cmorph resulting from limb adjustments and normalization of amsu-b rainfal. In *Prepr. 14th Conf. on*

Satellite Meteorology and Oceanography, Atlanta, GA, Amer. Meteor. Soc.,, 2006.

R.J. Joyce, J.E. Janowiak, P.A. Arkin, and P.P. Xie. CMORPH: A method that produces global precipitation estimates from passive microwave and infrared data at high spatial and temporal resolution. *Journal of Hydrometeorology*, 5 (3):487–503, 2004.

C. Kidd and E.C. Barrett. The use of passive microwave imagery in rainfall monitoring. *Remote Sensing Reviews*, 4:415–450, 1990.

C. Kidd and G. Huffman. Global precipitation measurement. *Meteorological Applications*, 18, Issue 3:334–353, 2011.

C. Kidd and C. Muller. The university of birmingham passive microwave - infrared combined algorithm. In F. Houssain and M. Gebremichael, editors, *Satellite Applications for Surface Hydrology*. Springer-Verlag: Dortrecht, the Netherlands;, 2009.

C. Kidd, D.R. Kniveton, M.C. Todd, and T.J. Bellerby. Satellite rainfall estimation using a combined passive microwave and infrared algorithm. *Journal of Hydrometeorology*, 4:1088–1104, 2003.

C. Kidd, P. Bauer, J. Turk, G.J. Huffman, R. Joyce, K.-L. Hsu, and D. Braithwaite. Inter-comparison of high-resolution precipitation products over northwest europe. *Journal of Hydrometeorology*, 13:67–83, 2012.

G.E. Klazura and D.A. Imy. A description of the initial set of analysis products available from the nexrad wsr-88d system. *Bulletin of the American Meteorological Society*, 74:1293–1312, 1993.

T. Kohonen. *Self-Organizing Map*. Springer-Verlag, New York, 1995.

T. Kubota, S. Shige, H. Hashizume, K. Aonashi, N. Takahashi, S. Seto, Y.N. Takayabu, T. Ushio, K. Nakagawa, K. Iwanami, M. Kachi, and K. Okamoto. Global precipitation map using satellite-borne microwave radiometers by the gsmap project: Production and validation. *IEEE Transactions on Geoscience and Remote Sensing*, 45:2259–2275, 2007.

R.J. Kuligowski. A self-calibrating real-time goes rainfall algorithm for short-term rainfall estimates. *Journal of Hydrometeorology*, 3:112–130, 2002.

C. Kummerow and L. Giglio. A passive microwave technique for estimating rainfall and vertical structure information from space. part i: Algorithm description. *Journal of Applied Meteorology*, 33:3–18, 1994.

C. Kummerow, W. S. Olson, and L. Giglio. A simplified scheme for obtaining precipitation and vertical hydrometeor profiles from passive microwave sensors. *IEEE Transactions on Geoscience and Remote Sensing*, 34:1213–1232, 1996.

C. Kummerow, W. Barnes, T. Kozu, J. Shiue, and J. Simpson. The tropical rainfall measurement mission (trmm) sensor package. *Journal of Atmospheric and Oceanic Technology*, 15:809–816, 1998.

C. Kummerow, W. Berg, J. Thomas-Stahle, and H. Masunaga. Quantifying global uncertainties in a simple microwave rainfall algorithm. *Journal of Atmospheric and Oceanic Technology*, 23(1):23–37, 2006.

C. Kummerow, Y. Hong, W.S. Olson, S. Yang, R.F. Adler, J. McCollum, R. Ferraro, G. Petty, D.B. Shin, and T.T. Wilheit. The evolution of the Goddard profiling algorithm (GPROF) for rainfall estimation from passive microwave sensors. *Journal of Applied Meteorology*, 40(11):1801–1820, 2001.

G. Liu and J. Curry. Retrieval of precipitation from satellite microwave measurements using both emission and scattering. *Journal of Geophysical Research*, 97:9959–9974, 1992.

S. Lovejoy and B. Mandelbrot. Fractal properties of rain and a fractal model. *Tellus, Ser. A*, 37:209–232, 1985.

A. Mariotti, N. Zeng, and K.M. Lau. Euro-mediterranean rainfall and enso - a seasonally varying relationship. *Geophysical research letters*, 29:art. no.1621, 2002.

F. S. Marzano, A. Mugnai, G. Panegrossi, N. Pierdicca, E. A. Smith, and J. Turk. Bayesian estimation of precipitating cloud parameters from combined measurements of spaceborne microwave radiometer and radar. *IEEE Transactions on Geoscience and Remote Sensing*, 37:596–613, 1999.

F.S. Marzano, M. Palmacci, D. Cimini, G. Giuliani, and F.J. Turk. Multivariate statistical integration of satellite infrared and microwave radiometric measurements for rainfall retrieval at the geostationary scale. *IEEE Transactions on Geoscience and Remote Sensing*, 42:1018–1032, 2004.

I. Mason. A model for assessment of weather forecasts. *Australian Meteorological Magazine*, 30:291–303, 1982.

J. Mejia and I. Rodriguez-Iturbe. On the synthesis of random fields sampling from the spectrum: An application to the generation of hydrologic spatial processes. *Water Resources Research*, 10:705– 711, 1974.

M. Menabde, D. Harris, A. Seed, G. Austin, and D. Stow. Multiscaling properties of rainfall and bounded random cascades. *Water Resources Research*, 33:2823– 2830, 1997a.

M. Menabde, A. Seed, D. Harris, and G. Austin. Self-similar random fields and rainfall simulations. *Journal of Geophysical Research*, 102:13,509– 13,515, 1997b.

M. Menabde, A. Seed, G. Harris, and G. Austin. Multiaffine random field model of rainfall. *Water Resources Research*, 35:509– 514, 1999.

S. Michaelides, V. Levizzani, E. Anagnostou, P. Bauer, T. Kasparis, and J.E. Lane. Precipitation: Measurement, remote sensing, climatology and modeling. *Atmospheric Research*, 94(4):512–533, 2009.

J.R. Miller. A climatological z-r relationship for convective storms in the northern great plains. In *Preprints, 15th Conf. on Radar Meteorology, Champaign-Urbana, IL, Amer. Meteor. Soc., 153-154.*, 1972.

A. Mugnai, E. A. Smith, and G. J. Tripoli. Foundations for statistical-physical precipitation retrieval from passive microwave satellite measurements. part ii: Emission-source and generalized weighting-function properties of a timedependent cloud-radiation model. *Journal of Applied Meteorology*, 32:17–39, 1993.

A. Mugnai, E.A. Smith, G.J. Tripoli, S. Dietrich, V. Kotroni, K. Lagouvardos, and C.M. Medaglia. Explaining discrepancies in passive microwave cloud-radiation databases in microphysical context from two different cloud-resolving models. *Meteorology and Atmospheric Physics*, 101(3-4):127–145, 2008.

P. Northrop. A clustered spatial-temporal model of rainfall. *Proc R. Soc. London, Ser. A,*, 454:1875–1888, 1998.

W. S. Olson, F. J. LaFontaine, W. L. Smith, R. T. Merrill, B. A. Roth, and T. H. Achtor. precipitation validation in dmsp special sensor microwave/lmager calibration/validation final report volume ii. Technical report, Washington, DC: Naval Res. Lab., 1991.

W. S. Olson, C.D. Kummerow, Y. Hong, and W.-K. Tao. Atmospheric latent heating distributions in the tropics derived from satellite passive microwave radiometer measurements. *Journal of Applied Meteorology*, 38:633–664, 1999.

T. M. Over and V. K. Gupta. A space-time theory of mesoscale rainfall using random cascades. *Journal of Geophysical Research*, 101:26,319–26,331, 1996.

G. Panegrossi, S. Dietrich, F.S. Marzano, A. Mugnai, E.A. Smith, X. Xiang, G.J. Tripoli, P.K. Wang, and J.P.V. Poiares Baptista. Use of cloud model microphysics for passive microwave-based precipitation retrieval: Significance of consistency between model and measurement manifolds. *Journal of the Atmospheric Sciences*, 55(9):1644–1673, 1998.

M. C. Peel, B. L. Finlayson, and T. A. McMahon. Updated world map of the kppen-geiger climate classification. *Hydrology and Earth System Sciences*, 11: 1633–1644, 2007.

C.P. Péguy. Une tentative de dlimitation et de schmatisation des climats intertropicaux. *Revue de gographie de Lyon*, 36(1):1–6, 1961.

S. Perica and E. Foufoula-Georgiou. Linkage of scaling and thermodynamic parameters of rainfall: Results from midlatitude mesoscale convective systems. *Journal of Geophysical Research*, 101:7431–7448, 1996a.

S. Perica and E. Foufoula-Georgiou. Model for multiscale disaggregation of spatial rainfall based on coupling meteorological and scaling descriptions. *Journal of Geophysical Research*, 101:26,347–26,361, 1996b.

G. W. Petty. Physical retrievals of over-ocean rain rate frommultichannel microwave imagery. part i: Theoretical characteristics of normalized polarization and scattering indices. *IEEE Transactions on Geoscience and Remote Sensing*, 54:79–99, 1994.

D. Pozo-Vázquez, M.J. Esteban-Parra, F.S. Rodrigo, and Y. Castro-Diez. A study of nao variability and its possible non-linear influences on european surface temperature. *Climate Dynamics*, 17:701–715, 2001.

C. Price, L. Stone, B. Rajagopalan, and P. Alpert. A possible link between el nino and precipitation in israel. *Geophysical research letters*, 25:3963–3966, 1998.

X. Rodó. Reversal of three global atmospheric fields linking changes in sst anomalies in the pacific, atlantic and indian oceans at tropical latitudes and midlatitudes. *Climate Dynamics*, 18:203–217, 2001.

X. Rodó, E. Baert, and F.A. Comin. Variations in seasonal rainfall in southern europe during the present century: Relationships with the north atlantic oscillation and the el nino southern oscillation. *Climate Dynamics*, 13:275–284, 1997.

I. Rodriguez-Iturbe, D. R. Cox, and P. S. Eagleson. Spatial modelling of total storm rainfall. *Proc R. Soc. London, Ser. A,*, 403:27–50, 1986.

D. Rosenfeld, D.B. Wolff, and E. Amitai. The window probability matching method for rainfall measurements with radar. *Journal of Applied Meteorology*, 33:683–693, 1994.

A. Rossa, P. Nurmi, and E. Ebert. Overview of methods for the verification of quantitative precipitation forecasts. In S. Michaelides, editor, *Precipitation: Advances in Measurement, Estimation and Prediction*, pages 417–450. Springer, 2008.

B. Rudolf. Management and analysis of precipitation data on a routine basis. In Sevruk and M. Lapin, editors, *International Symposium on Precipitation and Evaporation*, pages 69–76. Slovak Hydrometeorology Institution, 1993.

G.-H. Ryu, B.-J. Sohn, C. Kummerow, E.-K. Seo, and G. Tripoli. Improved goddard profiling (gprof) database over the korean peninsula and its impact on trmm tmi rainfall. *Proc. of SPIE*, 7859, 78590A, 2010.

M.R.P. Sapiano. An evaluation of high resolution precipitation products at low resolution. *International Journal of Climatology*, 30:1416–1422, 2010.

D. Schertzer and S. Lovejoy. Physical modeling and analysis of rain and clouds by anisotropic scaling multiplicative processes. *Journal of Geophysical Research*, 92:9693– 9714, 1987.

R. Sibson. A brief description of natural neighbor interpolation. In V. Barnett, editor, *Interpreting Multivariate Data*, chapter 2, pages 21–36. Chichester: John Wiley, 1981.

E. Smith and D. Philips. Measurements from satellite platforms, annual satellite report no. nass-11542, 1971-72, ssec, university of wisconsin, 1-53. Technical report, 1972.

E. A. Smith, X. Xiang, A. Mugnai, and G. Tripoli. Design of an inversion-based precipitation profile retrieval algorithm using an explicit cloud model for initial guess microphysics. *IEEE Transactions on Geoscience and Remote Sensing*, 54:53–78, 1994.

E.A. Smith, J.E. Lamm, R. Adler, J. Alishouse, K. Aonashi, E. Barrett, P. Bauer, W. Berg, A. Chang, R. Ferraro, J. Ferriday, S. Goodman, N. Grody, C. Kidd, D. Kniveton, C. Kummerow, G. Liu, F. Marzano, A. Mugnai, W. Olson, G. Petty, A. Shibata, R. Spencer, F. Wentz, T. Wilheit, and E. Zipser. Results of wetnet pip-2 project. *Journal of the Atmospheric Sciences*, 55: 1483–1536, 1998.

E.A. Smith, G. Asrar, Y. Furuhama, A. Ginati, A. Mugnai, K. Nakamura, R.F. Adler, M.-D. Chou, M. Desbois, J. F. Durning, J. K. Entin, F. Einaudi, R. R. Ferraro, R. Guzzi, P. R. Houser, P. H. Hwang, T. Iguchi, P. Joe, R. Kakar, J. A. Kaye, M. Kojima, K.-S. Kummerow, C. Kuo, D. P. Lettenmaier, V. Levizzani, N. Lu, A. V. Mehta, C. Morales, P. Morel, T. Nakazawa, S. P. Neeck, K. Okamoto, R. Oki, G. Raju, J. M. Shepherd, J. Simpson, B.-J. Sohn, E. F. Stocker, W.-K. Tao, J. Testud, G. J. Tripoli, E. F. Wood, S. Yang, and W. Zhang. International global precipitation measurement (gpm) program and mission: An overview. In Vincenzo Levizzani, J. Turk, and P. Bauer, editors, *Measuring Precipitation from Space - EURAINSAT and the future*, chapter 48, pages 611–654. Springer, 2007.

T. M. Smith, P.A. Arkin, J. J. Bates, and G. J. Huffman. Estimating bias of satellite-based precipitation estimates. *Journal of Hydrometeorology*, 7: 841–856, 2006.

B.J. Sohn, H.-J. Han, and E.-K. Seo. Validation of satellite-based high-resolution rainfall products over the korean peninsula using data from a dense rain gauge network. *Journal of Applied Meteorology and Climatology*, 49(4):701–714, 2010.

S. Sorooshian, K.-L. Hsu, X. Gao, H.V. Gupta, B. Imam, and D. Braithwaite. Evaluation of PERSIANN system satellite-based estimates of tropical rainfall. *Bulletin of the American Meteorological Society*, 81(9):2035–2046, 2000.

E. Stokstad. Scarcity of rain, stream gages threatens forecasts. *Science*, 285: 1199–1200, 1999.

F.J. Tapiador, C. Kidd, V. Levizzani, and F.S. Marzano. A neural networks-based fusion technique to estimate half-hourly rainfall estimates at 0.1^o resolution from satellite passive microwave and infrared data. *Journal of Applied Meteorology*, 43:576–594, 2004.

K.E. Taylor. Summarizing multiple aspects of model performance in a single diagram. *Journal of Geophysical Research-Atmospheres*, 106(D7):7183–7192, 2001.

Y. Tian and C.D. Peters-Lidard. A global map of uncertainties in satellite-based precipitation measurements. *Geophysical Research Letters*, 37(24), 2010.

Y. Tian, C.D. Peters-Lidard, J.B. Eylander, R.J. Joyce, G.J. Huffman, R.F. Adler, K.-L. Hsu, F.J. Turk, M. Garcia, and J. Zeng. Component analysis of errors in satellite-based precipitation estimates. *Journal of Geophysical Research*, 114:D24101, 2009.

Y. Tian, C.D. Peters-Lidard, and J.B. Eylander. Real-time bias reduction for satellite-based precipitation estimates. *Journal of Hydrometeorology*, 11:1275–1285, 2010.

M.C. Todd, C. Kidd, D. Kniveton, and T.J. Bellerby. A combined satellite infrared and passive microwave technique for estimation of small-scale rainfall. *Journal of Atmospheric and Oceanic Technology*, 18:742–755, 2001.

F.J. Turk and S.D. Miller. Toward improving estimates of remotely-sensed precipitation with modis/amsr-e blended data techniques. *IEEE Transactions on Geoscience and Remote Sensing*, 43:1059–1069, 2005.

F.J. Turk, B.-J. Sohn, H.-J. Oh, E.E. Ebert, V. Levizzani, and E.A. Smith. Validationg a rapid-update satellite precipitation analysis acrosso telescoping space and time scales. *Meteorology and Atmospheric Physics*, 105:99–108, 2009.

F.J. Turk, P. Arkin, E.E. Ebert, and M.R.P. Sapiano. EVALUATING HIGH-RESOLUTION PRECIPITATION PRODUCTS. *Bulletin of the American Meteorological Society*, 89(12):1911–1916, 2008.

D. Veneziano and V. Iacobellis. Multiscaling pulse representation of temporal rainfall. *Water Resources Research*, 38:1138, 13PP, 2002.

D. Veneziano, R. L. Bras, and J. D. Niemann. Nonlinearity and self-similarity of rainfall in time and a stochastic model. *Journal of Geophysical Research*, 101:26,371– 26,392, 1996.

G.A. Vicente, J.C. Davenport, and R.A. Scofield. The role of orographic and parallax correction on real time, high resolution satellite rain rate observation. *International Journal of Remote Sensing*, 23:221–230, 2002.

L. Vincent and P. Soille. Watersheds in digital spaces: an efficient algorithm based on immersion simulations. *IEEE Transactions on Pattern Analysis and Machine Intelligence*, 13:583–598, 1991.

E. C. Waymire, V. K. Gupta, and I. Rodriguez-Iturbe. A spectral theory of rainfall intensity at the meso-beta scale. *Water Resources Research*, 20:1465–1483, 1984.

F. Weng, L. Zhao, R. Ferraro, G. Poe, X. Li, and N. Grody. Advanced microwave sounding unit cloud and precipitation algorithms. *Radio Science*, 38:8068–8079, 2003.

H. S. Wheater, V. S. Isham, D. R. Cox, R. E. Chandler, A. Kakou, P. J. Northrop, L. Oh, C. Onof, and I. Rodriguez-Iturbe. Spatial-temporal rainfall fields: Modelling and statistical aspects. *Hydrology and Earth System Sciences*, 4:581–601, 2000.

T. T. Wilheit, A. T. C. Chang, and L. S. Chiu. Retrieval of monthly rainfall indices from microwave radiometric measurement using probability distribution functions. *Journal of Atmospheric and Oceanic Technology*, 8:118–136, 1991.

P. Willems. A spatial rainfall generator for small spatial scales. *Journal of Hydrometeorology*, 252:126–144, 2001.

C. J. Wilmott, C. M. Rowe, and W. D. Philpot. Small-scale climate maps: A sensitivity analysis of some common assumptions associated with grid-point interpolation and contouring. *American Cartographer*, 12:5–16, 1985.

WMO. World weather watch - twenty-second status report on implementation - wmo-no. 986. Technical report, World Meteorological Organization (WMO), 2005.

P. Xie and P. A. Arkin. Global monthly precipitation estimates from satellite-observed outgoing longwave radiation. *Journal of Climate*, 11:137–164, 1998.

P. Xie and P.A. Arkin. Gauge-based monthly analysis of global land precipitation from 1971 to 1994. *Journal of Geophysical Research*, 101:19023–19034., 1996a.

P. Xie and P.A. Arkin. Analyses of global monthly precipitation using gauge observations, satellite estimates and numerical model predictions. *Journal of Climate*, 9:840–858, 1996b.

P. Xie and P.A. Arkin. Global precipitation: a 17-year monthly analysis based on gauge observations, satellite estimates, and numerical model outputs. *Bulletin of the American Meteorological Society*, 78:2539 – 2558, 1997.

P. Xie, J. E. Janowiak, P. A. Arkin, R. F. Adler, A. Gruber, R. Ferraro, G. J. Huffman, and S. Curtis. Gpcp pentad precipitation analyses: An experimental dataset based on gauge observations and satellite estimates. *Journal of Climate*, 16:2197–2214, 2003.

P. Xie, A. Yatagai, M. Chen, T. Hayasaka, Y. Fukushima, C. Liu, and S. Yang. A gauge-based analysis of daily precipitation over east asia. *Journal of Hydrometeorology*, 8:607–626, 2007.

A. Xiong, P. Xie, J.-Y. Liang, Y. Shen, R. J. Joyce, J. E. Janowiak, and P. A. Arkin. Merging gauge observations and satellite estimates of daily precipitation over china. In *Fourth Int. Precipitation Working Group Workshop, Beijing, China*, pages 358–363, 2008.

E. Xoplaki. *Climate variability over the Mediterranean.* PhD thesis, University of Bern, Switzerland, 2002.

E. Xoplaki, F.J. Gonzalez-Rouco, J. Luterbacher, , and H. Wanner. Mediterranean summer air temperature variability and its connection to the large-scale atmospheric circulation and ssts. *Climate Dynamics*, 20:723–739, 2003.

D. Yakir, S. Lev-Yadun, and A. Zangvil. El nino and tree growth near jerusalem over the last 20 years. *Global Change Biology*, 2:101–105, 1996.

K.K. Yilmaz, T.S. Hogue, K.-L. Hsu, S. Sorooshian, H.V. Gupta, and T. Wagener. Intercomparison of rain gauge, radar, and satellite-based precipitation estimates with emphasis on hydrologic forecasting. *Journal of Hydrometeorology*, 6:497–517, 2005.

I.I. Zawadzki and U. Ro. Correlations between maximum rate of precipitation rate and mesoscale parameters. *Journal of Applied Meteorology*, 17:1327–1334, 1978.

I.I. Zawadzki, E. Torlaschi, and R. Sauvageau. The relationship between mesoscale thermodynamic variables and convective precipitation. *Journal of Atmospheric Sciences*, 38:1535–1540, 1981.

D.A. Zeweldi and M. Gebremichael. Evaluation of CMORPH Precipitation Products at Fine Space-Time Scales. *Journal of Hydrometeorology*, 10(1): 300–307, 2009.

L. Zhao and F. Weng. Retrieval of ice cloud parameters using the advanced microwave sounding unit. *Journal of Applied Meteorology*, 41:384–395, 2002.